Universities of Florence, Perugia, Pisa, Vienna

DEPARTMENT OF CIVIL AND ENVIRONMENTAL ENGINEERING
International Doctorate in Civil and Environmental Engineering - XXXI cycle

PhD Thesis

On the estimation of soil saturated hydraulic conductivity: from local to field scale

Sulla stima della conduttività idraulica di saturazione: dalla scala locale alla scala di campo

Zur Bestimmung der gesättigten hydraulischen Leitfähigkeit des Bodens: von der lokalen Skale zur Feldskale

PhD candidate: Tommaso Picciafuoco

Austrian supervisor:
Prof. Günter Blöschl

Italian supervisors:
Prof. Corrado Corradini

Prof. Renato Morbidelli

Prof. Alessia Flammini

2019

Table of Contents

List of Figures

List of Tables

Nomenclature

Acronyms

1D	one-dimensional
3D	three-dimensional
CHP	Constant Head well Permeameter
CTP	CSIRO Tension disc Permeameter
DRI	Double-Ring Infiltrometer
DTM	Digital Terrain Model
EM	ElectroMagnetic
GCV	Generalized Cross-Validation
GMER	Geometric Mean Error Ratio
GP	GUELPH constant head well Permeameter
GPR	Ground Penetrating Radar
HDS	Heat Dissipation Sensor
HOAL	Hydrological Open-Air Laboratory
HYPRES	HYdraulic PRoperties of European Soils
MC	Monte Carlo simulation technique
OLS	Ordinary Least Squares
PDF	Probability Density Function
PTF	PedoTransfer Function
PTF_{MLR}	PedoTransfer Function obtained applying the Multiple Linear Regression technique

PTF_R	PedoTransfer Function obtained applying the Ridge regression technique
REV	Representative Elementary Volume
RMSE	Root Mean Square Error
RS	Rainfall Simulator
SAR	Synthetic Aperture Radar
SCM	undisturbed Soil Core sampling Method
SFH	Simplified Falling-Head technique
SRI	Single-Ring Infiltrometer
SVM	Support Vector Machines
TDR	Time Domain Reflectometry
TP	Tension Permeameter
USDA	United States Department of Agriculture
VIF	Variance Inflation Factor
WRC	Water Retenstion Curve

Greek symbols

α	parameter (Parlange et al., 1982)
$\boldsymbol{\beta}$	vector of regression coefficients
v	velocity of propagation
ψ	soil water matric capillary head
ψ_{av}	soil water matric capillary head at the wetting front
ρ	correlation coefficient
ρ_a	air density
ρ_w	water density
σ^2	variance

τ	group effect (ANOVA)
θ	volumetric water content
θ_r	residual water content
θ_s	water content at saturation
ϵ	error ratio
ε	random error
$\boldsymbol{\varepsilon}$	error vector
ε_{ra}	apparent relative permittivity

Other symbols

A	area
CV	Coefficient of Variation
c	velocity of light in free space
cl	clay content
D	diffusivity
el	elevation
F	cumulative infiltration
F'	cumulative dynamic infiltration (Parlange et al., 1982)
$\tilde{F}$	variance ratio (ANOVA)
G	integral capillary drive
H	total number of observations (ANOVA)
h_w	water depth
$\boldsymbol{I}$	identity matrix
$\bar{I}$	areal-average infiltration rate
J	total number of groups (ANOVA)
K	hydraulic conductivity

K_a	air conductivity
K_r	relative conductivity function
K_s	saturated hydraulic conductivity
$\bar{K}_s$	areal-average saturated hydraulic conductivity
$\bar{K}_s^f$	geometric mean of six values of K_s averaged over 80 m^2
n	number of measurements (bootstrap method)
om	organic matter content
P	pressure
q	infiltration rate
R^2	coefficient of determination
r	rainfall rate
r_0	disc radius
S	sorptivity
SS	sum of squares (ANOVA)
S_e	effective saturation
s	slope angle
sa	sand content
si	silt content
t	time
t_p	time to ponding
t_0	equivalent time origin (Philip, 1957a,b,c, 1969)
W_{95}	width of the normalized 95 % confidence interval
$\boldsymbol{X}$	matrix of regressors
$\tilde{\boldsymbol{X}}$	standardized matrix of regressors
$\boldsymbol{y}$	vector of dependent variables

Abstract

The soil saturated hydraulic conductivity, K_s, has a key role in the partitioning of rainfall into runoff and infiltration. The commonly used instruments for in-situ measurements of K_s have frequently provided conflicting results. This thesis presents a comparison of K_s estimates obtained by three classical devices, i.e. the double ring infiltrometer (DRI), the Guelph version of the constant-head well permeameter (GP) and the CSIRO version of the tension permeameter (CTP). A distinguishing feature of this study is the use of steady deep flow, obtained from controlled rainfall-runoff experiments, as a benchmark of K_s at "local" and field scales to assess the reliability of the above methods. The DRI overestimates K_s, the GP gives conflicting estimates of K_s with substantial overestimation in laboratory experiments and underestimation at the plot scale, whereas the CTP yields average K_s values with errors of 24 % in the plot-scale experiment and 66 % in the laboratory experiments. The DRI yields a better estimate of the K_s spatial variability as compared to the GP and CTP, but a separate calibration should be made to correct the overestimation of K_s values. The reasons for such discrepancies within and between the measurement methods are not yet fully understood.

Spatially representative estimates of K_s are needed for simulating catchment scale surface runoff and infiltration. Classical methods for measuring K_s at the catchment scale are time-consuming. Important insights can be obtained by experiments aimed at understanding the controls of K_s in an agricultural setting and identifying the minimum number of samples required for estimating representative plot scale K_s values. This thesis presents results from a total of 131 double-ring infiltrometer measurements at 12 plots in a small Austrian catchment. A statistical analysis of K_s across the catchment suggests that K_s is only slightly influenced by physical soil characteristics,

while land use is the main control. The highest values of K_s were observed in arable fields, with a median and a coefficient of variation (CV) about 3 times and 75 %, respectively, of those in grassland areas. An uncertainty analysis aimed at determining the minimum number of K_s measurements necessary for estimating the geometric mean of K_s over a given area with a specified accuracy suggests that, beyond a specific and plot-size dependent number of measurements, the benefit of extra measurements is small. The width of the confidence interval of the geometric mean of K_s decreases with the number of measurements and increases with the size of the sampled plot. Applications of these findings for designing field campaigns are discussed.

Classical field techniques to determine K_s at the plot scale are complex and time-consuming, therefore the development of pedotransfer functions, PTFs, to derive K_s from easily available soil properties is of utmost importance. However, PTFs have been generally developed at the point scale, while application of hydrological modeling requires field scale estimates. In this thesis, values of field-scale saturated hydraulic conductivity, $\bar{K}_s$, measured in a number of areas within the Austrian catchment, have been used to derive two PTFs by multiple linear regression (PTF_{MLR}) and ridge regression (PTF_R). Calibration and validation of the PTFs indicate that the PTF_R provides better estimates with smaller average errors. This suggests that the ridge regression is a valid alternative to the widely used multiple linear regression technique. Predictions of $\bar{K}_s$ by the PTFs in the areas where infiltration measurements were not performed have also been made to obtain a map of $\bar{K}_s$ for the whole catchment. To obtain a spatial resolution suitable for catchment hydrological modeling, an interpolation of the available soil properties is required. Two alternative approaches have been used: (A) soil properties have been first interpolated with successive application of the PTFs, (B) the PTFs have been first applied in the sites where soil properties were available and then interpolated. The map of $\bar{K}_s$ obtained by the PTF_{MLR} was found not to be representative of the $\bar{K}_s$ spatial variability because of the almost uniform values within the catchment, which is not realistic. On the other hand, the map generated by the PTF_R on the basis of approach (A) has a much more variable spatial pattern of $\bar{K}_s$ which is consistent with the catchment morphology and soil characteristics.

Sommario

La conduttività idraulica di saturazione, K_s, riveste un ruolo fondamentale nella ripartizione delle precipitazioni in deflusso superficiale e infiltrazione. Gli strumenti comunemente utilizzati per la misura in-situ di K_s forniscono frequentemente dei risultati contrastanti. Questo lavoro di tesi presenta un confronto riguardante la stima di K_s ottenuta attraverso tre strumenti classici, nello specifico l'infiltrometro a doppio anello (DRI), il permeametro a carico costante della Guelph (GP) e il permeametro ad anello della CSIRO (CTP). La caratteristica che contraddistingue questo studio è l'utilizzo del deflusso profondo in condizioni stazionarie, ottenuto attraverso degli esperimenti controllati di pioggia-ruscellamento, come criterio di riferimento per la stima di K_s alla scala locale e di plot allo scopo di valutare l'affidabilità dei suddetti strumenti. Il DRI sovrastima largamente K_s, il GP fornisce dei risultati contrastanti con una notevole sovrastima riscontrata negli esperimenti eseguiti in laboratorio e una sottostima in quelli alla scala di plot, mentre CTP restituisce valori mediati di K_s con errori del 24 % e 66 % per gli esperimenti eseguiti rispettivamente in campo ed in laboratorio. Il DRI consente di ottenere una stima migliore della variabilità spaziale di K_s in confronto al GP e al CTP, tuttavia una procedura di calibrazione dovrebbe essere eseguita al fine di correggere il problema di sovrastima dei valori di K_s. Il motivo delle differenze osservate nei risultati ottenuti con un singolo strumento e tra diversi strumenti non è ancora compreso a fondo.

Al fine di simulare il deflusso superficiale e l'infiltrazione alla scala di bacino sono necessarie delle stime spaziali rappresentative di K_s. Le metodologie classiche per la misura di K_s alla scala di bacino sono estremamente dispendiose in termini di tempo. Conoscenze importanti possono essere tuttavia ottenute attraverso esperimenti finalizzati alla comprensione dei fattori che

influenzano la variabilità di K_s in ambiente agricolo e all'identificazione di un numero minimo di misure necessario alla stima di valori rappresentativi di K_s alla scala di plot. Questa tesi presenta i risultati ottenuti attraverso 131 misure eseguite con infiltrometro a doppio anello in 12 siti di misura appartenenti ad un piccolo bacino austriaco. Un'analisi statistica di K_s in tutto il bacino suggerisce che tale parametro è influenzato in maniera lieve dalle caratteristiche fisiche e topografiche del suolo, mentre la destinazione d'uso del terreno risulta essere il fattore dominante. I valori maggiori di K_s sono stati osservati nei campi coltivati, con una mediana circa 3 volte maggiore ed un coefficiente di variazione (CV) del 75 % rispetto a quelli osservati nei terreni erbosi. Un'analisi di incertezza mirata alla determinazione del numero minimo di misure di K_s necessario per stimarne la media geometrica su un'area di specifiche dimensioni e con una specifica accuratezza suggerisce che, oltre un certo numero di misure specifico per ciascun sito di misura e dipendete dalla grandezza del plot, il vantaggio che si ottiene attraverso misure aggiuntive è modesto. L'ampiezza dell'intervallo di confidenza della media geometrica di K_s diminuisce all'aumentare del numero di misure ed aumenta con le dimensione del plot campionato. Possibili applicazioni dei risultati alla progettazione di campagne di misura sono inoltre discusse.

Le tecniche di misura classiche per la determinazione di K_s alla scala di plot e di bacino sono complesse e dispendiose in termini di tempo, pertanto lo sviluppo di funzioni di pedotrasferimento, PTFs, per poter derivare K_s a partire da altre proprietà del suolo di più facile reperimento assume grande importanza. Tuttavia, le PTFs sono state generalmente sviluppate alla scala locale, mentre nelle applicazioni di modellistica idrologica sono richieste stime a scala di campo. In questa tesi, valori di conduttività idraulica di saturazione alla scala di campo, $\bar{K}_s$, misurati in un certo numero di aree all'interno del bacino austriaco, sono stati utilizzati per derivare due PTFs attraverso le tecniche di regressione lineare multipla (PTF_{MLR}) e di regressione ridge (PTF_R). La calibrazione e la validazione delle PTFs indicano che la PTF_R fornisce stime migliori con errori medi più piccoli. Ciò suggerisce che la regressione ridge sia una valida alternativa alla più largamente utilizzata regressione lineare multipla. Nelle aree in cui non erano state eseguite misure, i valori di $\bar{K}_s$ sono stati predetti attraverso le due PTFs al fine di realizzare una

mappa di $\bar{K}_s$ per l'intero bacino. Per poter ottenere una risoluzione spaziale appropriata per la modellazione idrologica a scala di bacino, è stato necessario eseguire un'interpolazione le proprietà del suolo disponibili. Due approcci alternativi sono stati adottati: (A) le proprietà del suolo sono state prima interpolate e successivamente sono state applicate le PTFs, (B) la PTFs sono state prima applicate in quei siti dove le proprietà del suolo erano disponibili a poi sono stai interpolati i valori risultanti. La mappa di $\bar{K}_s$ ottenuta con $\mathrm{PTF}_{\mathrm{MLR}}$ non è rappresentativa della variabilità spaziale di $\bar{K}_s$ come si evince dalla distribuzione dei valori la quale risulta essere circa uniforme in tutto il bacino, cosa che non può essere considerata realistica. D'altro canto, la mappa generate attraverso la $\mathrm{PTF}_{\mathrm{R}}$ sulla base dell'approccio (A) present un andamento spaziale che è coerente con la morfologia del bacino e con le caratteristiche del suolo.

Kurzfassung

Die gesättigte hydraulische Leitfähigkeit des Bodens, K_s, spielt eine entscheidende Rolle bei der Aufteilung des Niederschlags in Oberflächenabfluss und Infiltration. Die üblicherweise verwendeten Instrumente und Methoden für In-situ-Messungen von K_s haben häufig zu widersprüchlichen Ergebnissen geführt. Diese Dissertation stellt einen Vergleich von Bestimmungsmethoden für K_s dar, die mit drei klassischen Messgeräten erhalten wurden, nämlich dem Doppelringinfiltrometer (DRI), der Guelph-Version des Permeameters mit konstantem Wasserspiegel (GP) und der CSIRO-Version des Saugspannungspermeameters (CTP). Ein kennzeichnendes Merkmal dieser Studie ist die Verwendung stationärer Infiltrationsbedingungen bei kontrollierten Niederschlag-Abflussexperimenten, die als Benchmark für die Messungen auf der lokalen Skale und der Feldskale verwendet werden, um deren Zuverlässigkeit zu bewerten. Die DRI Methode überschätzt K_s stark, die GP Methode ergibt widersprüchliche Schätzungen mit einer erheblichen Überschätzung in den Laborexperimenten und einer Unterschätzung auf der Feldskale, während die CTP Methode durchschnittliche Werte mit Fehlern von 24 % auf der Feldskale und 66 % in den Laborexperimenten liefert. Die DRI Methode liefert eine bessere Schätzung der räumlichen Variabilität im Vergleich zu GP und CTP, es sollte jedoch eine separate Kalibrierung vorgenommen werden, um die Überschätzung der K_s Werte zu korrigieren. Die Gründe für die Abweichungen innerhalb und zwischen den Messverfahren sind noch nicht vollständig verstanden.

Für die Simulation von Oberflächenabfluss und Infiltration in Einzugsgebieten sind räumlich repräsentative Schätzungen von K_s erforderlich. Die klassischen Messmethoden für K_s auf der Einzugsgebietskala sind zeitaufwändig. Wichtige Erkenntnisse können durch Experimente gewonnen werden,

die darauf abzielen, die Einflussfaktoren auf K_s in einer landwirtschaftlich genutzten Landschaft zu verstehen, und die Mindestanzahl von Messwerten zu ermitteln, die für die Bestimmung repräsentativer Werte von K_s erforderlich sind. Diese Arbeit präsentiert Ergebnisse von insgesamt 131 Doppelring-Infiltrometermessungen auf 12 Messflächen in einem kleinen österreichischen Einzugsgebiet. Eine statistische Analyse von im gesamten Einzugsgebiet zeigt, dass diese nur geringfügig von den physikalischen und topographischen Bodeneigenschaften beeinflusst wird, während die Landnutzung einen wichtigen Einflussfaktor darstellt. Die höchsten K_s Werte wurden auf Ackerflächen beobachtet, wobei der Median bzw. der Variationskoeffizient (CV) etwa das Dreifache bzw. 75 % der Werte auf Grünland betragen. Eine Unsicherheitsanalyse, die darauf abzielt, die minimale Anzahl von K_s Messungen zu bestimmen, die für die Ermittlung des geometrischen Mittels über eine bestimmten Fläche mit vorgegebener Genauigkeit erforderlich ist, zeigt, dass der Nutzen zusätzlicher Messungen über eine bestimmte und von der Plotgröße abhängige Anzahl von Messungen hinaus gering ist. Das Konfidenzintervall des geometrischen Mittels von K_s nimmt mit der Anzahl der Messungen ab und steigt mit der Größe der Fläche auf der gemessen wird. Die Anwendung dieser Erkenntnisse für die Planung von Feldkampagnen wird diskutiert.

Klassische Methoden zur Bestimmung von K_s auf der Feldskale und der Einzugsgebietsskale sind komplex und zeitaufwändig, daher ist die Entwicklung von Pedotransferfunktionen (PTFs) zur Ableitung von K_s aus leicht verfügbaren Bodeneigenschaften von äußerster Wichtigkeit. PTFs wurden jedoch im Allgemeinen auf der Punkteskala entwickelt, während die Anwendung für die hydrologische Modellierung eine Schätzung auf der Feldskale erfordert. In dieser Arbeit wurden Werte für die gesättigte hydraulische Leitfähigkeit auf der Feldskale, die auf einer Reihe von Flächen innerhalb des österreichischen Einzugsgebiets gemessen wurden, verwendet, um zwei PTFs durch multiple lineare Regression (PTF_{MLR}) und Ridge-Regression (PTF_R) abzuleiten. Die Kalibrierung und Validierung der PTFs zeigt, dass die PTF_R Methode bessere Schätzungen mit kleineren durchschnittlichen Fehlern liefert. Dies legt nahe, dass die Ridge-Regression eine gültige Alternative zu der weit verbreiteten linearen Regressionsmethode ist. Die PTFs wurden auch verwendet, um $\bar{K}_s$ auf Flächen zu berechnen, auf denen keine Infiltrationsmessungen durchgeführt

wurden, um eine $\bar{K}_s$ Karte des gesamten Einzugsgebiets zu erhalten. Um eine für die hydrologische Modellierung des Einzugsgebiets geeignete räumliche Auflösung zu erhalten, ist eine Interpolation der verfügbaren Bodeneigenschaften erforderlich. Dafür wurden zwei alternative Ansätze verwendet: (A) Bodeneigenschaften wurden zuerst interpoliert, und dann wurden die PTFs angewendet. (B) Die PTFs wurden zuerst an den Standorten angewendet, an denen Bodeneigenschaften verfügbar waren, und dann interpoliert. Die durch die $\mathrm{PTF}_{\mathrm{MLR}}$ erhaltene Karte erwies sich aufgrund der nahezu gleichen Werte innerhalb des Einzugsgebiets als nicht repräsentativ für die räumliche Variabilität, was nicht realistisch ist. Andererseits weist die mittels $\mathrm{PTF}_{\mathrm{R}}$ auf der Grundlage des Ansatzes (A) erzeugte Karte ein viel variableres räumliches Muster von $\bar{K}_s$ auf, das mit der Einzugsgebietsmorphologie und den Bodeneigenschaften konsistent ist.

Chapter 1

Introduction

The soil saturated hydraulic conductivity, K_s, is a key parameter controlling various hydrological processes, such as rainfall partitioning into infiltration and surface runoff and transport of pollutants in saturated and unsaturated soils. Accurate estimates of K_s are needed for modeling point infiltration into homogeneous (Philip, 1969; Chow et al., 1988; Corradini et al., 1997; Smith, 2002) and layered soils (Corradini et al., 2000, 2011; Govindaraju et al., 2012), and are also essential at the field scale to properly represent the effect of horizontal soil heterogeneity on the infiltration process in distributed rainfall-runoff models. Smith and Goodrich (2000) and Govindaraju et al. (2001) presented two models that can simulate areal-average infiltration of rainfall into vertically homogeneous soils exhibiting horizontal random variation of saturated hydraulic conductivity. Later, Govindaraju et al. (2006) extended their previous model incorporating a coupled spatial variability of K_s and rainfall rate. The above-mentioned areal models have in common the essential requirement of a spatial characterization of K_s, which in the absence of sampled data can be synthetically approximated by a log-normal random field with areal-average value, $\bar{K}_s$, and coefficient of variation, $CV(K_s)$, fixed in advance.

A detailed representation of the natural spatial variability of hydraulic soil properties, and particularly of K_s, is crucial because the last quantity exhibits a high degree of variability (Nielsen et al., 1973; M. L. Sharma et al., 1987; Loague and Gander, 1990). Many factors influence K_s spatial variability, such as soil

structure (Dexter et al., 2004), texture (Puckett et al., 1985; Saxton et al., 1986; Jabro, 1992; Baiamonte et al., 2017), landscape position (Wagger and Denton, 1989; Mohanty et al., 1994), land cover, management practices (Ziegler et al., 2006; Zimmermann and Elsenbeer, 2008; Alletto and Coquet, 2009; Bonell et al., 2010; Picciafuoco et al., 2018b), and spatial scale (Schulze-Makuch et al., 1999; Sobieraj et al., 2004; Lai and Ren, 2007). Furthermore, previous studies have shown the effects of K_s spatial variability on various hydrological aspects, such as the runoff hydrograph, the overland flow estimation and the peak discharge (Woolhiser et al., 1996; Taskinen et al., 2008; Hu et al., 2015), highlighting how an inaccurate spatial characterization of K_s could lead to misguided results. Accounting for K_s spatial variability is therefore essential.

Several techniques are available for in-situ estimation of K_s through infiltration measurements (McKenzie et al., 2002). The most commonly used devices are: tension permeameters (TP), e.g. the CSIRO disc permeameter (CTP) (Perroux and White, 1988), single ring infiltrometers (SRI) (Lassabatère et al., 2006), double-ring infiltrometers (DRI) (Swartzendruber and Olson, 1961a,b), constant-head well permeameters (CHP), e.g. the GUELPH permeameter (GP) (Reynolds and Erlick, 1985), rainfall simulators (RS), e.g. the GUELPH rainfall simulator (Tossell et al., 1987). Undisturbed soil core sampling (SCM) is also used. The choice of the device influences the estimated values of K_s (Angulo-Jaramillo et al., 2000; Muñoz-Carpena et al., 2002; Verbist et al., 2013; Bagarello et al., 2014; Morbidelli et al., 2017) due to different factors such as the volume of soil investigated, the duration of the measurement, the theoretical framework (e.g., 1D or 3D infiltration) and the estimates of other soil parameters (e.g., soil sorptivity, saturated water content) necessary to derive the value of K_s applying specific equations.

Investigations have been made to compare the estimates provided by different measurement tools in order to understand their reliability in the K_s estimation (Boers et al., 1992; Vanderlinden et al., 1998; Reynolds et al., 2000; Verbist et al., 2013). The results highlighted great differences between the values observed with different instruments used in the same area. Consequently, although intercomparison of different methods is useful, a proper assessment of these techniques would be required to identify a reliable bechmark to validate K_s measurements (Reynolds et al., 2000; Lai et al., 2010).

An important issue affecting in-situ K_s estimation is the time required to perform the measurements. In fact, most field techniques rely on the attainment of a steady-state flow rate, so that the measuring process is usually time-consuming. Speeding up the measurement operations is one of the greatest challenges to be faced when the spatial scale increases. Some approaches rely upon the reduction of the number of measurements required to obtain the same information content of the entire data-set (Vieira et al., 1981; Skøien and Blöschl, 2006; Ahmed et al., 2015). Others use faster measurement techniques (Muñoz-Carpena et al., 2002; Bagarello et al., 2004) or indirect methods – i.e. pedotransfer functions (PTFs) – (Wösten et al., 1999; Schaap et al., 2001).

Usually PTFs are developed from existing soil databases by examining the relationships between easily available input data (e.g., textural properties or topographic variables) and hard-to-measure soil parameters that have to be predicted at the local scale (e.g., retention curve or saturated hydraulic conductivity). However, many PTFs available in literature are not suitable for applications in different regions (Tietje and Tapkenhinrichs, 1993; Kern, 1995; Cornelis et al., 2001; Wagner et al., 2001; Nemes et al., 2003). Therefore, attempts have been made to recalibrate published pedotransfer functions adjusting the parameters to soil conditions different from those used in their development (Abdelbaki, 2016).

As above-mentioned, in order to apply the models for estimating field-scale infiltration, K_s can be represented as a random variable through $\bar{K}_s$ and $CV(K_s)$. In principle, the last two quantities could be estimated using pedotransfer functions. However, PTFs already developed allow to derive K_s only at the local scale and therefore a procedure of upscaling or alternatively PTFs able to provide directly $\bar{K}_s$ should be defined. If a PTF providing saturated hydraulic conductivity values at the plot scale was developed, a continuous map of $\bar{K}_s$ could be produced for a given catchment.

The main objectives of this work are:

1. to validate in-situ K_s measurements carried out by classical techniques.

   Three widely used devices (DRI, CTP and GP) have been tested (Morbidelli et al., 2017). The benchmark relies upon controlled rainfall-runoff experiments designed to reach saturation and steady

flow conditions in two deep soils set up at the laboratory and the field/plot scale. Steady conditions are detected by measurements of soil moisture content, surface flow, and deep flow. The last quantity is considered as the "correct" representation of the areal-average K_s value.

2. realization of a variety of experiments by the classical devices to highlight the elements that control K_s values in an agricultural setting and to define the minimum number of samples required for estimating a representative value of K_s at the plot scale (Picciafuoco et al., 2018b).

   A total of 131 DRI measurements were made on 12 plots in a small Austrian catchment. Measurements were collected in both grasslands and arable lands to deduce the effects of different land management operations on the K_s spatial variability. A statistical analysis has been performed to understand the confidence in the estimate of the areal average value of K_s for different land uses, plot areas and sample sizes. Guidelines for planning measurement campaigns with double-ring infiltrometers, when time and resources are limited, are also given.

3. calibration and validation of two PTFs to determine plot-scale K_s values (Picciafuoco et al., 2018a).

   In this context a new data-set of $\bar{K}_s$ representative of different catchment areas has been generated from the outcomes of point 2. The multiple linear regression and ridge regression techniques have been used to define the pedotransfer functions, $\mathrm{PTF_{MLR}}$ and $\mathrm{PTF_{R}}$, respectively

4. derivation and comparison of two maps with $\bar{K}_s$ values predicted by two alternative methodologies for the Austrian catchment (Picciafuoco et al., 2018a).

Before addressing the above issues, a synthetic description of the infiltration theory is presented to highlight as the saturated hydraulic conductivity is involved in model for point and field-scale infiltration into homogeneous and heterogeneous soils.

Chapter 2

A short account of infiltration theory

Research activity has been limited for many years to the development of local, or point, infiltration models for vertically homogeneous soils (Green and Ampt, 1911; Philip, 1957a,b,c; Smith and Parlange, 1978; Parlange et al., 1982; Dagan and Bresler, 1983; Corradini et al., 1997). However, natural soil vertical profiles are frequently not homogeneous. In the last case, hydrological simulations can schematize local infiltration by a two-layered vertical profile (Mualem et al., 1993; Taha et al., 1997) with a sealing layer over a more permeable soil layer or vice versa. Several models for local infiltration into crusted soils were developed adapting the Green-Ampt model (Hillel and W. R. Gardner, 1970; Ahuja, 1983; Smith, 1990). Later on, Corradini et al. (2000) developed a model to represent point infiltration under complex rainfall pattern and for any two-layered soil.

In applied hydrology, upscaling of point infiltration models to the field and catchment scale is required to estimate the areal-average infiltration. This is a challenge even for vertically homogeneous soils because of the natural horizontal heterogeneity of soil properties and particularly of the saturated hydraulic conductivity (Russo and Bresler, 1981, 1982). Smith and Goodrich (2000) proposed a semi-empirical model to determine the areal-average infiltration rate into areas with K_s considered as a log-normally distributed random variable. However, in addition to the heterogeneity of K_s, the rainfall rate, r,

is also characterized by spatial variability (Goodrich et al., 1995; Krajewski et al., 2003) and their interaction makes the estimate of areal infiltration very complex (Morbidelli et al., 2006). A semi-analytical/conceptual model of the expected areal-average infiltration was then developed combining a random variability of K_s and r (Govindaraju et al., 2006) which was also extended including an empirical representation of the run-on process (Morbidelli et al., 2006).

The infiltration models generally consider a soil surface placed horizontally or with a low slope that does not affect the physical process. However, in most real situations, infiltration occurs in surfaces characterized by different gradients, therefore the role of surface slope on infiltration has to be quantified. The results obtained by some theoretical and experimental investigations (K. D. Sharma et al., 1983; Poesen, 1984; Philip, 1991; Essig et al., 2009; Morbidelli et al., 2015) lead to rather conflicting conclusions on the estimate of K_s in sloping surfaces.

2.1 Richards' equation

Under conditions of horizontally homogeneous soil the water movement in the vertical direction is governed by the one-dimensional soil water flow and continuity equations. The flow rate per unit cross-sectional area, q, is given by Darcy (1856) law:

$$q = -K(\psi)\left(\frac{\partial \psi}{\partial z} - 1\right) \tag{2.1}$$

where K is the soil hydraulic conductivity, ψ the soil water matric capillary head and z is the soil depth assumed positive downward. The infiltration rate, q_0, is expressed by equation (2.1) applied at the soil surface.

The mass conservation equation, in the absence of changes in the water density and porosity, as well as of sinks and sources, is given by:

$$\frac{\partial \theta}{\partial t} = -\frac{\partial q}{\partial z} \tag{2.2}$$

where t is the time and θ the volumetric water content. Substitution of

equation (2.1) in equation (2.2) leads to the θ-based Richards equation:

$$\frac{\partial \theta}{\partial t} = \frac{\partial}{\partial z}\left[D(\theta)\frac{\partial \theta}{\partial z} - K(\theta)\right] \tag{2.3}$$

where $D(\theta) = K(\theta)\mathrm{d}\psi/\mathrm{d}\theta$ is the soil diffusivity. In order to solve equation (2.3) it is necessary to define the soil water hydraulic properties $K(\theta)$ and $\psi(\theta)$ (Mualem, 1976; van Genuchten, 1980).

Since the Richards equation is highly nonlinear, analytical solutions can only be derived for specific initial and boundary conditions. The initial condition at time $t = 0$ for $z \geq 0$ is $\theta = \theta_i$, while the upper boundary conditions at the soil surface are:

$$\begin{array}{lll} z = 0 & 0 < t \leq t_p & q_0 = r \\ z = 0 & t_p < t \leq t_r & \theta_0 = \theta_s \\ z = 0 & t_r < t & q_0 = 0 \end{array}$$

where t_p the time to ponding, t_r the rainfall duration and θ_s is the volumetric water content at saturation (the subscripts i and s denote initial and saturation quantities, respectively, while 0 stands for quantities at the soil surface). Finally, the lower boundary condition at a depth z_b which is not reached by the wetting front is $\theta(z_b) = \theta_i$ for $t > 0$. Therefore, the Richards equation allow to derive θ_0 for $0 < t \leq t_p$ when $q_0 = r$. For $t > t_p$ the vertical profile of θ can be derived and then q_0 through the Darcy law.

2.2 Point infiltration in vertically homogeneous soils

2.2.1 Philip model

Philip (1957a,b,c, 1969) proposed an infiltration model obtained through an analytical series solution of the Richards equation under the conditions of vertically homogeneous soil, constant initial moisture content, and saturated soil surface with immediate ponding. For early to intermediate times, the infiltration capacity can be expressed through the first two terms as:

$$f_c = \frac{1}{2}St^{-1/2} + B \tag{2.4}$$

where S is the sorptivity, depending on soil properties and initial moisture content, and B is a quantity ranging from $0.38 \cdot K_s$ to $0.66 \cdot K_s$. The sorptivity represents the soil capability of absorbing water and its magnitude is usually proportional to the amount of water absorbed and to the velocity of the process. For $t \to 0$, B can be neglected in comparison to the first term on the right-hand side of equation (2.4), while for $t \to \infty$, the equation is replaced by:

$$f_c = K_s \tag{2.5}$$

The first term of equation (2.4) represents infiltration due to capillarity and the second due to gravity. Substituting $f_c = \mathrm{d}F/\mathrm{d}t$, the integration of equation (2.4) yields the cumulative infiltration, F:

$$F = St^{1/2} + Bt \tag{2.6}$$

Philips model was later extended to include the more realistic hypothesis of non-immediate ponding. For constant rainfall rate $r > K_s$, surface saturation occurs at a time $t_p > 0$ and following Chow et al. (1988) infiltration can be described through an equivalent time origin, t_0, for potential infiltration after ponding as:

$$t_p = \frac{S^2 \left(r - \frac{B}{2}\right)}{2r(r - B)^2} \tag{2.7}$$

$$t_0 = t_p - \frac{1}{4B^2}\left[(S^2 + 4BF_p)^{1/2} - S\right]^2 \tag{2.8}$$

$$f_c = \frac{1}{2}S(t - t_0)^{-1/2} + B \qquad t > t_p \tag{2.9}$$

with $f_c = r$ for $t \leq t_p$. For unsteady rainfall and $\theta = \theta_s$, for $t > t_p$, infiltration can be estimated through a similar procedure.

2.2.2 Green-Ampt model

The original Green and Ampt (1911) model represents infiltration into homogeneous soils under the conditions of continuously saturated soil surface

and uniform initial soil moisture as:

$$f_c = K_s \left[1 - \frac{\psi_{av} \, (\theta_s - \theta_i)}{F} \right] \tag{2.10}$$

where ψ_{av} is the soil water matric capillary head at the wetting front. To express the infiltration as a function of time, this equation can be solved after the substitution $f_c = \mathrm{d}F/\mathrm{d}t$. The resulting integrated equation (Chow et al., 1988) is:

$$F = K_s t - \psi_{av}(\theta_s - \theta_i) \ln \left[1 - \frac{F}{\psi_{av}(\theta_s - \theta_i)} \right] \tag{2.11}$$

Equation (2.11) can be applied under the assumption of immediate ponding. Under more general conditions, with a constant rainfall rate $r > K_s$, that begins at the time $t = 0$, surface saturation is reached at a time $t_p > 0$. For $t \leq t_p$ the infiltration rate at the surface q_0 is equal to r and later to the infiltration capacity. At the time to ponding, $F = rt_p$ and $f_c = r$ which substituted in equation (2.10) allow to determine t_p as:

$$t_p = -\frac{(\theta_s - \theta_i) K_s \psi_{av}}{r(r - K_s)} \tag{2.12}$$

Substituting $f_c = \mathrm{d}F/\mathrm{d}t$, the integration of equation (2.10) yields:

$$F = F_p - \psi_{av}(\theta_s - \theta_i) \ln \left(\frac{F - \psi_{av}(\theta_s - \theta_i)}{F_p - \psi_{av}(\theta_s - \theta_i)} \right) + K_s(t - t_p) \qquad t > t_p \tag{2.13}$$

The extension of equation (2.11) to unsteady rainfall is straightforward.

2.2.3 Three-parameter semi-analytical model

Parlange et al. (1982) presented a three-parameter model, obtained through analytical integration of the Richards equation, expressed as:

$$f_c = K_s \left(1 + \frac{\alpha}{\exp\left[\frac{\alpha F'}{G(\theta_s - \theta_i)} \right] - 1} \right) \tag{2.14}$$

where $F' = F - K_i t$ is the cumulative dynamic infiltration, α is a parameter related to the behavior of hydraulic conductivity and diffusivity as functions

of θ, and G is the integral capillary drive defined as:

$$G = \frac{1}{K_s} \int_{\theta_i}^{\theta_s} D(\theta) \mathrm{d}\theta \tag{2.15}$$

Equation (2.14) can be applied to determine t_p and f_c for any rainfall pattern and, for $t > t_p$, it can be rewritten under the condition of surface saturation in the form:

$$\left[(1-\alpha)K_s - K_i\right](t - t_p) = F' - F'_p - \frac{(\theta_s - \theta_i)K_s G}{K_d} \ln \left(\frac{\exp\left[\frac{\alpha F'}{(\theta_s - \theta_i)G}\right] - 1 + \frac{\alpha K_s}{K_d}}{\exp\left[\frac{\alpha F'_p}{(\theta_s - \theta_i)G}\right] - 1 + \frac{\alpha K_s}{K_d}} \right) \tag{2.16}$$

where $K_d = K_s - K_i$ and $F'_p = F'(t_p)$. The quantities F'_p and t_p are the values of F' and t, respectively, at which equation (2.14) with $f_c = r(t_p)$ is first satisfied. The value of α usually ranges from 0.8 to 0.85 (Smith, 2002).

2.2.4 Semi-analytical/conceptual model

For complex rainfall patterns the models presented in the previous subsections cannot be applied in principle because the assumption of uniform initial soil moisture cannot be met for successive storms. Models combining infiltration and soil moisture redistribution are the best solution when complex rainfall patterns, which are rather common under natural conditions, have to be considered (Basha, 2011a,b).

Dagan and Bresler (1983) developed an analytical model starting from depth integrated forms of the Darcy and continuity equations and using simplifications in the initial and surface boundary conditions that reduce practical applications at the local scale.

A more general model was formulated by Corradini et al. (1997) starting from the same integrated equations of Dagan and Bresler (1983) then combined with a conceptual representation of the wetting soil moisture profile. To highlight the structure of the model, a specific rainfall pattern which allows to describe all the involved components is used here.

Let us consider a stepwise rainfall pattern involving successive periods of rainfall with constant $r > K_s$, separated by periods with $r = 0$ (Figure 2.1). We denote by t_1 the duration of the first pulse, t_2 and t_3 the beginning and end of the second pulse, respectively, and t_4 the beginning of the third pulse. The model was derived considering a soil with a constant value of θ_i. In addition, as the event progresses in time, a dynamic wetting profile represented by a distorted rectangle through a shape factor $\beta(\theta_0) \leq 1$ was assumed. The resulting ordinary differential equation is:

$$\begin{aligned}\frac{\mathrm{d}\theta_0}{\mathrm{d}t} =& \frac{(\theta_0 - \theta_i)\beta(\theta_0)}{F'\left[\frac{\mathrm{d}\beta(\theta_0)}{\mathrm{d}\theta_0}(\theta_0 - \theta_i) + \beta(\theta_0)\right]} \cdot \\ & \left[q_0 - K_0 - \frac{(\theta_0 - \theta_i)G(\theta_i, \theta_0)\beta(\theta_0)pK_0}{F'}\right]\end{aligned} \tag{2.17}$$

where p is a parameter linked with the profile shape of θ, F' is the cumulative dynamic infiltration rate, and $G(\theta_i, \theta_0)$ is the integral capillary drive expressed by equation (2.15), modified by the substitution of θ_s with θ_0 and K_s with K_0. Equation (2.17) can be applied for $0 < t < t_2$ with an analytical approximation of the profile shape of $\theta(z)$ (Corradini et al., 1994). Functional forms for β and p were obtained by calibration using results provided by the Richards equation applied to a silty loam soil.

Equation (2.17) can be solved numerically. For $q_0 = r$ it gives $\theta_0(t)$ until time to ponding t_p', then for $t_p' < t \leq t_1$ it provides the infiltration capacity ($q_0 = f_c$) and for $t_1 < t < t_2$, with $q_0 = 0$, it describes the redistribution process ($\mathrm{d}\theta/\mathrm{d}t < 0$). The second rainfall pulse leads to a new time to ponding, t_p'', but reinfiltration occurs according to two alternative approaches determined by a comparison of r and the downward redistribution rate. The shape of the soil water content profiles associated with different infiltration-redistribution-reinfiltration stages are shown in Figure 2.1.

2.3 Point infiltration into vertically heterogeneous soils

A two-layer approximation, with each layer being schematized as homogeneous, is frequently used to set up models of infiltration for vertically not

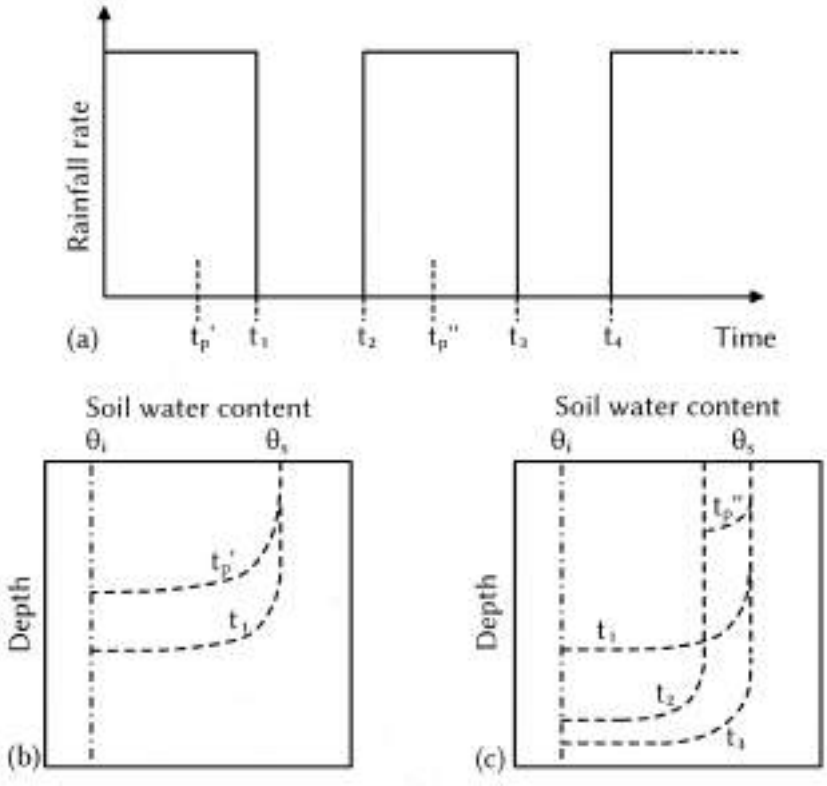

Figure 2.1 - (a) rainfall pattern selected to describe the semi-analytical/conceptual model for point infiltration; (b) and (c) profiles of soil water content at various times and associated with different infiltration-redistribution stages. Figure shown in Singh (2017) as Figure 45.1.

homogeneous natural soils.

A special case of layered soil profile is that of a sealing layer at the surface, resulting from the impact of raindrops impact on the soil. The direct effect of the presence of a sealing layer at the soil surface is to reduce ponding time and infiltration rate during rainfall (Römkens et al., 1986a,b). The process of formation of a sealing layer was accurately examined by Mualem and Assouline (1989) and Mualem et al. (1993), and that of disruption was considered by Bullock et al. (1988), Emmerich (2003), and Morbidelli et al. (2011). Evidence of the role of crusted soils in semiarid regions has been recently provided by L. Chen et al. (2013). Green-Ampt-based models for infiltration into stable crusted soils were proposed by Hillel and W. R. Gardner (1970), Ahuja (1983), and Vandervaere et al. (1998), while efficient approaches which represent transient infiltration into crusted soils are proposed by Smith (1990)

and Philip (1998).

On the other hand, vertical profiles with a more permeable upper layer are observed in the hydrological practice and can be also used, for example, as a first approximation in the representation of infiltration into vertically homogeneous soils with grassy vegetation (Morbidelli et al., 2014). For this layering type Chow et al. (1988) and Corradini et al. (2000) presented two models characterized by fairly limited complexity. The classical Green-Ampt equations are applied until the wetting front is in the upper layer, then equations are provided to determine F and f_c. Corradini et al. (2000) formulated a semi-analytical/conceptual model applicable to any horizontal two-layered soil, where either layer may be more permeable. The same elements previously used by Corradini et al. (1997) are adopted in each layer and integrated at the interface between the two layers using the boundary conditions expressing continuity of flow rate and capillary head. Until water does not infiltrate in the lower layer, the Corradini et al. (1997) model is used, then, when the wetting front enters the lower layer, a system of two ordinary differential equations is provided to describe the time evolution of the soil moisture profile and the infiltration rate.

2.4 Areal infiltration over heterogeneous surfaces

The mathematical problem of infiltration at the field scale cannot be addressed analytically and the use accurate Monte Carlo (MC) simulation techniques imposes an enormous computational effort for routine applications. Considering the horizontal spatial heterogeneity of saturated hydraulic conductivity, MC simulations were used, for instance, by M. L. Sharma (1979), Maller and M. L. Sharma (1981), and Saghafian et al. (1995) in specific studies focused on describing field-scale infiltration. MC simulations were also used by Sivapalan and Wood (1986) to validate a relation they developed for areal average and variance of infiltration rate under a time-invariant rainfall rate. A less frequent alternative to MC sampling for the representation of the random variability of a soil property is the Latin Hypercube sampling (McKay

et al., 1979) adopted by Smith and Goodrich (2000) to develop a simple parameterized approach for areal-average infiltration. Even though performing simulations with many realizations of a random variable is often too expensive in terms of computational effort for practical applications, MC simulations are useful to parameterize simple semi-empirical approaches or to validate semi-analytical models. Along these lines, Govindaraju et al. (2001) developed a semi-analytical/conceptual model for estimating the expected areal-average infiltration into vertically homogeneous soils under a uniform rainfall spatial distribution and random horizontal pattern of K_s (see also Corradini et al., 2002). Later on, Govindaraju et al. (2006) combined in the model the random variability of both rainfall and saturated hydraulic conductivity. Finally, Morbidelli et al. (2006) incorporated in the last model a semi-empirical/conceptual component to consider the run-on process. The combined effect of soil surface sealing and spatial variability in soil properties on infiltration and runoff was investigated by Assouline and Mualem (2002, 2006) using a dynamic model of seal formation (Assouline and Mualem, 1997).

2.4.1 Semi-empirical approach

Smith and Goodrich (2000) proposed a semi-empirical model to determine the areal-average infiltration rate, $\bar{I}$, into areas with random spatial variability of K_s. The local infiltration is described through the three-parameter equation of Parlange et al. (1982), which, in addition to K_s, takes into account a parameter α that varies between 0 and 1 and accounts for the soil type, and the soil integral capillary drive, G. The last quantity can be related to soil sorptivity:

$$G = \frac{S^2}{2K_s(\theta_s - \theta_i)} \tag{2.18}$$

A log-normal probability density function (PDF) of K_s with a mean value $\bar{K}_s$ and a coefficient of variation $CV(K_s)$ is selected and only one realization of the random variable is considered. A runoff area of uniform soil type with random heterogeneity in hydraulic properties and composed of a number of runoff paths (ensemble) is assumed. Each runoff path is a single sample, their sum constitutes the total area. The ensemble behavior is simulated using the Latin Hypercube sampling method. The PDF is divided into N equal probability

ranges and the first moment of each sub-area is used to determine a sample value $K_{s,i}$ with $i = 1, \ldots, N$. The areal-average infiltration rate is obtained as:

$$\bar{I}(t) = \frac{1}{N} \sum_{i=1}^{N} f_c(t, K_{s,i}, G_i) \tag{2.19}$$

Under a rainfall rate r a part of the area (characterized by $K_s > r$) has an infiltration rate equal to r, while the remaining part (characterized by $K_s < r$) has an infiltration rate equal to K_s. In order to account for this effect, an areal effective value of K_s, K_e, related to the PDF of K_s and to the value of r, is considered.

Finally, on the basis of a large number of simulations carried out for many $CV(K_s)$ and r, a relationship is provided for the scaled areal-average infiltration rate, $\bar{I}_e^*$, linked with the corresponding scaled cumulative depth, F_e^*, as:

$$\bar{I}_e^* = 1 + (r_e^* - 1) \left\{ 1 + \left[\frac{r_e^* - 1}{\alpha} \left(e^{\alpha F_e^*} - 1 \right) \right]^c \right\}^{1-1/c} \qquad r_e^* > 1 \tag{2.20}$$

with

$$c \cong 1 + \frac{0.8}{\left[CV(K_s) \right]^{1.3}} \left[1 - e^{-0.85(r_b^* - 1)} \right] \tag{2.21}$$

where $\bar{I}_e^* = \bar{I}_e / K_e$, $F_e^* = F_e / [(\theta_s - \theta_i) G]$, $r_e^* = r / K_e$, and $r_b^* = r / \bar{K}_s$.

2.4.2 Semi-analytical/conceptual model

Govindaraju et al. (2001) formulated a semi-analytical model to estimate the expected field-scale infiltration rate $\langle \bar{I}(F) \rangle$ under the condition of negligible run-on and uniform rainfall rate. The model accounts for K_s horizontal heterogeneity assuming it as a random variable with log-normal PDF characterized by a mean value $\bar{K}_s$ and a coefficient of variation $CV(K_s)$. The study area is partitioned into N cells, each with a single value of K_s, and $\langle \bar{I}(F) \rangle$ is estimated averaging through a large number of K_s realizations. As the number of cells N tends to infinity, a continuous spatial variation of K_s is considered and the expected value of $\bar{I}$ is given by:

$$\langle \bar{I}(F) \rangle = r \left[1 - M(K_c, 0) \right] + \frac{\psi(\theta_s - \theta_i) + F}{F} M(K_c, 1) \tag{2.22}$$

with M expressed (Z. Q. Chen et al., 1994) by:

$$\begin{aligned} M(K_c, \xi) &= \int_0^{K_c} k^{\xi} p_k(k) \mathrm{d}k \\ &= \exp\left(\xi\mu_y + \frac{\sigma_y^2 \xi^2}{2}\right)\left[1 - \frac{1}{2}\mathrm{erfc}\left(\frac{\ln(K_c) - \mu_y}{\sqrt{2}\sigma_y} - \frac{\sigma_y \xi}{\sqrt{2}}\right)\right] \end{aligned} \tag{2.23}$$

where ξ is a generic argument of the function, μ_y and σ_y^2 are the mean and the variance of the random variable $Y = \ln(K_s)$, and K_c is the maximum value of K_s leading to surface saturation determined by:

$$K_c = \frac{Fr}{\psi(\theta_s - \theta_i) + F} \tag{2.24}$$

Finally, to relate the expected time, $\langle t \rangle$, and F the following relation is provided:

$$\begin{aligned} \langle t \rangle =& \frac{F}{r}\big(1 - M(K_c, 0)\big) + \\ & \left[F + \psi(\theta_s - \theta_i)\ln\left(\frac{\psi(\theta_s - \theta_i)}{\psi(\theta_s - \theta_i) + F}\right)\right] M(K_c, -1) + \\ & \psi(\theta_s - \theta_i)\sum_{i=1}^{\infty} \frac{M(K_c, i)}{(i+1)r^{i+1}} \end{aligned} \tag{2.25}$$

The model, that can be also adopted for applications with time-dependent rainfall, was later extended by Govindaraju et al. (2006) to account for random variability of both K_s and r, and finally by Morbidelli et al. (2006) to incorporate the run-on effect.

2.5 Two-phase flow in porous media

When water infiltrates into an initially dry porous medium, the infiltrating water replaces air in the voids. Under natural conditions, the movement of air is generally small (Parlange and Hill, 1979). Therefore, all the above-mentioned solutions of the flow equation, which assume that air can move freely within the porous medium and remain practically at atmospheric pressure so that its impact on the movement of water can be neglected, can be applied. However, under conditions of flood irrigation or intense rainfall air

can be compressed and reduce significantly the infiltration rate (McWhorter, 1971; Dixon and Linden, 1972; Touma et al., 1984; Wang et al., 1997). Solving the problem of two-phase flow in porous medium presented an increased interest since oil can replace air in the two-phase definition and thus address practical issues related to the oil industry. Different approaches were developed (McWhorter, 1971; Morel-Seytoux, 1973; Wooding and Morel-Seytoux, 1976; Weir and Kissling, 1992; Sander et al., 1993; Weeks et al., 2003). The basic equation describing the flux of water, q_w, affected by the flux of air, q_a, was formulated, following McWhorter (1971), by Sander et al. (1988, 1993) in the form:

$$\begin{aligned} q_w(t) = &\left[1-\kappa(\theta)\right] D(\theta)\frac{\partial\theta}{\partial z} + \\ &\left[1-\kappa(\theta)\right]\left(1-\frac{\rho_a}{\rho_w}\right)K(\theta) + \\ &(q_w+q_a)\kappa(\theta) \end{aligned} \tag{2.26}$$

where ρ_a and ρ_w are the air and water densities respectively, and $\kappa(\theta)$ is an increasing function of θ between 0 and 1 defined by McWhorter (1971) as:

$$\kappa(\theta) = \frac{K(\theta)}{K(\theta)+K_a(\theta)} \tag{2.27}$$

with $K_a(\theta)$ being the air conductivity function.

Chapter 3

Soil hydraulic properties

Unsaturated soils contain two fluid phases, i.e. soil water and soil air, and an immobile phase, the soil matrix. In an universal definition, soil hydraulic properties describe macroscopic relations between the chemical potential, the phase concentration, and the transmission behavior of water and gases in soil (Durner and Flühler, 2005). These relations depend on multiple factors, including temperature, pore space geometry, surface properties of the soil matrix, chemical composition of the soil solution, and properties of the wetting and non-wetting fluids that occupy the complementary parts of the pore space. Two-phase flow systems have historically been described using fluid pressures and volumetric water contents as primary variables.

To come to a reasonable definition of water content, we must average the amount of water over a certain soil volume. A practical choice is to choose the smallest volume that contains all structural elements of the pore system in sufficient abundance, i.e. the representative elementary volume REV (Hubbert, 1956; Bear, 1972). In fine-textured non-structured soils, such as fine sands, volumes of 1 cm^3 or less might be sufficiently large to yield a reliable average for soil porosity, while in soils with shrinkage cracks the REV is as large as the whole soil profile (Durner and Flühler, 2005). Therefore, the size of the REV will vary in different spatial directions. If we extend the REV concept to characterize structural properties of natural soils, we see that no single REV exists, because enlarging the averaging volume will lead to the inclusion of new structural elements of larger size. Averaging the local phase fractions

in an REV, and associating the resulting value to the central point of the averaging volume leads to the definition of spatially continuous variables such as water content, air content, soil density, porosity, or water potential.

3.1 Hydraulic functions

The dependence of water content from the water potential, $\theta(\psi)$ is usually called *water retention curve* (WRC) and, in principle, it can be determined by monitoring simultaneously the state variables ψ and θ at an identical point in space during a hydraulic process that changes the systems state. The dependence of the hydraulic conductivity K on water content is called *hydraulic conductivity curve* and it can be determined by inverting equation (2.1) or equation (2.3). For the use in simulation models, these constitutive relationships must be expressed in a continuous way over the whole moisture range, from dryness to saturation.

Numerous expressions have been proposed to describe the water retention characteristic (Brooks and Corey, 1964; Brutsaert, 1967; Campbell, 1974; van Genuchten, 1980). All these curves describe a continuous change of water content from a maximum value, θ_s, which represents the saturated water content, to a minimum value, θ_r, which is the residual water content. The transition from full to partial saturation takes place at a characteristic pressure head (often called bubbling pressure or air entry pressure) that is related to a characteristic width of the largest pores, and thereby depends on soil texture and structure. The slope of the WRC at pressures lower than the air entry pressure depends on the width of the pore-size distribution.

Empirical studies (van Genuchten and Nielsen, 1985) showed that the parametric expression proposed by van Genuchten (1980) is particularly suited to describe the WRC:

$$\theta(\psi) = \theta_r + \frac{\theta_s - \theta_r}{[1 + (\alpha|\psi|)^n]^{1-1/n}} \tag{3.1}$$

which can be also rewritten as:

$$S_e = [1 + (\alpha|\psi|)^n]^{1/n-1} \tag{3.2}$$

where $S_e = {}^{(\theta(\psi)-\theta_r)}/_{(\theta_s-\theta_r)}$ is called effective saturation, $\alpha > 0$ is related to the inverse of the air entry pressure head, and $n > 1$ and $m > 0$ are related to the pore-size distribution. The van Genuchten (1980) equation (3.1) has become a standard in numerical modeling of water transport in unsaturated porous media.

Similar to the water retention characteristic, the dependence of the hydraulic conductivity on water content, water saturation, or pressure head, is generally expressed by a simple parametric expression. Common to all expressions is the use of a scaling function, the so-called relative conductivity function, $K_r(\theta)$, applied to the saturated conductivity:

$$K(\theta) = K_s \cdot K_r(\theta) \tag{3.3}$$

Simple empirical expression for the $K(\theta)$ relation have been proposed, amongst others, by W. R. Gardner (1958), Brooks and Corey (1964), and by combining the van Genuchten (1980) and the Mualem (1976) models. The most frequently used are the exponential model (W. R. Gardner, 1958):

$$K(\theta) = K_s \cdot \exp(\alpha\psi) \tag{3.4}$$

the power function (Brooks and Corey, 1964):

$$K(\theta) = K_s \cdot S_e^{\beta} \tag{3.5}$$

or the van Genuchten/Mualem model:

$$K(\theta) = K_s \cdot S_e^{\delta} \left[1 - \left(1 - S_e^{n/n-1} \right)^{1-1/n} \right]^2 \tag{3.6}$$

where α and β are empirical coefficients, and δ is an empirical parameter called tortuosity factor.

3.2 Determining soil hydraulic properties

In general, soil hydraulic properties can be estimated with direct or indirect methods. Direct methods are based on flow experiments in the field or with soil samples in the laboratory, and rely on the observations of flow attributes,

such as water potential or water content. Indirect methods are used to estimate hydraulic properties from more easily measured data, often using regression or neural network algorithms. However, all the estimation procedures involved in the indirect methods need the result of direct measurements as benchmark for validation.

Measurements of soil hydraulic properties are useful for the following objectives:

1. Soil hydraulic properties are often needed for a hydraulic classification of soils, in a similar manner as the particle size distribution is used for a textural classification (indirect methods are often appropriate for this group).
2. Soil hydraulic properties are used in numerical simulation of water transport by Richards' equation. Estimation of water recharge through the vadose zone for water balance calculations is a classic application, but very important is its use for agricultural, ecological, and environmental purposes, such as irrigation control, fertilizer management, and contaminant fate modeling.
3. Accurate measurements are crucial to better understand the hydrological processes.

The demand on accuracy, resolution, precision, and reliability of the measurements is moderate for the first objective, while it is higher for the second and third ones. Especially for the third objective, the precision, reliability, and validity of measurements are of utmost importance, in order to avoid misinterpretations.

Determining soil hydraulic properties is a demanding procedure for numerous reasons. Soils are porous media with a three-dimensional arrangement of interconnected voids that form a highly complex pore system and the microscopic properties of the pore system determine the macroscopic hydraulic behavior. A complete knowledge of soil water flow requires a thorough understanding of processes on scales much smaller than the usual measurement scale and the ability to express effective hydraulic properties at scales much larger than the measurement scale (Durner and Lipsius, 2005).

A specific problem in the determination of soil hydraulic properties derives

from the difficulty in the control and validation of measurement results:

- The soil pore system is not a stable structure and the measurement process itself changes the system (Ghezzehei and Or, 2003), therefore, repetitive measurements on the same soil sample by different laboratories are impractical. Furthermore, the sampling process itself often causes severe disturbance, and undisturbed sampling is almost impossible.
- Different measurement methods use different sample volumes and sample numbers.
- Natural soils exhibit considerable temporal variability (Mapa et al., 1986; Ahuja et al., 1998; Leij et al., 2002), therefore measurements at the same site may yield different results if applied at different times (van Es et al., 1999).
- Soil pore system is affected by a variety of interacting biological, chemical, and physical processes which may change the macroscopic hydraulic behavior.

On this basis, the determination of the spatial variability of hydraulic properties is probably the greatest problem (Nielsen et al., 1973; Nielsen et al., 1986). In the following subsections a short account of both indirect and direct methodologies (separated in laboratory and field methods) for measuring the soil hydraulic properties is provided, with a particular focus on the techniques for in-situ estimation of the saturated hydraulic conductivity.

3.2.1 Indirect estimation of hydraulic functions

The difficulty of performing soil hydraulic measurements in laboratory or field is often used as incentive for developing indirect methods using widely available data. The general method is to define physical relations or find statistical correlations between predictors, such as soil texture, and soil hydraulic properties. Two main classes of indirect methods can be identified: semi-physical and empirical approaches.

Semi-physical models

Semi-physical methods recognize the shape similarity between the cumulative particle-size distribution and the water retention characteristic (Schaap, 2005). The Arya and Paris (1981) model uses information from j particle-size classes to estimate j pairs of water contents and pressure heads, assuming that the bulk density is the same for each class. Haverkamp and Parlange (1986) built a semi-physical model upon the assumption that the pore radius is linearly related to the particle radius. Combined with the capillary law that links pore size to capillary pressure, a retention characteristic curve can be derived from a cumulative particle-size distribution.

Empirical models

Empirical methods, often called pedotransfer functions (PTFs) after Bouma (1987), generally focus on simple statistical models to estimate hydraulic properties. Contrary to most physically based models, empirical methods often require limited – but easily accessible – input data such as sand, silt, or clay percentages and porosity, although more elaborate combinations of input data are also possible (Rawls et al., 1991; Wösten et al., 2001). Pedotransfer functions can be broadly classified in (Schaap, 2005):

- *Class PTFs:* provide hydraulic properties for particular soil classes. The advantages of class PTFs are their simplicity (essentially, they consist of simple tables) and modest requirements regarding input data. Only class information is necessary, thus enabling estimates of hydraulic properties from qualitative field data. Class PTFs for the 12 USDA textural classes were reported by Rawls et al. (1982), Rawls and Brakensiek (1985), and Schaap and Leij (1998), among others. Wösten et al. (1999) provided average van Genuchten (1980) retention and unsaturated conductivity parameters for 12 soil classes based on the FAO textural classification. A drawback of class PTFs is that discrete changes of hydraulic properties occur between two adjacent classes (e.g. loam to sandy loam, or topsoil to subsoil). Such changes may not always be realistic, especially for small-scale applications, instead continuous PTFs provide continuously varying estimates that may be more useful in such cases.

- *Continuous PTFs:* estimate parameters of retention or conductivity models, such as the Brooks and Corey (1964), Mualem (1976), and van Genuchten (1980) equations. Contrary to class PTFs, these models estimate hydraulic parameters that vary continuously with input data.

These are developed by examining the relationships between input data (e.g., textural properties or topographic variables) and soil hydraulic parameters that have to be predicted (e.g., retention curve or saturated hydraulic conductivity) from existing soil databases. Schaap et al. (2001) developed a neural network-based software named ROSETTA which allows to estimate the van Genuchten water retention parameters and the saturated hydraulic conductivity by applying five hierarchical PTFs generated with a large number of data obtained from three databases (Schaap and Leij, 1998). Wösten et al. (1999) developed a database of European soil properties (HYPRES) and used it to derive pedotransfer functions for water retention and saturated hydraulic conductivity. The use of large databases to develop pedotransfer function provides the ability of capturing a wide range of combinations and relationships among soil properties making the obtained PTFs applicable in different scenarios. However, it has been highlighted in multiple studies that PTFs available in literature are not always applicable with acceptable accuracy in regions other than those they were developed for (Tietje and Tapkenhinrichs, 1993; Kern, 1995; Cornelis et al., 2001; Wagner et al., 2001; Nemes et al., 2003). For this reason, attempts have been made to recalibrate published pedotransfer functions adjusting the parameters to soil conditions different from those used in the development phase (Abdelbaki, 2016).

3.2.2 Direct estimate of hydraulic functions by laboratory measurements

Laboratory methods have the advantage of being conducted in a controlled environment, however, they are subject to the limitation that inevitably some disturbances are introduced in manipulating the sample, even if "undisturbed" soil cores are taken. In addition, the measurements may be affected by hydraulic effects not present in the field (Muñoz-Carpena et al., 2002). Furthermore, Santos et al. (1999) pointed out the importance of in-situ methods to

obtain reference values against which laboratory methods should be tested.

Hydrostatic equilibrium methods

Hydrostatic equilibrium methods can be used to determine the WRC. Nimmo (2002) compiled a table with useful guidelines for the selection of the most appropriate method for a given purpose, considering aspects of sample size, measurement range, difficulty, duration, and cost. Examples of hydrostatic equilibrium methods are:

- *Hanging water column:* a sample is placed on a fine sand bed and suction is applied by moving a hanging water column below the sample level. After equilibrium, the water content ad the corresponding head are determined. The water column is then moved to derive a different couple of θ and ψ values.
- *Suction table:* the method is similar to the hanging water column, but instead of a water column, a controlled vacuum is applied to the water phase. Water contents are measured after equilibrium with different vacuum pressures.
- *Pressure plate extractor:* a sample is placed on a porous plate inside a pressure container. Air pressure is applied to the container, which induces displacement of water through the porous plate. After reaching equilibrium, water content is determined in relation to different air pressure values.
- *Centrifuge method:* an initially saturated sample is placed in a centrifuge and spinned with a specific velocity. After the centrifugal and capillary forces reach equilibrium the saturation can be determined. The pressure range depends on the applied velocity of the centrifuge.

Steady-state flux methods

Steady-state methods aim at obtaining the hydraulic conductivity at a particular saturation, by inversion of Darcy's law. The procedure is based on the assumption that the rate of flow is proportional to the pressure gradient.

Steady-state in water flow is reached by applying either constant head or constant flux boundary conditions at the top or the bottom of soil samples. A

flux boundary condition can be realized by drip irrigation, by spraying, or by pumping water via a porous plate onto the top of the sample. For methods that aim at the saturated hydraulic conductivity K_s, it is important that the flow resistance of the experimental device is kept smaller than the resistance of the soil because, considering that K_s is extremely dependent on continuous macropores along the flow direction, any change of soil structure (compaction, sealing of water entry surface) must be avoided. Examples of steady-state flux methods are:

- *Constant head permeameter:* water is applied by means of a Mariotte device at the top of a soil sample at a constant head, and K_s is calculated by equation (2.5) when a steady-state flux is reached. This method is often used as a benchmark for evaluating other methods (Reynolds et al., 2000).
- *Drip infiltrometer method:* the drip infiltrometer method (Dirksen, 1991) determines the hydraulic conductivity by infiltration. Typically, the soil sample is placed on a sand box with a hanging water column. Water is applied from a reservoir through needles at the top of a sample. Tensiometers are placed in the soil at different depths and the pressure head can be controlled by adjusting the height of a hanging water column. Measurements start after the steady-state is reached. By measuring the flux q and the pressure heads ψ, the unsaturated hydraulic conductivity $K(\psi)$ is calculated for each compartment between two tensiometers by Darcy's law.
- *Atomized water spray method:* water is delivered uniformly to the soil surface with a controlled atomized spray (Dirksen and Matula, 1994), with the advantage that large samples can be analyzed.
- *Disc infiltrometer method:* in the disc infiltrometer method (Šimůnek et al., 1999), water is applied at negative pressure using a tension disc, placed at the top of the sample. The soil profile is instrumented with both time domain reflectometry (TDR) probes and tensiometers, and the measured data are analyzed using Wooding (1968) analytical solution which requires steady-state infiltration rates at different supply pressure heads.

Transient methods

Transient methods are used to determine hydraulic conductivity or diffusivity, and since they do not require equilibrium, are much more rapid compared to the previous methods. Examples are:

- *Falling head permeameter:* is used to determine K_s for samples with low conductivity. The upper surface of the soil sample is connected to a water reservoir and, as water flows, the pressure difference between the upper and the lower level decreases. The saturated hydraulic conductivity is calculated by:

$$K_s = \frac{1}{(t_2 - t_1)} \frac{A_R L_S}{A_S} \ln\left(\frac{h_{w_2}}{h_{w_1}}\right) \tag{3.7}$$

  where A_R and A_S are the areas of the reservoir and the soil sample, respectively, L_S is the height of the soil sample, and h_{w_1} and h_{w_2} are the water depths at times t_1 and t_2, respectively, measured in the reservoir.
- *Continuous inflow/outflow method:* a soil sample is placed on a membrane plate in contact with a pressure-controlled reservoir. The reservoir headspace is controlled by air pressure manipulation to initiate water flow in the soil sample. Theoretically, both $\theta(\psi)$ and $K(\psi)$, up to the air-entry value of the membrane plate, including saturation can be measured.
- *Wind's evaporation method:* Wind's evaporation method (Wind, 1968) aims at determining simultaneously $\theta(\psi)$ and $K(\psi)$. Tensiometers are installed at regular depth intervals in a saturated soil sample. The sample is placed on a balance and its surface is exposed to free or forced evaporation. Weight and pressure heads are recorded periodically and after completing the experiment, the volumetric water content of the sample is determined, allowing to recalculate the total water contents during the experiment.
- *Hot-air method:* the hot-air method (Arya et al., 1975) determines the diffusivity $D(\theta)$. Hot air is blown over the surface of an initially uniformly wet soil column. After the evaporation is stopped,the sample is cut in layers and θ is measured in each layer. The diffusivity can be

caluclated from:

$$D(\theta) = \frac{1}{2t} \left.\frac{\mathrm{d}x}{\mathrm{d}\theta}\right|_x \int_{\theta_x}^{\theta_i} x \mathrm{d}\theta \tag{3.8}$$

where t is the time, θ_i is the initial water content, and θ_x is the water content at distance x from the evaporating surface.

3.2.3 Direct estimate of hydraulic functions by field measurements

Laboratory experiments have the advantage of being comparatively quick and precise, but they often lead to soil physical properties that are not representative for the field situation. Direct in-situ measurements of hydraulic and retention properties still provide perhaps the most reliable approach for determining hydraulic properties, despite their high cost and extreme time demands (Tseng and Jury, 1993). Two distinct types of field procedures are in common use: internal drainage flux method and infiltration methods. Infiltration methods can be further distinguished in ponded infiltration methods, tension infiltration methods and infiltration from wells or bore holes.

Field methods have the advantage of dealing with soil in natural conditions. However, small-scale heterogeneity in soil conditions may introduce large variation in measured values (Muñoz-Carpena et al., 2002). Since most field measurements are confined to produce a single measurement at a single field location, adequate evaluation of field hydraulic properties requires a large number of measurements.

3.2.3.1 Internal drainage method

The internal drainage method is regarded as a reference method to measure in-situ unsaturated hydraulic properties for both homogeneous and layered soils (Hillel et al., 1972). In the method, large rings, of about 2 m in diameter, are inserted into the soil. Within each ring, tensiometers and TDR probes are installed, and water is ponded on the soil surface until the soil is wetted beyond the maximum depth for which the determinations are desired. Both θ and ψ are monitored for weeks. Because θ and ψ determination is needed

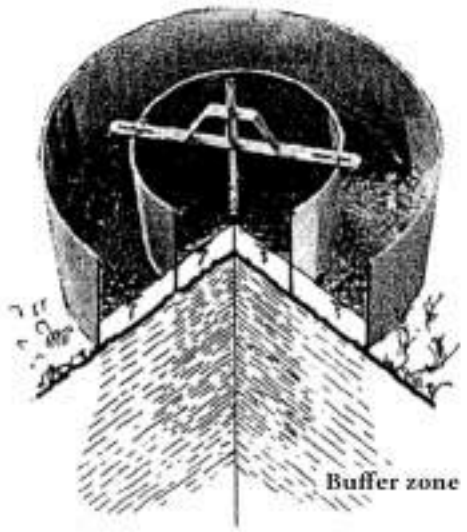

Figure 3.1 - Double-ring infiltrometer. Buffer zone due to infiltration below the outer ring.

over a long period of time, the method is particularly time- and equipment-intensive, and thus costly, especially if several sites must be monitored to estimate spatial variability.

3.2.3.2 Infiltration methods

Ponded infiltration methods

Ring infiltrometers are probably the most widely used device for measuring field infiltration rates (Wu et al., 1997), and the technique is useful in the estimation of the in-situ field saturated hydraulic conductivity. Since the single-ring infiltrometer leads to estimates of the infiltration rate that decrease as the ring diameter increase (Marshall and Stirk, 1950), the double-ring infiltrometer (DRI) was designed with two concentric rings of different dimensions in order to enable the formation of a buffer area that minimizes lateral flow from the inner ring (Figure 3.1). This allows to reduce the measurement error and to consider the infiltration process as 1D.

A few studies have been conducted on how the size of the DRIs affects the measurements. Swartzendruber and Olson (1961a,b) conducted a series of double-ring infiltration experiments with different sizes of outer rings. They found that the effect of the outer ring (buffer) brings the infiltration

velocity close to the one-dimensional infiltration rate, and the measurements error due to lateral flow becomes negligible as the diameter of the outer ring increases to 120 cm with an inner ring diameter of 100 cm. Ahuja et al. (1976) reported that when an outer ring of 90 cm diameter was used with an inner ring of 30 cm diameter, the lateral flow was almost eliminated. Furthermore, he reported that even when an outer ring of 60 cm diameter was used, the effect of lateral flow on the final infiltration rate was negligible. In the present work a set-up of diameters equal to 30 cm and 60 cm for the inner and outer ring, respectively, was chosen.

The infiltration rate is the velocity at which water enters the soil. At early times, when the soil is far from saturation, the infiltration rate is usually high because the process is driven by capillary forces. However, when the soil reaches saturation, the water seepage is only due to the gravitational force and the infiltration rate reduces down to a constant value. The infiltration rate in unsaturated conditions below the double-ring infiltrometer can be represented by the following equation, valid for 1D flow:

$$q = -K\frac{\psi - z - h_w}{z} \tag{3.9}$$

where h_w is the water depth inside the inner ring. For an homogeneous soil, when $t \to \infty$, equation (2.5) can be applied.

The technique consists of pushing the two concentric steel rings about 10 cm into the ground and pouring water inside them until the water level equalizes in the two rings. The reduction of the inner ring water level due to infiltration is recorded at regular time steps, and the measurement ends when steady state of the infiltration is detected. Measurements can be influenced by the water level inside the two rings. For example, if the water depth in the outer ring is higher as compared to the inner ring, the difference in hydraulic head between the two water surfaces can generate a water flow from the outer towards the inner ring (Figure 3.2), which could produce a reduction of the recorded infiltration rate or even a change of sign. It is thus fundamental to maintain the same water level inside the two rings.

In order to be able to determine K_s, a steady infiltration rate must be detected which means that DRI measurements should last at least three or four hours.

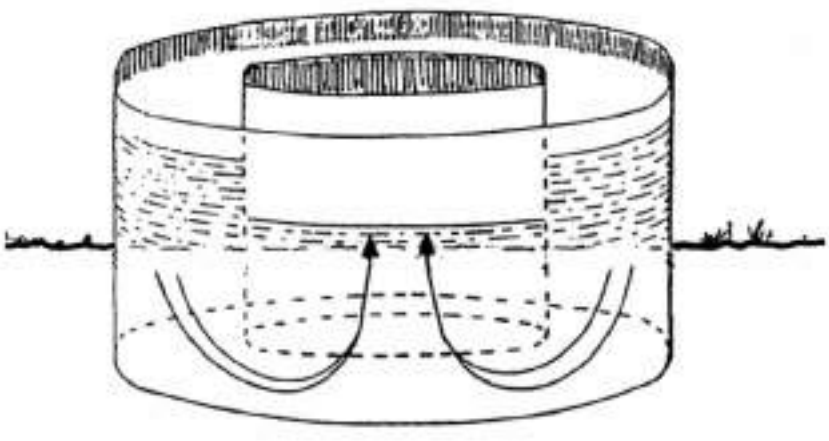

Figure 3.2 - Incorrect water flow from the outer towards the inner ring due to different water levels inside the instrument.

Tension disc infiltration

A tension disc infiltrometer is a constant head infiltrometer that can operate at either a positive or a negative head and thus it can be used for determination of both saturated and unsaturated hydraulic properties. While ponded infiltration is used to determine K_s, tension infiltrometer also provides an opportunity to estimate unsaturated hydraulic properties.

The CSIRO disc permeameter was designed by Perroux and White (1988), as an evolution of the "sorptivity tube" by Clothier and White (1981). Figure 3.3 shows the configuration for the application of a water potential at the surface $\psi_0 > 0$ (ponded infiltration). The supply pressure is the distance between the air bubble exit point and the soil surface, and is selected by adjusting the three level-adjustment screws. The egress of water from the reservoir and air-entry side-tube before the initiation of flow is prevented by fine stainless steel meshes at the bottom of the reservoir and side tube. The air-entry side-tube initially contains water whose volume is adjusted approximately equal to the volume between the permeameter head and the soil surface. This water is rapidly deposited on the soil surface by opening the side-tube stopcock to start infiltration.

To install the permeameter, a thin-walled metal ring, with a 20 cm diameter, is partly inserted into the soil and any disturbed soil around the perimeter is

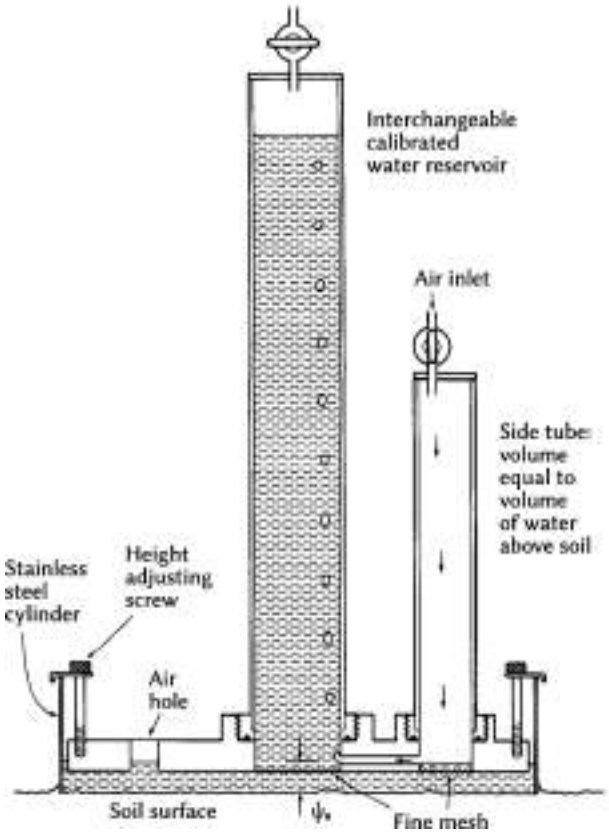

Figure 3.3 - CSIRO tension disc permeameter for supplying water at positive pressures. The volume of the side-tube is equal to the volume between the soil surface and the permeameter, and it is supplied to the surface at the beginning of infiltration.

pressed down. The distance from the top of the ring to the soil is adjusted to contain the selected head of water and the permeameter. No contact material is necessary here. The empty permeameter is placed on the ring and the adjustment screws are altered to give the required ψ_0. The permeameter, as well as the air-entry side-tube, is filled of water, being careful that both stopcocks are closed. The infiltration begins after the side-tube stopcock is opened allowing the side-tube water volume to be rapidly deposited over the soil. Infiltrated volumes are recorded as a function of time.

The estimate of K_s relies upon the measurement of the steady volumetric flow rate q_0 at successive time-steps. This is linked to K_s by the following

equation (Wooding, 1968; White and Sully, 1987):

$$q_0 = \pi r_0 K_s + 4 r_0 \frac{b S_0^2}{\theta_s - \theta_i} \tag{3.10}$$

where $S_0 = S(\psi_0)$, r_0 is the disc radius, and b is a dimensionless constant, equal to 0.55 for natural soils.

The value of sorptivity S_0 can be evaluated at early times using:

$$\lim_{t \to 0} \frac{\mathrm{d}F}{\mathrm{d}t^{-1/2}} = S_0 \tag{3.11}$$

For one-dimensional infiltration Philip (1969) argued that capillarity should dominate the infiltration process for $t < t_{grav}$, with t_{grav} the time when gravity force begins to influence the one-dimensional flow. White and Sully (1987) found that, in the field, t_{grav} varies between 0.08 and 34 h, therefore the linearity of $F\, t^{-1/2}$ implied by equation (3.11) is expected to hold for as little as 6 s to as long as at least 2450 s. According to Perroux and White (1988) linearity is usually found for at least 60 s.

Infiltration from wells and bore holes

Tension disc and ring infiltrometer are constrained to the near-surface and are easily influenced by microtopography. These limitations can be partly overcome by infiltration from bore holes.

The Guelph permeameter is a constant head well permeameter used to measure in-situ hydraulic conductivity, employing the Mariotte principle. Flow from the permeameter is assumed to reach a steady-state after a transient state during which the soil saturated bulb and the wetting zone increase in size by moving quasi-spherically from the infiltration surface (Figure 3.4). At the steady-state, the saturation bulb remains constant in size while the wetting front continues to increase (Reynolds and Erlick, 1985). The constant head level in the well hole is established and maintained by regulating the position of the air tube, which is located in the center of the permeameter reservoir. As the water level in the reservoir falls, a vacuum is created in the air space above the water. The vacuum can only be relieved when air of ambient atmosphere pressure, which enters at the top of the air tube, bubbles

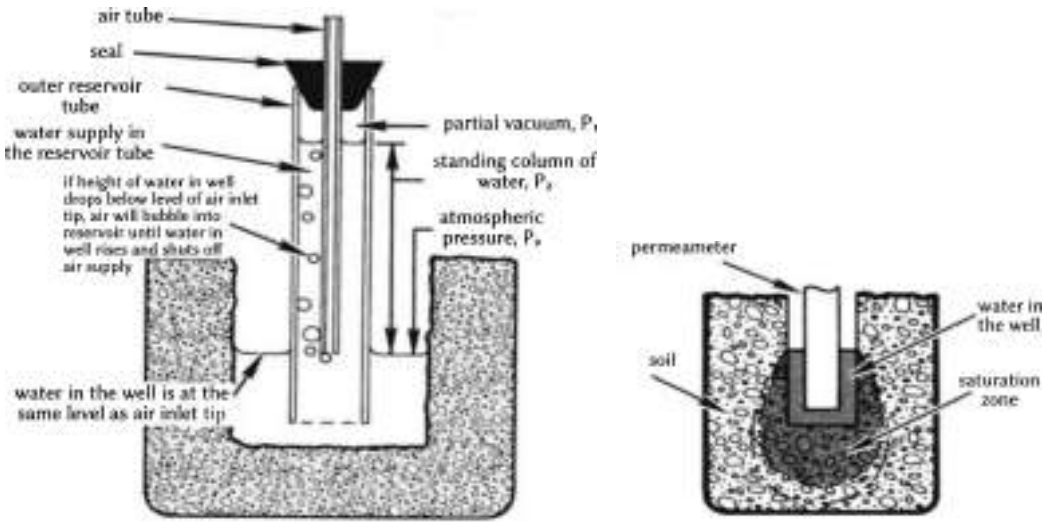

Figure 3.4 - GUELPH permeameter: (a) in-hole constant-head permeameter and (b) saturated zone around borehole, i.e. saturation bulb.

out of the air inlet tip and rises to the top of the reservoir. Whenever the water level in the well begins to drop below the air inlet tip, air bubbles emerge from the tip and rise into the reservoir air space. The vacuum is then partially relieved and water from the reservoir reintegrates water in the well. The whole process is controlled by the Mariotte principle:

$$P_0 = P_1 + P_2 \tag{3.12}$$

where P_0 is the atmospheric pressure at the water surface inside the well hole, P_1 is the negative pressure inside the reservoir, and P_2 is the positive pressure associated to the column of water. The outflow of water from the well at steady-state can be measured by observing the water level reduction inside the reservoir. The rate of this constant outflow of water, together with the diameter of the well, and height of water in the well can be used to accurately determine the field saturated hydraulic conductivity. The experiment has to be repeated two times using two different water heads of 5 and 10 cm in order to estimate K_s through the analytical solution given by Reynolds and Erlick (1985).

3.2.4 Measurement of soil water content

The measurement of soil water content has undergone revolutionary advancements in the last 20 years. From having gravimetric sampling and neutron moderation as the primary field methods in the early 1980s, we now have numerous options, such as time domain reflectometry (TDR), capacitance (and impedance) devices, ground penetrating radar (GPR), airborne/satellite active radar, and passive microwave methods (Topp and Ferré, 2005). These five newer methods are all based on electromagnetic (EM) measurements.

The unique electrical properties of water, both pure and in the soil, form the basis of indirect electromagnetic water content measurements in soil. The relative dielectric permittivity of water, approximately equal to 80, is generally more than an order of magnitude larger than that of other soil components (1 for air and between 3 and 5 for soils). As a result, the bulk dielectric permittivity of a soil was found to be a function of the volumetric water content, with only a slight dependence on the volume fraction of solids and electrical conductivity (Topp et al., 1980). The velocity of propagation, v, of an EM wave is defined as (Von Hippel, 1954):

$$v \approx \frac{c}{\sqrt{\varepsilon_{ra}}} \tag{3.13}$$

where c is the velocity of light in free space and ε_{ra} is the apparent relative permittivity of the medium. The volumetric water content can be derived applying, for example, the relationship derived by (Topp and Reynolds, 1998):

$$\theta = 0.155\sqrt{\varepsilon_{ra}} - 0.176 \tag{3.14}$$

Time domain reflectometry probes

Over the past 30 years, the TDR has been used to measure water content at many scales and under a broad range of conditions (Topp and Reynolds, 1998; Robinson et al., 2003) and has become a standard method of water content measurement. Most TDR instruments (Figure 3.5a) launch a fast rise voltage step along a transmission line (probe) buried in the soil or the medium of interest. The voltage pulse propagates as a planar EM wave, traveling in the

soil and guided by the probe. The measured v is used into equations (3.13) and (3.14) to give the soil volumetric water content through which the EM wave has propagated. The configuration of the probe determines the extent and shape of the measured soil sample.

Capacitance measurements

Capacitance devices (Figure 3.5b) determine the apparent capacitance of a probe placed in or near a soil (Paltineanu and Starr, 1997; C. M. K. Gardner et al., 1998). The capacitance probe (along with the soil) forms part of an inductance-capacitance resonant circuit with a specific frequency that depends upon the water content of the soil near the probe.

Ground penetrating radars

The GPR is a geophysical method that uses electromagnetic signals that propagate as waves to map the subsurface structure. Typical wave penetration would be 1 to 3 m in silty sands and non-saline clays while low frequency GPR waves can penetrate tens of meters in dry, non-saline sandy soils (Topp and Ferré, 2005). A GPR transmitter and receiver (Figure 3.5c) are placed on the ground surface to minimize any effect of above-ground features, and then are moved to obtain images of soil interfaces in the soil or localized objects. As with the TDR, the primary information used for water content estimates is the velocity of the signal, and equations (3.13) and (3.14) can be used to relate this velocity to the volumetric water content. Unlike TDR, the EM wave transmitted from a GPR signal travels unguided through the medium. Therefore, the traversed path length must be defined in order to translate the recorded pulse travel times to velocities. To define the path length, either discreet buried targets (e.g., buried pipes) or flat surfaces (e.g., a water table) can be used if their depth is known. The resulting water content from this method is a linear weighted average of the water contents along the travel path of the wave (Huisman et al., 2003).

(a) (b) (c)

Figure 3.5 - Instruments for soil water content measurement: (a) a two-rods TDR probe, (b) a capacitive probe, and (c) a GPR set-up.

Active microwave remote sensing

Active microwave remote sensing (radar) is similar in principle to air-launched surface reflection GPR that can be mounted on either airborne or space-borne platforms. Synthetic Aperture Radars (SARs) in the 1 to 10 GHz frequency range are most commonly used for soil water content estimation (Boisvert et al., 1996). A microwave pulse is generated by a transmitter, and this signal is directed towards the ground target via a transmitting antenna. The backscattered signal travels back to the radar receiving antenna. A receiver then amplifies the signal, which is processed electronically to provide the transmission time, signal amplitude and signal phase. The transmission time to and from the target is used to determine the range or distance to the target. The relative permittivity of the soil surface is the primary factor determining the strength of the signal returned to the sensor from the target. Using current approaches, soil water measurements from SAR are limited to surfaces without significant vegetation cover and to a depth which ranges from 1 to 10 cm.

Passive microwave remote sensing

In the passive microwave method, the ground surface is the source of the EM signal. This signal is detected and interpreted for estimation of water content. This method measures the natural thermal emission of the land

surface using very sensitive detectors that are tuned to specific frequency bands in the microwave region (Jackson, 1993). Interpretations are made as follows: (i) normalize brightness temperature to emissivity; (ii) remove effects of vegetation; (iii) account for surface roughness effects; (iv) relate emissivity to relative permittivity; and, finally, (v) convert relative permittivity to water content using an equation similar to equation (3.14).

3.2.5 Measurement of water potential

Soil water potential reflects the energy state of water in porous media and thus drives movement of water. The water potential is commonly measured as pressure head, with units of water column length (m). The lack of single measurement technology, covering the entire energy range of interest from moist to dry conditions, presents a challenge to the measurement of soil water potential. Tensiometry, which is an accurate and widely used technique to determine soil water (matric) potential, requires extensive maintenance and is restricted to relatively wet conditions (Durner and Or, 2005). Other instruments for water potential measurement measure are heat dissipation sensors (HDS), gypsum blocks, granular matrix sensors, or filter paper. At the dry end of the moisture range, thermocouple psychrometers, which use equilibrium water vapor pressure (relative humidity) in soil air, are often used.

Tensiometers

Tensiometers are probably the most widely used measurement technology for soil water potential and are particularly suited for the measurement of soil water energy status at high water contents.

A water-filled reservoir, connected to a pressure-sensing element (transducer), is brought into contact with the soil through a rigid porous membrane, which is permeable for water and impermeable for air (usually a porous ceramic cup). When the matric potential of the soil is lower (more negative) than in the tensiometer water from the tensiometer is attracted by the surrounding porous media, thereby creating suction sensed by the pressure gauge. Water flows until equilibrium is reached and the suction inside the tensiometer equals the soil matric potential.

Gypsum blocks

The method is based on measuring water content or water content-related properties in well-characterized reference porous media that are in hydrostatic equilibrium with the surrounding soil. Classic porous reference materials are blocks of gypsum, fiberglass, or nylon. Recently, granular matrix sensors, which consist of gypsum wafers embedded in granular matrix (Scanlon et al., 2002), have been realized. The relationship between water content and water potential of the sensor needs to be initially calibrated and subsequently it can be used to infer the matric head of the surrounding soil.

Heat dissipation sensors

Similar to gypsum blocks and granular matrix sensors, HDSs infer water potential by measuring a water content–dependent property in a porous medium which is in hydraulic equilibrium with the surrounding soil. A HDS consists of a heating element and a thermocouple embedded within a porous ceramic matrix. The measurement is based on the rate of temperature rise recorded at a line heat source embedded in the ceramic. The rate of heat dissipation in a porous medium is dependent on specific heat capacity, thermal conductivity, and density. Since these properties are greatly affected by the water content, heat dissipation can be related by a calibration relation to water potential.

Chapter 4

Case study

In order to address the multiple objectives of this investigation, measurements of saturated hydraulic conductivity were performed at three experimental systems. The assessment of the reliability of different measurement techniques for in-situ estimation of K_s through rainfall-runoff experiments (work objective 1) required a highly controlled experimental system in order to monitor all the quantities in play. Therefore, measurements with DRI, CSIRO-TP (CTP) and GUELPH-CHP (GP) were performed at both the laboratory and the field experimental systems located at the University of Perugia, Italy. On the other hand, to understand the controls of K_s spatial variability in an agricultural setting and the confidence related to the estimation of the areal average value of K_s for different land uses, plot areas and sample sizes (work objective 2), measurements carried out with DRIs at the Hydrological Open-Air Laboratory (HOAL) located in Petzenkirchen, Austria, were employed. The same observations were also used to generate continuous maps of $\bar{K}_s$ for the HOAL catchment by means of two developed pedotransfer functions (work objectives 3 and 4).

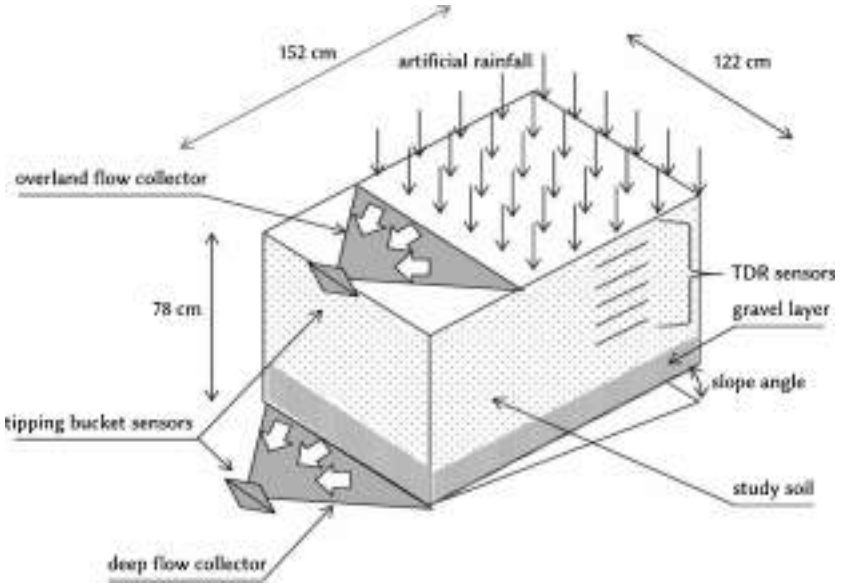

Figure 4.1 - Laboratory physical model with adjustable slope angle. The sensors for surface and deep flow as well as the probes for soil moisture content measurements by TDR method are also indicated.

4.1 Study area

4.1.1 Laboratory system

The basic element of the laboratory system consists of a physical model (Figure 4.1) realized by a tank filled with homogeneous soil 152 cm long, 122 cm wide, and 78 cm deep, which can be adjusted with a slope gradient, γ, ranging from 1° to a maximum of 15°. The lateral and lower boundaries of the tank are not permeable. Transparent walls are used to observe the wetting front evolution during infiltration experiments.

Rainfall is artificially produced by a generator (Figure 4.2a) consisting of sprinklers (Spraying Systems Co.) of water under pressure supplied by a pump. Raindrops of average and maximum diameter (1 mm and <1.5 mm, respectively) significantly lower than those observed in natural rainfalls (Poesen, 1984) were generated. A proper choice of the sprinkler combined with an adjustment of the water pressure enables us to obtain a specific rainfall rate of interest, with values up to about 50 mm h^{-1}. Before the beginning of each experiment the average value of rainfall rate is determined through a

(a) (b) (c)

Figure 4.2 - Generator of artificial rainfall: (a) water sprinklers; (b) and (c) water pressurization system.

sheet-metal pan placed on the tank. It catches the rainfall over the soil surface that generates a water flow measured at the outlet. Moreover, the spatial distribution of rainfall rate is also checked in advance by a grid of pans placed over the sheet-metal. For each sprinkler the rain rate spatial distribution is almost uniform.

Surface runoff and percolated water are measured by two tipping bucket sensors that provide continuous data of the flow collected by two triangular metal elements. Deep flow is collected at the downstream boundary of the core, while surface flow is collected at the outlet of the soil surface exposed to rainfall during the experiments. Previous studies (Essig et al., 2009; Morbidelli et al., 2015, 2016) confirmed that the downstream boundary of the tank does not produce significant changes in the hydrographs of surface and deep flow.

The water content profile is monitored using a time domain reflectometry (TDR) device (TRASE-BE, Soil Moisture Equipment Corp., Goleta, CA, USA). Up to five buriable three-rod waveguides with wire-to-wire spacing of 1.25 cm and length 8 cm are inserted horizontally at different depths (Figure 4.1), taking care that the metal rods are in close contact with soil. Each probe provides measurements of soil moisture associated with the corresponding depth, but in any case the zone of influence is a small soil volume around itself. Zegelin et al. (1989) showed that three-wire probes embedded horizontally in a field

profile during a rainfall event can be used to follow the wetting front and water redistribution, as well as to estimate the amount of infiltrated water with error less than 10 %.

The porous medium for the experiments is taken from a natural fine-textured soil divided into different diameter classes, after removing stones and roots. Then, by recombining fixed quantities of material of each class a homogeneous bare soil layer of 67 cm is obtained. A gravel layer with a depth of 7 cm is set at the bottom of the soil tank in order to speed up the outflow of percolated water. Some soils selected on the basis of the USDA soil classification are used for the laboratory experiments. These soils, characterized by saturated hydraulic K_s less than the maximum rainfall rate, r, available from the artificial rainfall generator, enable us to perform experiments in a range of r/K_s values that is sufficiently wide for investigating the main aspects of the infiltration process.

4.1.2 Field experimental system

The field experimental system is located in Perugia, central Italy, in a hilly area of about 1 ha, with an altitude of 328 m a.s.l., near the Civil and Environmental Engineering Department of Perugia University. It consists of two data assimilation areas (Figure 4.3). The first one is equipped with a hydro-meteorological station including sensors of rainfall rate, wind speed and direction, solar radiation, air temperature and relative humidity, all operative 2 m above the soil surface with time resolution of 5 minutes, and a Class A evaporation pan (Figure 4.4). The second one is composed of two 9×9 m plots characterized by a loam (naturally-vegetated surface) and silt loam (bare surface) soils according to the USDA soil classification (Linsley et al., 1992) and consists of:

- TDR sensors for continuous measurements of soil moisture content and tipping bucket sensors for surface, intermediate, and deep flows (Figure 4.5);
- an artificial rainfall generator (Figure 4.6) including appropriate sprinklers (Spraying Systems Co.) of water under pressure. The rainfall was almost spatially uniform, as checked in advance by a grid of pans and is

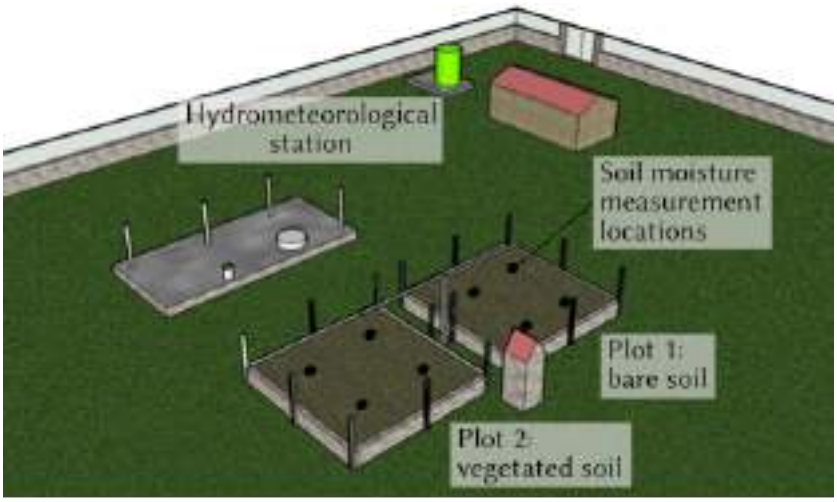

Figure 4.3 - Schematic representation of the field experimental system.

characterized by drops of average and maximum diameter of 1 mm and <1.5 mm, respectively.

The bare-surface plot was artificially created starting from a natural soil that was subsequently divided into different diameters classes and then properly meshed to obtain a silt loam soil, in the absence of stones and roots. The material was carefully packed to a thickness of 70 cm and placed on an underlying drainage layer with thickness of 10 cm to allow air to escape freely. The heterogeneity of the soil hydraulic properties was expected to be somewhat more pronounced than in the laboratory soil because differences in soil packing become more significant with increasing the spatial scale and cannot be totally eliminated. The plot is laterally bounded to avoid lateral water fluxes and the main soil hydraulic properties were earlier deduced under natural rainfall events by Morbidelli et al. (2011, 2014). In this study, based on the use of artificial rainfall, the saturated soil water content was updated to the maximum observed value.

Four vertical profiles of soil moisture were monitored by TDR equipment (TRASE-BE, Soil Moisture Equipment Corp., Goleta, CA, USA) with four buriable three-rod waveguides of length 20 cm inserted horizontally at 5, 15, 25, and 35 cm depths below the soil surface. The system as a whole enables us to investigate the movement of the wetting front during infiltration,

Figure 4.4 - Hydro-meteorological station located at the field experimental system.

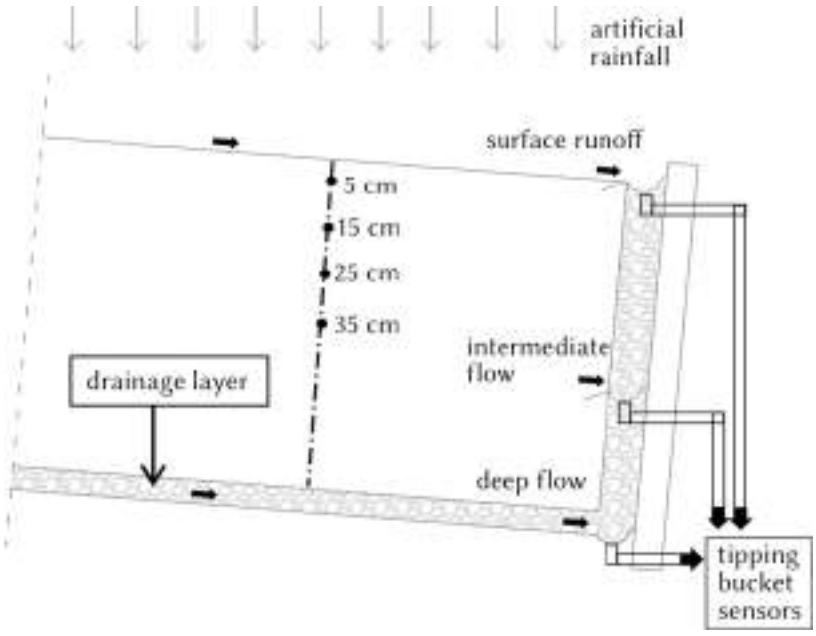

Figure 4.5 - Vertical section of the experimental plot with soil water content measurements at different depths and surface, intermediate, and deep flow collectors.

Figure 4.6 - Artificial rainfall generator of the field experimental system.

redistribution, and reinfiltration periods. Data from the probes were collected at intervals of 30 minutes, and the universal calibration curve of Topp et al. (1980) was used to calculate soil moisture content from the TDR signal.

Surface, intermediate (at about 40 cm depth), and deep (at 70 cm depth) flows were measured with time resolution of 5 minutes by three tipping bucket systems.

4.1.3 Hydrological Open-Air Laboratory (HOAL)

The HOAL catchment (Figure 4.7) is located in Petzenkirchen, in the western part of Lower Austria, close to the Institute for Land and Water Management Research. The natural surface water outlet of the catchment is the Seitengraben stream, which exhibits a mean annual flow of $4.1\,\mathrm{l\,s^{-1}}$. The stream receives inflow from twelve inlets which include two erosion gullies, five tile drains, two springs, two tributaries from wetlands and the piped inlet stream. The basin has an elevation that ranges from 268 to 323 m a.s.l., an area of $0.66\,\mathrm{km^2}$, and a mean slope of 8 %. Most of the catchment surface is arable land (87 %), while the rest is forested (6 %), paved (2 %) or used as

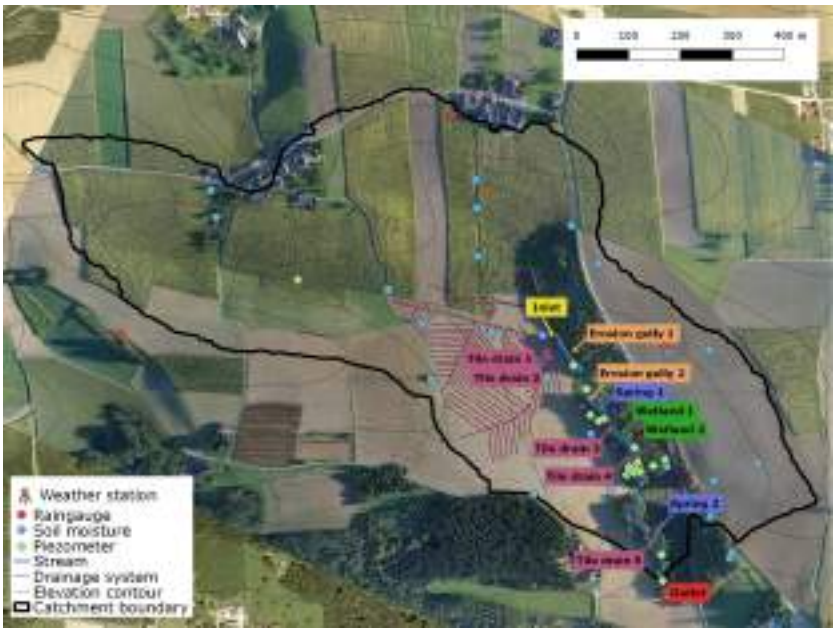

Figure 4.7 - Map of the HOAL catchment, Petzenkirchen, Austria.

pasture (5 %). The climate can be characterized as humid with a mean annual temperature of 9.5 °C and a mean annual precipitation of 823 mm yr^{-1} from 1990 to 2014 (Blöschl et al., 2016). Due to shallow, low permeable soils and the use of the catchment area as agricultural land, the concave part of the catchment was tile drained in the 1940s to reduce water logging (purple lines in Figure 4.7). The estimated drainage area from the tile drains is about 15 % of the total catchment. The pipes drain into the main stream at four locations: two tile drain systems, tile drain 3 and 4, do not dry out during the year, while two are ephemeral, tile drain 1 and 2 (Figure 4.7). The uppermost 25 % of the stream was piped in the 1940s to enlarge the agricultural production area, and the pipe enters the main stream at inlet. There are two clearly visible springs that directly discharge into the stream, spring 1 is perennial, while spring 2 is not. In the south-eastern part of the catchment is a small wetland close to the stream which permanently seeps into the stream via two rivulets (wetland 1 and 2). The wetland is fed by springs at the upper part of the wetland and usually responds very quickly to all types of rainfall due to its high saturation state.

During low-intensity events in summer, the flow in the main stream

responds to rainfall with substantial delay as the soil usually offers a lot of storage capacity, depending on soil moisture. During major storms, saturation overland flow occurs across the fields (mainly in the depression areas along the talweg and close to the stream) and enters the stream at two locations (erosion gullies 1 and 2). During high-intensity thunderstorms in summer and spring, infiltration excess overland flow tends to occur with a very substantial, fast contribution from the tile drainage system. During infiltration excess overland flow events, all forms of erosion from interrill to gully erosion may occur on the fields that are poorly covered by crops (such as after soil management). During very dry periods in summer, the high clay contents causes shrinking cracks which act as macropores for re-infiltration during subsequent events. In winter, rain-on-snow runoff may occur as saturation overland flow during large events and even minor events will lead to a significant increase in streamflow due to high soil moisture contents.

A basic monitoring infrastructure was installed in the catchment. All of the instruments are operated at a temporal resolution of 1 min with the exception of the piezometers, where groundwater levels are recorded at temporal resolutions of 5 to 30 min. Four raingauges (red dots in Figure 4.7) were strategically placed to monitor spatial rainfall patterns. The weather station, located approximately in the center of gravity of the catchment, monitos air temperature, air humidity, wind speed and direction (all at three heights), incoming and outgoing solar and long-wave radiation, raindrop size distribution, snow depths, soil heat flux and soil temperatures at different depths. A total of 12 flumes were installed to monitor discharge at 1 min resolution from the inlet piped stream, tile drains, erosion gullies, springs, tributaries from wetlands and from the outlet of the catchment. A total of 23 piezometers (green dots in Figure 4.7) were installed to monitor groundwater level and water temperature.

The HOAL catchment is also provided with a dedicated monitoring infrastructure. Eddy-correlation stations were placed to understand the spatial distribution of land-atmosphere interactions. A soil moisture monitoring network (cyan dots in Figure 4.7) was set up, and TDR sensors were installed at four depths below ground surface. Due to agricultural manipulation of the fields, 11 stations are temporary and are removed and replaced once or

twice a year, while 20 stations, installed on pasture lands, are permanent. To understand the dynamics of nutrients such as phosphorus and nitrogen and their compounds, a water quality monitoring network was installed at the tributaries within the HOAL. The above-mentioned flumes were equipped with in-situ sensors for electrical conductivity, temperature, turbidity, pH, nitrate and chloride with sampling intervals of 1 min.

Winter wheat, winter barley, maize, rapeseed and soy are the main types of crop cultivated in the catchment. Crop rotation is associated with green manure in order to ensure natural fertilization of the soil. However, nitrogen fertilizers and natural fertilizers, e.g. pig manure, are also applied before sowing, as well as plant protection agents, such as plant growth regulators, fungicides and broad-spectrum insecticides. The harvest of the winter crops usually occurs in July, while tillage and seedbed preparation are usually scheduled in late-August or September.

A soil survey campaign of 300 cores, sampled on the nodes of a 50×50 m grid (Figure 4.8 light-grey squares), allowed to map the textural composition of the catchment soil, providing information about organic matter content (*om*), clay (*cl*), silt (*si*), and sand (*sa*) percentages at multiple depths. According to the USDA soil classification, the topsoil of the catchment is constituted of silty loam for 75 %, silty clay loam for 20 %, and silt for 5 %. Furthermore, a high-resolution digital terrain model (DTM) was used to derive elevation (*el*) and local slope angles (*s*) across the catchment. Table 4.1 summarizes the information available in the 300 nodes of the grid.

4.2 Saturated hydraulic conductivity data

Three devices for local measurement of K_s were used on both the laboratory and the field experimental systems: a DRI, a CSIRO tension infiltrometer and a GUELPH permeameter.

Three measurements with each device were carried out in three different locations of the laboratory system and the results are reported in Table 4.2.

The same instruments were used to perform single point measurements of K_s in nine sub-areas of the field experimental system (Figure 4.9), identified using a 3×3 m grid, and the results are reported in Table 4.3.

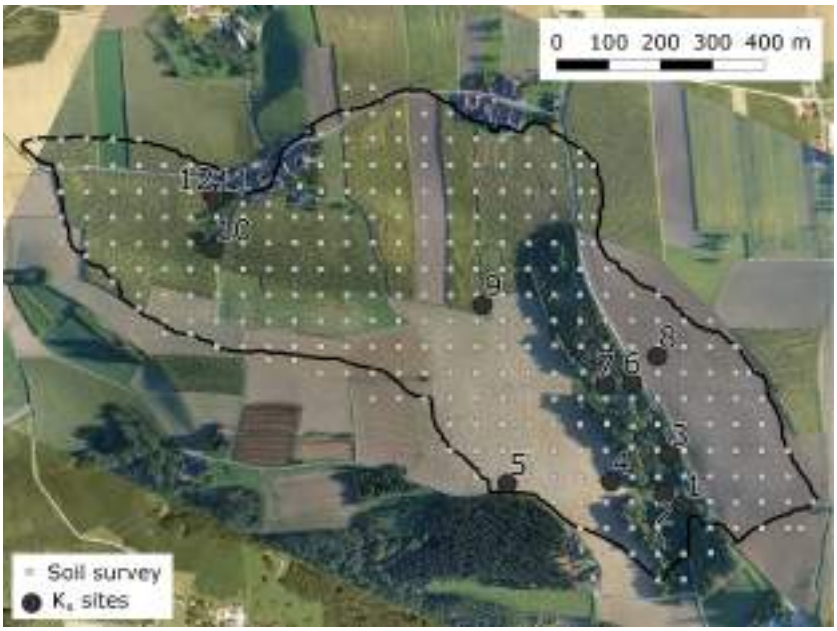

Figure 4.8 - HOAL catchment. Plots where DRI measurements were performed (dark-grey circles) and soil survey campaign locations (light-grey squares).

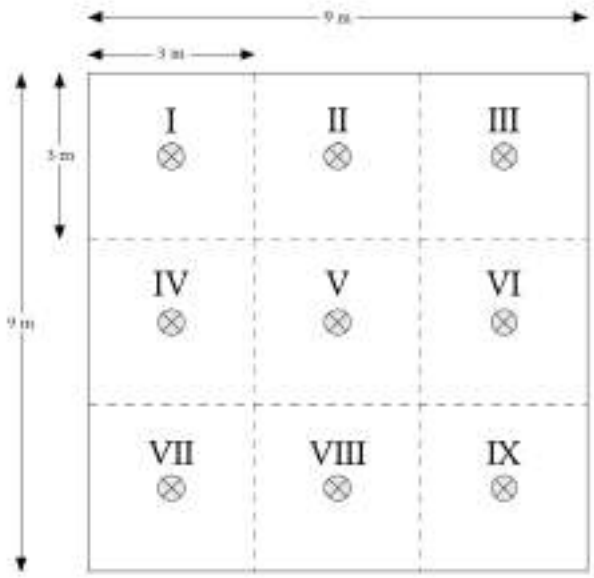

Figure 4.9 - Locations of in-situ measurements of saturated hydraulic conductivity (numbered from I to IX) in the field experimental plot.

Table 4.1 - General statistics of the data available in the 300 nodes of the grid of Figure 4.8. Min = minimum value; Max = maximum value; Mean = arithmetic mean; *CV* = coefficient of variation; *om* = organic matter content; *cl* = clay content; *si* = silt content; *sa* = sand content; *s* = slope angle; *el* = elevation.

Statistics	*om* (%)	*cl* (%)	*si* (%)	*sa* (%)	*s* (°)	*el* (m a.s.l.)
Min	0.5	6.6	48.6	3.4	0.5	257.6
Max	8.4	39.7	87.6	26.8	27.7	324.6
Mean	2.2	21.8	70.7	7.4	5.9	291.7
St.dev.	0.7	6.4	6.8	2.5	4.0	14.4
CV (%)	33.1	29.2	9.7	34.2	68.0	4.9

Table 4.2 - Saturated hydraulic conductivity, K_s (mm h^{-1}), of the laboratory soil estimated through different point measurement techniques. Mean = arithmetic mean.

Measurement	DRI	CTP	GP
I	15.0	11.6	39.0
II	15.0	6.1	13.7
III	15.0	23.1	3.8
Mean	15.0	13.6	18.8

Saturated hydraulic conductivity measurements were also performed at the HOAL catchment. A total of 131 locations, on 12 different plots, were chosen to sample K_s (dark-grey dots in Figure 4.8). The measurements were performed between March and September 2017 with the objective of evenly exploring both the grassland areas and the areas devoted to agricultural practices. However, due to restricted access to the cultivated areas during the crop growing season and tillage operations, the measurement campaign in those parts of the catchment was limited to the period between harvest and tillage, i.e. between July and September.

Among the available measurement techniques, double-ring infiltrometers were chosen because of the ease of installation and robustness in natural environments where tall grass, surface slope or strong wind may preclude the usage of other, more sensitive, devices. Due to the low cost of the equipment, simultaneous use up to four instruments was possible to speed up the

Table 4.3 - Saturated hydraulic conductivity, K_s ($mm\,h^{-1}$), of the 9×9 m study plot obtained through different point measuremen techniques in different subareas (see Figure 4.9). Mean = arithmetic mean; *CV* = coefficient of variation.

Sub-area	DRI	CTP	GP
I	72.0	4.0	3.2
II	36.0	8.2	4.3
III	6.0	12.1	1.4
IV	78.0	2.1	2.6
V	66.0	28.8	1.7
VI	18.0	26.0	2.6
VII	48.0	10.3	1.8
VIII	117.0	31.4	1.6
IX	102.0	17.7	2.0
Mean	60.3	15.6	2.4
CV (%)	61.2	69.7	39.6

procedures. On each plot, K_s measurements were performed with a spatial resolution of 3 m. Figure 4.10 shows examples of the different environmental conditions present on the plots. Figure 4.10a-b show the largest plot, plot 2, which consists of grassy land and is located close to the forested area of the catchment. Figure 4.10c-d represent plot 5 showing the winter wheat remains left on the field after the harvest, and Figure 4.10e-f show plots 11 and 12, both located in a naturally-vegetated orchard.

At the locations where the infiltration measurements were performed, soil textural composition and organic matter content were inferred from the survey data available on the 50×50 m grid. In addition, slope and elevation across the catchment were obtained from the DTM. Table 4.4 shows general statistics related to the data available at the 131 locations of the K_s measurements.

Table 4.4 - General statistics of the information available in the 300 nodes of the grid. Min = minimum value; Max = maximum value; Mean = arithmetic mean; *CV* = coefficient of variation; *om* = organic matter content; *cl* = clay content; *si* = silt content; *sa* = sand content; *s* = slope angle; *el* = elevation; K_s = saturated hydraulic conductivity.

Statistics	*om* (%)	*cl* (%)	*si* (%)	*sa* (%)	*s* (°)	*el* (m a.s.l.)	K_s (mm h^{-1})
Min	1.9	17.6	68.7	6.0	2.4	263.1	1.0
Max	3.4	23.0	73.8	11.5	13.0	316.4	130.0
Mean	2.6	20.3	71.3	8.4	6.1	279.3	25.1
St.dev.	0.4	1.1	1.5	1.2	1.9	16.3	25.8
CV (%)	13.8	5.6	2.1	14.7	31.7	5.8	102.7

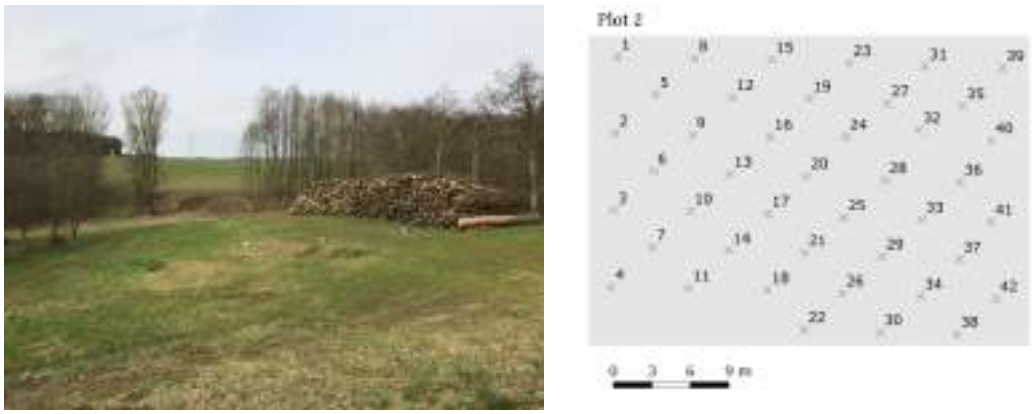

(a) **(b)**

Figure 4.10 - Plot 2, the largest plot located in the proximity of the forested area of the catchment and featuring a grassy meadow land; (a) measurement plot and (b) measurement scheme.

(c)

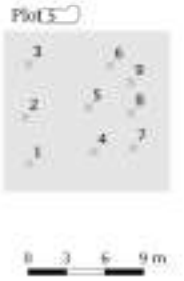

(d)

Figure 4.10 - Plot 5, a plot located in the cultivated area of the catchment; (c) measurement plot and (d) measurement scheme.

(e)

(f)

Figure 4.10 - Plots 11 and 12, both located in a naturally vegetated orchard; (e) measurement plot and (f) measurement scheme.

Chapter 5

Reliability assessment of K_s measurement techniques through rainfall-runoff experiments

Several experimental techniques are available for in-situ estimation of K_s through infiltration measurements (§ 3.2.3). The most commonly used devices are: tension permeameter (TP), e.g. the CSIRO disc permeameter (CTP), single ring infiltrometer (SRI), double-ring infiltrometer (DRI), constant-head well permeameter (CHP), e.g. the Guelph permeameter (GP), rainfall simulator (RS), e.g. the Guelph rainfall simulator. The choice of the device employed inevitably conditions the estimated values of K_s (Angulo-Jaramillo et al., 2000; Muñoz-Carpena et al., 2002; Verbist et al., 2013; Bagarello et al., 2014; Morbidelli et al., 2017) due to different factors such as the volume of soil investigated, the duration of the measurement, the theoretical framework (e.g., 1D or 3D infiltration) and the estimates of other soil parameters (e.g., soil sorptivity, saturated water content) necessary to derive the value of K_s applying specific equations.

Attempts have been made to compare the estimates provided by different measurement tools in order to understand their reliability in the K_s estimation. Burgy and Luthin (1956) compared the areal-average infiltration rate obtained

by SRI and DRI and did not find significant differences in the results obtained with the two devices. Sidiras and Roth (1987) carried out measurements of infiltration rate with DRI and RS for different surface conditions with the DRI results greater up to a factor of 5 than the RS ones. Boers et al. (1992) performed infiltration measurements by DRI, RS, and CHP and found conflicting results. Gupta et al. (1993, 1994) compared K_s values obtained with DRI, RS, and GP. In a given area, they found that the DRI and RS provided a variability of K_s lower than that observed by the GP. Vanderlinden et al. (1998) investigated the saturated hydraulic conductivity measured with CHP, TP, DRI, and falling-head borehole permeameter, under and outside an olive canopy. Their results highlighted significant differences among the selected techniques. Reynolds et al. (2000) compared positive-head TP, SRI, and undisturbed soil core sampling in three soil types with different management strategies. They found inconsistency among the K_s values obtained by the different techniques, with a ratio between the geometric means of K_s up to 10. The SCM did not provide representative estimates of K_s, and the TP, under high permeability conditions, yielded lower K_s values with respect to the other techniques. Emmerich (2003) performed a variety of K_s measurements by a TP on erodible pavement surfaces and obtained values of K_s much greater than the rainfall intensities from events that resulted in runoff production. Ronayne et al. (2012) compared in-situ measurements carried out at 32 locations in an alpine glacial till soil by using a minidisc infiltrometer, a DRI and the GP. The K_s estimates were found to be dependent on the measurement technique with areal geometric means ranging from 8 to 71 mm h^{-1} among the three devices. Verbist et al. (2013) investigated six measurement methods of K_s, including the TP, SRI, DRI, and CHP, at three locations with stony soils. They observed substantial differences among the estimates, with K_s ratios up to 10 at each site. The DRI and SRI estimates were found to be always higher than those from the other devices at all three locations.

In spite of these conflicting results, the aforementioned techniques are currently considered as reference points for developing new devices. As an example, Moret-Fernández et al. (2015) validated a modified version of the hood infiltrometer (Schwärzel and Punzel, 2007) to estimate K_s with a conventional TP on uncovered soil surfaces. Consequently, although intercomparison of

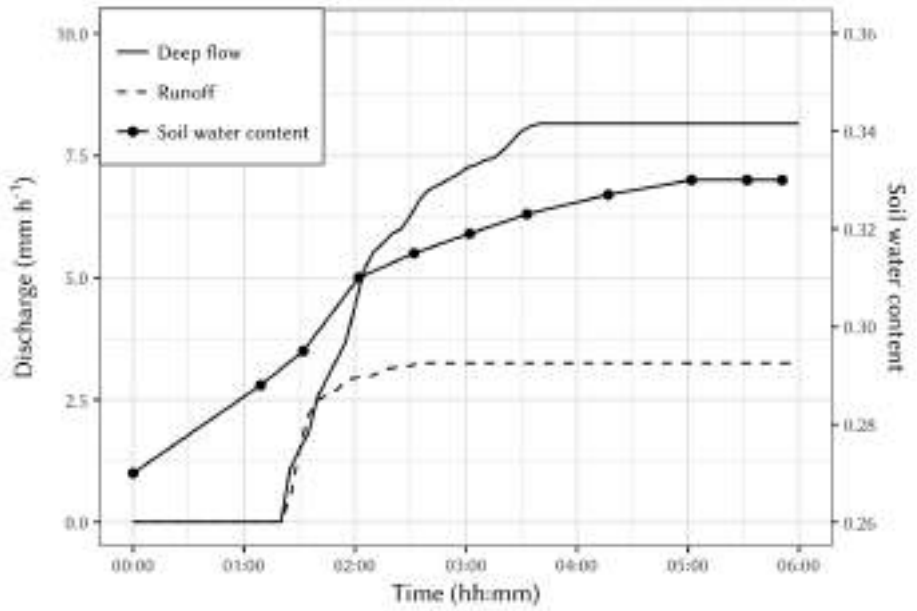

Figure 5.1 - Evolution in time of surface runoff, deep flow and soil water content during a rainfall-runoff laboratory experiment producing steady-state conditions. The artificially produced rainfall rate was equal to 11.4 mm h^{-1}.

different methods is useful, a proper assessment of these techniques requires a reliable bechmark to validate K_s measurements (Reynolds et al., 2000; Lai et al., 2010). In this work, such benchmark value has been derived through rainfall-runoff experiments, as detailed in the following section.

5.1 Rainfall-runoff experiments

The approach adopted in this investigation relies upon several rainfall-runoff experiments: a constant artificial rainfall rate is maintained upon the study area (laboratory and field) until steady-state conditions are reached for surface runoff, deep flow and soil moisture. When the soil moisture content is time invariant, the whole soil profile is saturated. The areal-average value of K_s is deemed equal to the deep flow in saturated conditions.

The laboratory rainfall-runoff experiments were performed prior to the point measurements of K_s (§ 4.2). Figure 5.1 shows the surface and deep flow hydrographs together with the trend of soil moisture content for a represen-

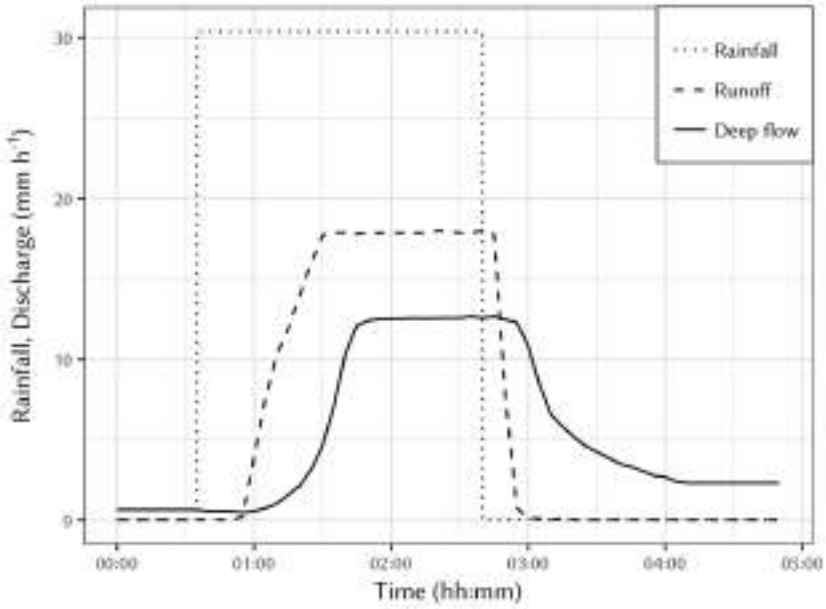

Figure 5.2 - Evolution in time of surface runoff and deep flow during a representative rainfall-runoff experiment at the field system. The rainfall rate is also reported.

tative experiment producing steady conditions. Under a rainfall intensity of 11.4 mm h^{-1} and duration 6 h, steady-state conditions were reached for the three quantities during the last hour, with soil water content equal to 0.33, surface runoff of 3.2 mm h^{-1} and deep flow rate of 8.2 mm h^{-1}. The observed steady values of the deep and surface flow rates indicate that the soil moisture vertical profile was time invariant, and the whole soil was under saturation. The steady soil moisture content, equal to the saturation value, detected by the TDR sensor supports this interpretation that leads to conclude that the areal-average value of K_s was equal to the steady deep flow rate of 8.2 mm h^{-1}.

Rainfall-runoff experiments at the field system were also realized prior to the measurements through infiltrometers (§ 4.2). Figures 5.2 and 5.3 highlight the results of a representative experiment carried out using a constant artificial rainfall rate of 30.4 mm h^{-1}. Examination of the time evolution of surface runoff, deep flow and soil water contents at four different locations and varying depths (5, 15, 25 and 35 cm) clearly indicates the existence of a steady-state period with a duration of 1 h prior to the cessation of rainfall and characterized by steady soil moisture content equal to θ_s. The values assumed

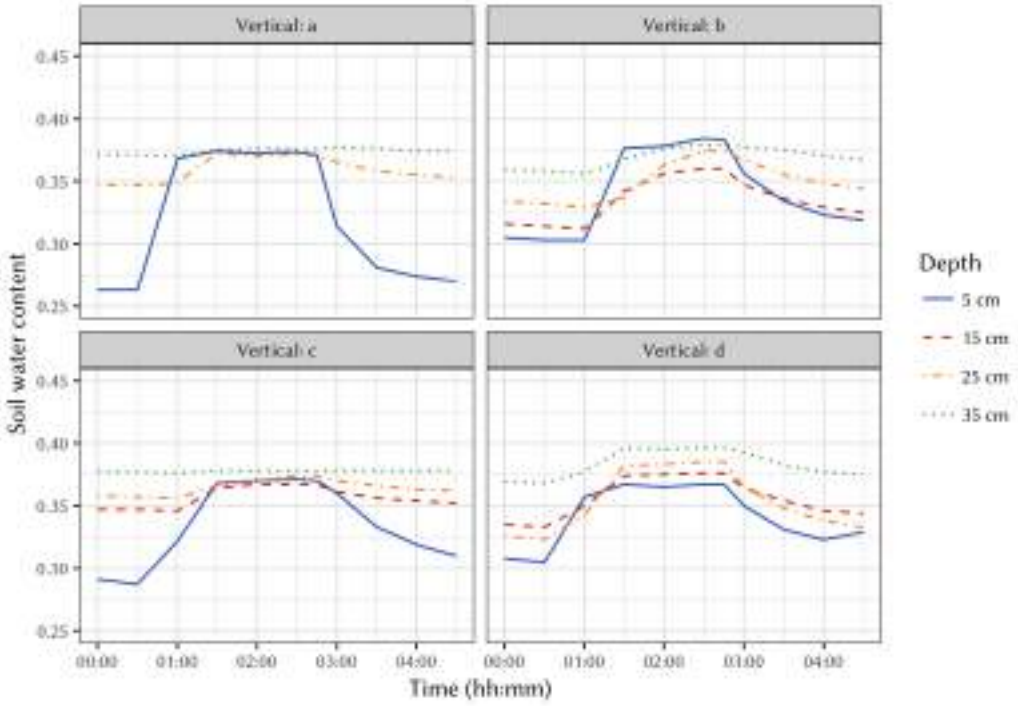

Figure 5.3 - Evolution in time of soil water content at different depths in four measurement locations (a-d) during a representative rainfall-runoff experiment at the field system.

by surface and deep flows at the steady-state are equal to 17.8 mm h^{-1} and 12.6 mm h^{-1}, respectively, while the values of θ_s, variable with depth at the four measurement locations (a-d), are shown in Figure 5.3 and reported in Table 5.1.

5.2 Results and discussion

As previously described, in addition to the rainfall-runoff experiments, measurements of K_s with DRI, CTP and GP were performed at both the laboratory (§ 4.1.1) and the field (§ 4.1.2) experimental systems. The results of the measurements are shown in Tables 4.2 and 4.3 for the laboratory and the field, respectively.

Because only minor variations of K_s were expected through the soil surface of the laboratory experimental system, the DRI, which provided a constant value of 15.0 mm h^{-1}, appears to be more reliable than the CTP and the GP

Table 5.1 - Volumetric soil moisture content observed during steady conditions at different depths in four locations of the field system soil.

Depth (cm)	Vertical			
	(a)	(b)	(c)	(d)
5	0.371	0.383	0.370	0.376
15	-	0.360	0.367	0.376
25	0.370	0.374	0.374	0.385
35	0.377	0.379	0.378	0.396

that gave values varying by a factor (ratio of maximum to minimum estimate of the same quantity) of 4 and 10, respectively. This variation indicates the extreme sensitivity of the last two instruments to small variations in the standard measurement procedures. Furthermore, the estimate of the K_s areal-average value derived by averaging over different measurements is substantially different from the benchmark value of $8.2\,\mathrm{mm\,h^{-1}}$, with errors of about 66 % and 129 % for the CTP and GP, respectively. Although providing consistent estimates, it is possible to note that the DRI also overestimates the K_s areal-average value with an error greater than 80 %.

As far as the data observed at the field experimental system are concerned, it can be observed that the reduction in soil moisture values with increasing depth (Figure 5.3) is less pronounced than it could be expected from drainage occurring within the soil profile. Soil moisture content values in the steady-state period, shown in Figure 5.3 and Table 5.1, suggest spatial variability in soil properties. In particular, θ_s values at locations b and d (Figures 5.3b and 5.3d) indicate a vertical variability of θ_s, which reaches 10 % within the site of Figure 5.3d. A slight horizontal heterogeneity of the steady soil moisture content can also be deduced from Figure 5.3 comparing the values at the same depth in the four monitored locations.

These results point out the possible presence of a spatial heterogeneity of K_s and therefore the selected devices for point measurements at the plot should reflect this variability with an areal-average value of K_s similar to that obtained by the rainfall-runoff approach. For each instrument, the coefficient of variation of K_s (Table 4.3) assumes reasonable values considering that it is

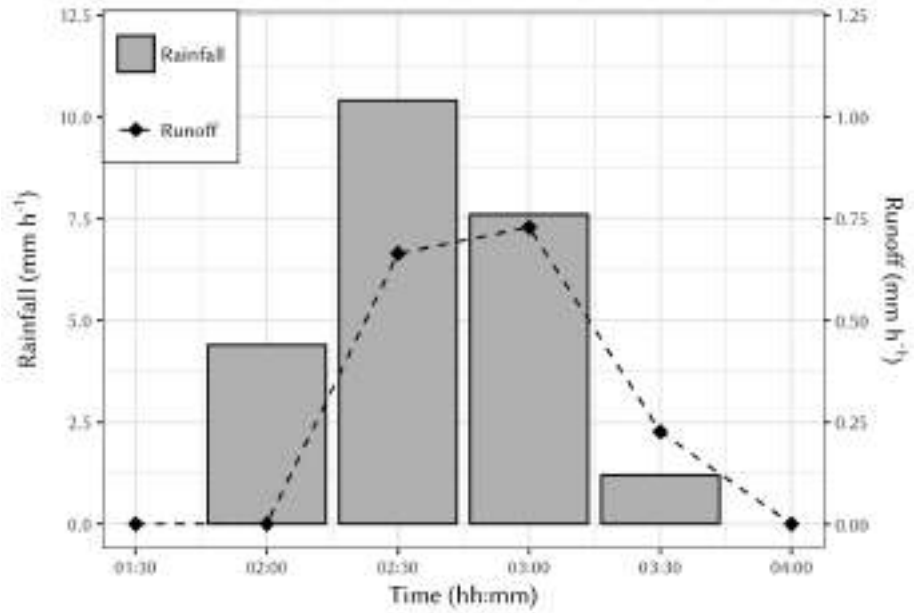

Figure 5.4 - Rainfall rate and surface runoff observed during the event of October 2, 2014, in the study plot.

within the typical range of 30-150 % found in natural soils (Ragab and Cooper, 1993; Mohanty et al., 1994). However, the areal-average value of K_s derived with the DRI overestimates the benchmark value (12.6 mm h^{-1}) by a factor of 5. Furthermore, the GP provides an underestimate by a factor of 5, whereas the average from CTP measurements is the closest to the plot average K_s value, with an error of 24 %.

Finally, some experimental results obtained for natural rainfall-runoff events supplement the aforementioned deduction about the magnitude of the average K_s value. As an example, Figure 5.4 shows results from a rainfall event with generation of surface runoff in a few parts of the plot where K_s had to be lower than the r value of 10.5 mm h^{-1}. The existence of portions of the plot with these values of K_s is consistent with the plot-average value of 12.6 mm h^{-1} because of the presence of soil heterogeneities. This view is also supported by some differences in the time evolution of the soil water content vertical profiles shown in Figures 5.3a–5.3d. On the other hand, the production of surface runoff with $r < 10.5$ mm h^{-1} indicates that the local values of K_s derived by the DRI (Table 4.3) throughout the plot and the associated plot-

Table 5.2 - Rainfall characteristics and volumetric soil moisture content associated with the rainfall events used before starting with the experiments of Tables 4.2 and 4.3.

	Laboratory system	Field system
Rainfall intensity ($mm\,h^{-1}$)	5.0	6.5
Rainfall duration (h)	12	12
Initial soil moisture	0.263	0.321*
Final soil moisture	0.330	0.372*

* Average value derived using all sensors set up in the plot.

average value are considerably overestimated because they should not lead to saturation at the soil surface.

An overall analysis of the experiments performed at the laboratory and plot scale highlights the following:

- the DRI leads to an overestimate of the areal-average value of K_s which is greatly variable from the laboratory to the study plot even though it is the only device, among those tested here, that provides reproducible results for the laboratory homogeneous soil;
- the GP yields conflicting results with K_s overestimated in laboratory but significantly underestimated at the plot scale;
- the CTP provides areal-average values of K_s closer to the expected one in the experimental plot, but produced a substantial error of 66 % in the laboratory soil where the observed K_s spatial variability appears to be excessive.

In addition, it is important to remark that the estimates of K_s were performed during the condition of steady deep flow, therefore excluding the presence of a crust layer. The absence of a sealing layer is also supported by the following experimental features: (a) the rainfall-runoff experiments started with high soil water content (Figures 5.1 and 5.3) obtained through light artificial rainfall of long duration generated in the previous day (Table 5.2); (b) the artificial raindrops impacted the soil surface with velocities considerably lower than those of natural raindrops because of their reduced size due to the characteristics of the rainfall generator and to the small distance (2 m) between the sprinklers and soil surface that excludes the raindrop

growth by coalescence. The elements (a) and (b) allowed us to avoid surface erosion, as deduced from the absence of cloudy surface water at the laboratory and plot outlets.

Furthermore, the conflicting results reported in previous studies on the measurements of K_s with different devices have been related to a variety of reasons, sometimes with particular emphasis to the differences in the point measurement areas. Gupta et al. (1993, 1994) found that at a given scale the extent of the K_s spatial variability increased with the sample size of each device, with larger values for the GP and Guelph infiltrometer and lower values for the RS technique. These results were obtained in natural soils with macropores, crop residues, and plant roots, therefore, the K_s estimates obtained through devices with larger sample size were considered to be closer to the areal-average K_s value. This suggested that the number of point measurements required to obtain an average K_s value representative of a given area should increase as the device sample size decreases. The role of sample size was also investigated by Lai and Ren (2007) who showed that the spatial variability of the observations taken with DRI in a heterogeneous soil was larger for smaller inner rings. Similar deductions were done by Reynolds et al. (2000) considering the presence in natural soils of macropores and other soil heterogeneities. The above analysis ascribed to soil structure a primary role in the estimate of K_s in natural soils, at both the point and field scale. Based on this, sample-size effect can be expected in the experiments of this investigation. However, this effect should be rather limited, considering that the soil heterogeneities were only due to the soil packing procedure, since macropores, cracks, stones, and other heterogeneities typical of natural soils were absent. In this context, we assumed that the selected numbers of point measurements by each device were appropriate to derive the K_s average value in the laboratory and plot experiments.

A further factor that can affect the estimate of K_s is air entrapment. Some paper pointed out that in natural soils entrapped air can influence point measurements of K_s, producing significant underestimates of the real values (Stephens et al., 1983; Gupta et al., 1994). Even though the presence of entrapped residual air cannot be excluded a priori, only minor effects are expected in our experiments because:

- the two soils were properly packed;
- air could escape freely through the soil lower boundary;
- all the measurements with the GP, CTP, and DRI were performed under the conditions of soils close to natural saturation at each depth;
- the values of K_s in the rainfall-runoff approach were deduced in a long period with steady surface and deep flow.

Chapter 6

Estimation of spatially representative plot-scale K_s

Saturated hydraulic conductivity, K_s, is a key parameter controlling various hydrological processes, therefore accurate estimates are needed in multiple infiltration models. A large number of factors influence K_s spatial variability, such as soil structure (Dexter et al., 2004), texture (Puckett et al., 1985; Saxton et al., 1986; Jabro, 1992; Baiamonte et al., 2017), landscape position (Wagger and Denton, 1989; Mohanty et al., 1994), land cover, management practices (Coquet et al., 2005; Ziegler et al., 2006; Zimmermann and Elsenbeer, 2008; Alletto and Coquet, 2009; Bonell et al., 2010), and spatial scale (Schulze-Makuch et al., 1999; Sobieraj et al., 2004; Lai and Ren, 2007).

Saturated hydraulic conductivity typically varies by at least two orders of magnitude in space. Baiamonte et al. (2017) performed 150 infiltration measurements in a Sicilian basin by applying the simplified falling-head technique (SFH) of Bagarello et al. (2014) and observed values of K_s that ranged from less than $1\,\mathrm{mm\,h^{-1}}$ to more than $8000\,\mathrm{mm\,h^{-1}}$. Similarly, Papanicolaou et al. (2015) conducted about 120 infiltration experiments on three hillslopes with different agricultural management practices in Iowa by means of semi-automated DRIs and observed K_s values that ranged from $0.15\,\mathrm{mm\,h^{-1}}$ to $360\,\mathrm{mm\,h^{-1}}$.

Woolhiser et al. (1996) examined the effects of K_s spatial variation on the interaction between infiltration and surface runoff at the hillslope scale

and found that runoff hydrographs were strongly affected by variations in saturated hydraulic conductivity, especially for small runoff events. Taskinen et al. (2008) investigated the effects of spatial variability of saturated hydraulic conductivity on overland flow in a small agricultural catchment by analyzing 2000 synthetic rainfall-runoff events generated from observed rainfall events with runoff modeled using different spatially variable K_s fields. They found the greatest differences in the first flow peak and in the rising part of the hydrograph. Hu et al. (2015) analyzed the effects of K_s variability on runoff simulations using the Limburg Soil Erosion Model in a small watershed on the Chinese Loess Plateau and found that total and peak discharges were underestimated if the spatial variability of K_s was completely ignored or only partially considered. Accounting for K_s spatial variability is therefore essential.

Most field techniques used to determine K_s, such as the traditional well permeameter and ring infiltrometers, rely on the attainment of a steady-state flow rate, so that the time required to carry out each measurement is usually high. Speeding up the measurement operations with the purpose of achieving detailed K_s maps over large areas is one of the greatest challenges to be faced when spatial scale increases. In order to reduce the time demand of extensive field measurement campaigns, the use of indirect methods (§ 3.2.1), the development of faster measurement techniques (e.g., those that estimate K_s in the transient stage of the infiltration process), or statistical analyses designed to extrapolate the essential information out of a smaller number of measurements are some of most frequently adopted approaches. Pedotransfer functions available in literature, developed for a large variety of soils, are largely employed for estimating K_s. However, macropores and other preferential flow paths often dominate the infiltration behavior even more than the characteristics of the soil matrix (as quantified by porosity, texture etc.), so it is usually of advantage not to rely on pedotransfer functions from the literature alone but to make at least a few K_s measurements in the catchment of interest (Bouma et al., 2011). Regarding the number of measurements required, Vieira et al. (1981) studied the spatial variability of 1280 field-measured infiltration rates using geostatistical concepts. They argue that 128 samples are sufficient to obtain nearly the same information as obtained

from 1280 samples. Ahmed et al. (2015) conducted an uncertainty analysis on 722 infiltration measurements in six roadside drainage ditches (grassy swales, i.e. shallow, open vegetated roadside drainage channels designed to convey stormwater runoff to storm sewers or receiving water bodies) and concluded that approximately 20 infiltration measurements is the minimum number to obtain, with an acceptable level of uncertainty, a representative geometric mean of K_s of a swale less than 350 m long. The identified minimum number is related to a 95 % confidence interval with a width of about 2 in logscale. Skøien and Blöschl (2006) found that the required number of samples depends on the spatial correlation of K_s as well as on the measurement setup. They investigated the effect of spacing (average distance between samples), extent (size of the domain sampled) and support (averaging area of one sample), i.e. the "scale triplet" as termed by Blöschl and Sivapalan (1995), on the estimates of the mean, the spatial variance and the integral scale of a variable in a landscape. For each of the chosen combinations of spacing, support and extent they generated 1000 synthetic random fields and sampled from them according to the selected scale triplet. In what they termed "single realization case", they compared the sample mean and sample variance with the mean and the variance of the entire random field of the same realization. They found that the estimation uncertainty of the mean increases when the spacing increases for a given number of samples. Small extents (relative to the underlying correlation length) imply that the samples are highly correlated and the underlying distribution can be well characterized from a limited number of samples. Skøien and Blöschl (2006) used numerically generated random fields, and actual observations of K_s may differ in terms of their sampling characteristics.

In order to understand the controls of saturated hydraulic conductivity of the soil surface in an agricultural setting and to identify the minimum number of samples needed for estimating a representative K_s at the plot scale, the results of a K_s measurement campaign performed in a small catchment in Austria with double-ring infiltrometers are used in a statistical analysis. Measurements collected at 12 different plots in both grasslands and arable lands (Figure 6.1) are selected to deduce the effects of different land management operations on the K_s spatial variability, and the results are reported in

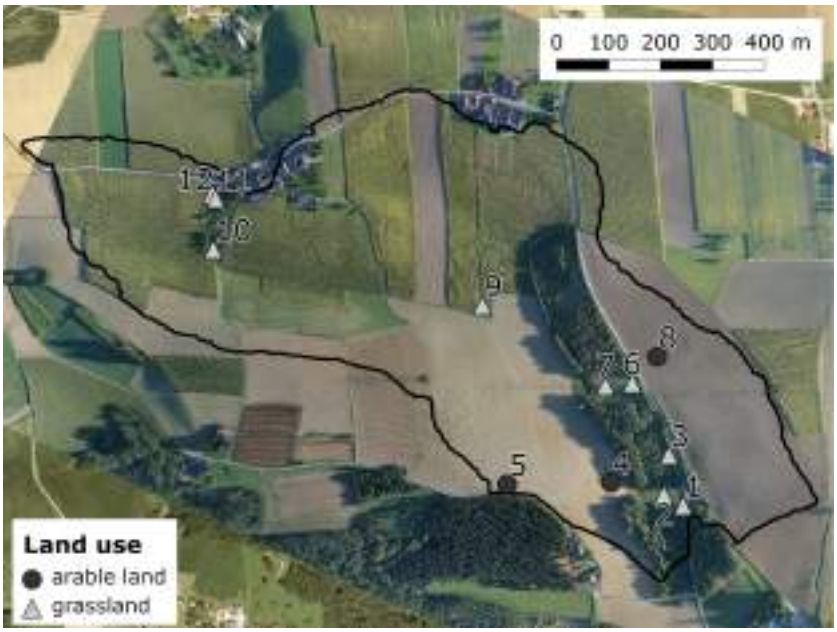

Figure 6.1 - Measurement plots in the HOAL catchment, Petzenkirchen, Austria. Dark-grey circles represent plots located in arable areas, light-grey triangles represent plots located in grassland areas.

Table 6.1.

An uncertainty analysis is also performed to understand the confidence in the estimate of the areal average value of K_s for different land uses, plot areas and sample sizes. Based on this analysis, guidance is given for planning measurement campaigns with double-ring infiltrometers when time and resources are limited.

6.1 Statistical analysis

The ANOVA method (Armstrong et al., 2000) has been selected for the analysis of variance of the experimental data associated to the different plots to understand whether the variability of K_s across the catchment is linked to specific soil physical characteristics of the measurement locations. An application of this method requires that specific assumptions on the experimental data are satisfied. In general terms, the results obtained for the study variable are subdivided into J groups and an observed value of a given group,

Table 6.1 - General statistics of the K_s values measured with double-ring infiltrometer. Min = minimum value; Max = maximum value; Mean = arithmetic mean; CV = coefficient of variation; Skew = skewness; $\text{Mean}_{\log}$ = arithmetic mean of the log-transformed values; $CV_{\log}$ = coefficient of variation of the log-transformed values; Arable land = K_s values measured in arable areas; Grassland = K_s values measured in grassy areas; Total = all K_s values.

Statistics	Arable land	Grassland	Total
Min (mm h^{-1})	2.0	1.0	1.0
Max (mm h^{-1})	130.0	84.0	130.0
Mean (mm h^{-1})	46.9	20.2	25.1
St. dev. (mm h^{-1})	35.5	20.3	25.8
CV (%)	75.6	100.3	102.7
Skew (-)	0.8	1.1	1.5
Median (mm h^{-1})	34.5	12.0	15.0
$\text{Mean}_{\log}$ (-)	3.5	2.4	2.6
$CV_{\log}$ (%)	27.7	50.6	47.9

j ($j = 1, \ldots, J$), can be expressed as a sum of the mean of all the available measurements, μ, the group effect, τ_j, representing the deviation of the group mean, μ_j, from μ and a random element reflecting the combined effects of natural variation between observations and measurement errors. The basic assumptions involved in the ANOVA method concern the random elements that should be normally distributed with the same variance in all groups, while the means μ_j can be variable from group to group. The available K_s data do not satisfy these two conditions, while log-transformed values of K_s have been found appropriate for the ANOVA method application (see also Snedecor and Cochran, 1980). The following procedure has been therefore used.

The entire data-set has been divided into J groups and a single transformed observation, $\ln(K_s)_{h,j}$, has been expressed as:

$$\ln(K_s)_{h,j} = \mu + \tau_j + \varepsilon_{h,j} = \mu_j + \varepsilon_{h,j} \qquad j = 1, \ldots, J \quad \text{and} \quad h = 1, \ldots, H \tag{6.1}$$

with H total number of observations, $\tau_j = \mu_j - \mu$ and with the quantities μ_j and $\varepsilon_{h,j}$ computed on the transformed data-set. On this basis, to highlight a possible absence of group effect, the null hypothesis of equality of the J

values of the mean has been tested starting from the quantity SS_t defined as:

$$SS_t = \sum_h \sum_j \left(\ln(K_s)_{h,j} - \mu\right)^2 \tag{6.2}$$

that can be rewritten as:

$$SS_t = SS_w + SS_b = \sum_h \sum_j \left(\ln(K_s)_{h,j} - \mu_j\right)^2 + \sum_j n_j \left(\mu_j - \mu\right)^2 \tag{6.3}$$

where SS_w is associated to the variation within each group, SS_b to the variation between each group and the catchment, and n_j is the number of observations in each group. The sample variance, σ_t^2, the "within variance", σ_w^2, and the "between variance", σ_b^2, have been then estimated by dividing each term of Equation (6.1) by the corresponding degree of freedom, df:

$$\sigma_t^2 = \frac{SS_t}{df_t} = \frac{SS_t}{H-1} \tag{6.4}$$

$$\sigma_w^2 = \frac{SS_w}{df_w} = \frac{SS_w}{H-J} \tag{6.5}$$

$$\sigma_b^2 = \frac{SS_b}{df_b} = \frac{SS_b}{J-1} \tag{6.6}$$

and the variance ratio, $\tilde{F}$, has been computed as:

$$\tilde{F}(J-1, H-J) = \frac{\sigma_b^2}{\sigma_w^2} \tag{6.7}$$

In order to test the null hypothesis, $\tilde{F}$ has been compared to the critical value, $\tilde{F}_{crit}\left(df_b, df_w\right)$, obtained from an F-distribution (Snedecor and Cochran, 1980) with df_w and df_b degrees of freedom with a significance level of 5 %. If $\tilde{F}$ is greater than the critical value, the null hypothesis of zero group effect has to be rejected and at least one of the μ_j values is significantly different from the grand mean. The above approach has been applied to different group ensembles:

1. ensemble obtained considering the plot locations as sources of variation to understand whether K_s variability is substantially linked to the specific physical and topographical characteristics of the measurement areas;
2. ensemble identified grouping areas with the same land use, considered because the outcomes of step (1) suggested a significant dependency of K_s variability on the plot location;
3. ensembles of plots characterized by the same land use to understand if (a) other plot-specific properties had a significant influence or (b) the observations could be considered as different sets sampled from the same population, even though collected at different locations in the catchment.

6.2 Uncertainty analysis

An analysis was performed with the aim of determining the uncertainty related to the estimate of an average K_s value for a specific area. The K_s geometric mean, $\bar{K}_s$, was chosen as the representative estimator of the areal average saturated hydraulic conductivity. Obviously, the higher the number of measurements used to estimate the geometric mean of K_s, the higher is the confidence that the estimate is representative of the true value of K_s for the considered area. However, since the measurements are very time consuming, understanding whether it is possible to reduce the number of measurements and still obtain a reliable average would enormously improve planning capabilities, e.g. when a measurement campaign has to be scheduled, and speed up the entire campaign.

In this study, an uncertainty analysis similar to that of Ahmed et al. (2015) was carried out. Three plots, 2, 11-12 and 7 were selected and for each data-set the non-parametric bootstrap method (Carpenter and Bithell, 2000) was used to estimate confidence intervals around the geometric mean for different numbers of samples. The method is particularly helpful whenever confidence intervals must be calculated for small data-sets, as in the case of plot 7 where only 9 measurements are available. As stated by Carpenter and Bithell (2000), we usually seek information about the value of a population parameter

(e.g. the mean, μ) by drawing a random sample $\boldsymbol{Y}$ from that population and constructing an estimate $\hat{\mu}(\boldsymbol{Y})$ of the value of μ from that sample. The bootstrap principle is to obtain information about the relationship between μ and $\hat{\mu}(\boldsymbol{Y})$ by looking at the relationship between $\hat{\mu}(\boldsymbol{y_{obs}})$ and $\hat{\mu}(\boldsymbol{Y^*})$, where $\boldsymbol{Y^*}$ is a resample characterized by the sample of the observations $\boldsymbol{y_{obs}}$. Because the method involves a resampling step – which can be done assuming a specific distribution for the parameter and sampling from it (i.e. parametric bootstrap) or without assuming any distribution for the parameter and sampling with replacement (i.e. non-parametric bootstrap) – it is often used for small data-sets.

In implementing the bootstrap method, the observations were assumed independent, sampling was done with replacement and the process was repeated 1000 times, as recommended for the 95 % confidence interval by Carpenter and Bithell (2000). From each sub-sample the geometric mean was estimated. A set of 1000 geometric mean values was obtained and the 95 % confidence interval was derived by calculating the 2.5 and 97.5 percentiles. The procedure was repeated changing the number of observations (n). The three aforementioned plots were chosen because they exhibited the same sampling density (about 1 measurement every 10 m^2), the same land cover (grass) but different number of observation points, i.e., 40, 20 and 9 for plots 2, 11-12 and 7, respectively. For each plot, the trend of the confidence interval was derived varying the number of observations n from 2 to the maximum number of data available on each plot. The three trends obtained were then normalized by the geometric mean of K_s of each plot to facilitate visual comparisons.

The second step of the analysis was performed for plot 2 because it was the one with the largest data-set. Six sub-areas of 55, 110, 165, 215, 280 and 345 square meters were considered, with larger sub-areas always containing all the smaller ones. In each sub-area, 4, 5, 6, 7, 8 and 9 measurements (n) were drawn, and the 95 % confidence intervals were estimated as above for a total of 36 area-sample number combinations. Finally, the widths, W_{95}, of the confidence intervals calculated as the difference between the 97.5 and 2.5 percentiles, were plotted against area for different sample numbers. The curves describe how the confidence in the estimation of $\bar{K}_s$ decreases when an equal number of measurements are performed on plots of increasing dimensions or how

many samples are needed to obtain a given accuracy.

6.3 Results and discussion

6.3.1 Controls on the spatial variability of saturated hydraulic conductivity

Figure 6.2 suggests that soil physical characteristics do not have a direct effect on K_s variability. A wider K_s variation range seems to be related to lower *om* (Figure 6.2a), higher *si* (Figure 6.2c) or lower *sa* (Figure 6.2d), however this may be caused by the variation of the physical characteristics with land use, rather than by a direct dependency of K_s on texture. Most likely, arable areas are characterized by lower percentages of *om* and *sa*, and higher percentage of *si*, therefore the corresponding wider variation range could be an expression of the treatment effect due to land use (investigated later), instead of a reflection of changes in soil textural composition. The weak relationship between K_s and soil textural composition is in contrast with experimental evidence of a strong connection between K_s and particle size distribution, and is likely related to the small variation of soil characteristics in the catchment (Rahmati et al., 2018). On the other hand, slope angle has a noticeable influence on K_s. In particular, higher values of K_s were observed at close to horizontal areas (Figure 6.2e), while the K_s range decreases with increasing slope angle s. This tendency is particularly evident for arable fields where land management operations disrupt the soil structure, increasing the void sizes and thus the capability of water to infiltrate by gravity. Figure 6.3 shows the relationship between slope angles and the textural components. No clear dependency of *s* on any of the considered soil characteristics can be detected, therefore, the observed influence of *s* on K_s (Figure 6.2e) is not related to changing soil attributes with slope, but it could be due to the effect of surface inclination on infiltration (Philip, 1991; Essig et al., 2009; Morbidelli et al., 2015) or to variations in soil properties not captured by texture such as macroporosity.

Notwithstanding the limited spatial variation of the physical and topographical soil attributes, saturated hydraulic conductivity varies substantially, with values ranging over two orders of magnitude, from a minimum of

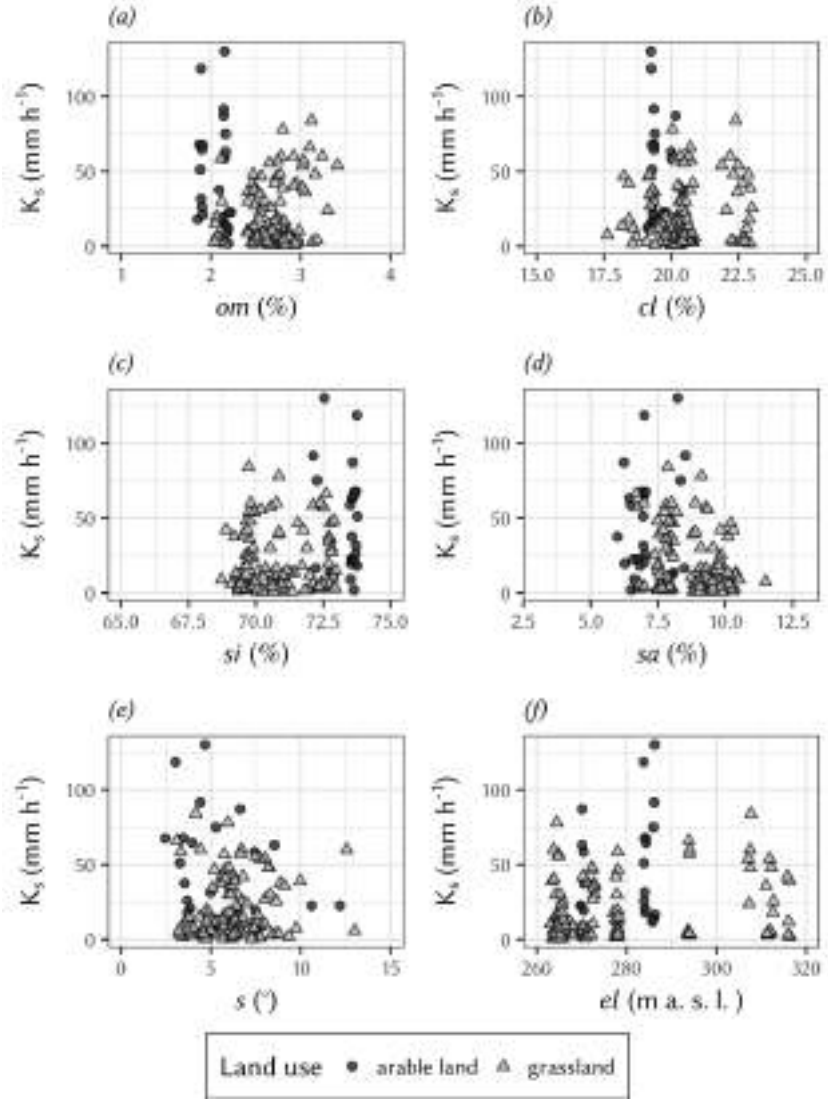

Figure 6.2 - Saturated hydraulic conductivity, K_s, observations plotted against (a) organic matter content, *om*; (b) clay content, *cl*; (c) silt content, *si*; (d) sand content, *sa*; (e) slope angle, *s*; (f) elevation, *el*. Dark-grey circles represent plots located in arable areas, light-grey triangles represent plots located in grassland areas.

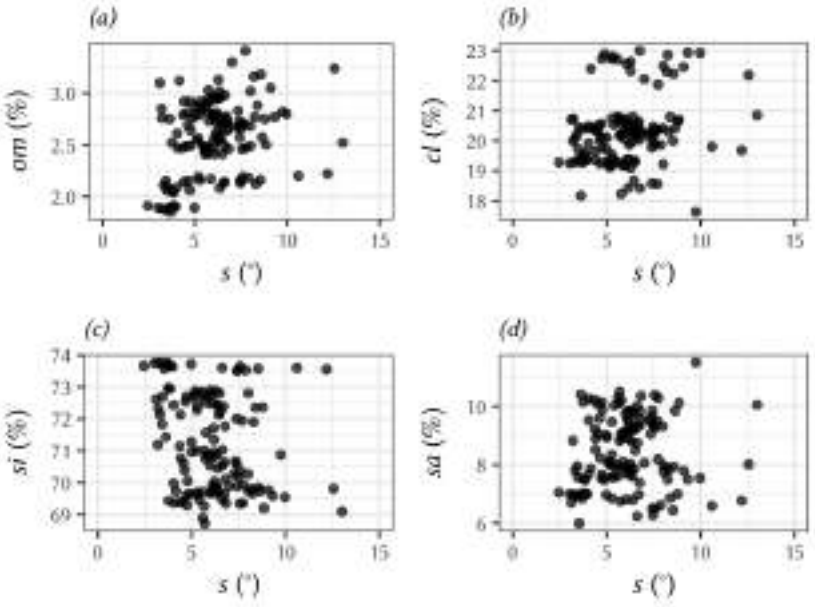

Figure 6.3 - Slope angles, *s*, plotted against (a) organic matter content, *om*; (b) clay content, *cl*; (c) silt content, *si*; (d) sand content, *sa*.

1 mm h^{-1} to a maximum of 130 mm h^{-1} (Table 6.1). The high spatial variability of K_s is a well-known characteristic of this parameter, regardless of the measurement technique applied, the geographical location, the land use or the soil type (Papanicolaou et al., 2015; Baiamonte et al., 2017).

Table 6.1 further shows the differences in the K_s variability between arable and grassy plots. While the K_s minima are basically identical for the two land uses, the maximum K_s observed in arable lands is more than 50 % higher than that on the grassy plots. This result can be explained by the fact that, after the harvest, i.e. the condition in which the infiltration measurements were performed, the remaining part of the plant as well as the root system are left in the ground until tillage. Therefore, the presence of the winter wheat root system, which can reach a depth of 2.2 m (Thorup-Kristensen et al., 2009), allows the establishment of a preferential flow regime that is more efficient than that of grassy soils, where the maximum rooting depth usually ranges from 30 cm to 70 cm (Brown et al., 2010). A uniform distribution of winter wheat remains in the field coupled with repeated land management of the investigated soils is also responsible for a more homogeneous, and

Table 6.2 - General statistics of the K_s values, grouped by plot. n.obs. = number of observations in each plot; Min = minimum value; Max = maximum value; Mean = arithmetic mean; CV = coefficient of variation; G.mean = geometric mean.

Plot	1	2	3	4	5	6
n. obs.	8	40	4	9	9	8
Min ($mm\,h^{-1}$)	1.5	1.0	6.0	2.0	18.0	2.0
Max ($mm\,h^{-1}$)	12.0	78.0	42.0	87.0	118.5	46.5
Mean ($mm\,h^{-1}$)	5.8	17.0	23.6	35.7	51.8	18.4
St. dev. ($mm\,h^{-1}$)	3.5	18.6	18.8	28.2	32.2	16.7
Median ($mm\,h^{-1}$)	5.3	12.0	23.3	22.5	51.0	12.8
CV (%)	60.8	109.0	79.4	78.9	62.2	90.6
G.mean ($mm\,h^{-1}$)	4.8	9.1	17.1	23.4	43.5	12.3
Plot	7	8	9	10	11	12
n. obs.	9	6	9	9	10	10
Min ($mm\,h^{-1}$)	3.0	12.0	1.8	3.0	3.0	2.0
Max ($mm\,h^{-1}$)	48.0	130.0	58.5	66.0	54.0	84.0
Mean ($mm\,h^{-1}$)	30.3	56.4	16.0	22.9	20.2	36.8
St. dev. ($mm\,h^{-1}$)	15.1	49.8	18.5	28.7	19.7	26.6
Median ($mm\,h^{-1}$)	34.5	45.8	7.0	4.0	12.0	40.5
CV (%)	49.8	88.3	115.7	125.3	97.6	72.2
G.mean ($mm\,h^{-1}$)	24.0	36.6	8.9	9.4	11.5	22.7

thus less variable, distribution of K_s across the area. The lower variability is reflected by a 25 % smaller CV in the arable fields than in the grassland areas. Land management operations repeated season after season, such as tillage or plowing, in addition to a uniform land cover of crops having the same growing period and therefore similar depths of the root system appear to partly cancel spatial variations due to different plant varieties and soil transformation mechanisms affecting the land surface, e.g. soil compaction, crust formation or soil swelling.

A site-by-site examination reveals very similar minima of saturated hydraulic conductivity on almost every plot (Table 6.2). On the other hand, the maxima vary greatly between different plots. CV assumes values greater than or equal to 50 % on each plot and its values closely reflect the overall

CV, thus indicating that the high K_s spatial variability is still traceable when the observation plots are individually considered. More information about plot differences and similarities is provided by Figure 6.4, which shows the boxplots of K_s on each measurement plot. As mentioned before, the minima vary little between plots, while the maxima vary a lot. There are differences related to land use: the first quartile in grassy fields (except plot 7) is less than or equal to the minima observed on arable plots 5 and 8, indicating that at least 25 % of the K_s values observed in natural conditions is lower than the minimum values observed when agricultural practices come into play. Moreover, about 50 % of the K_s values observed on arable plots 5 and 8 are greater than the maximum values measured on grassy plots 1, 3, 6, 7, 9 and 11 due to the fact that the median is greater than or equal to the maximum of each mentioned grassy plot. The boxplot analysis highlights a significant variability among the different measurement plots but it does not clarify if the detected variation is caused by specific physical and topographical characteristics, by different land uses or simply by the random nature of saturated hydraulic conductivity.

In order to understand whether the variability of K_s across the catchment is more related to the random nature of the parameter than to the measurement location or vice versa, an analysis of the variance was carried out. The first step of the analysis was therefore aimed at determining whether the plot characteristics have a significant influence on K_s spatial variability. Hence, the whole set of measurements was divided into $J = 12$ groups, representing the twelve measurement plots. Table 6.3a shows the results of the analysis of variance which was carried out on the log-transformed data. The ANOVA assumptions of normally distributed residuals and homoscedasticity were tested with the Shapiro-Wilk test (Shapiro and Wilk, 1965) and the Breusch-Pagan test (Breusch and Pagan, 1979), respectively. The variance between different plots, $\sigma_b^2 = 4.1$, is almost three times higher than the variance within each plot, $\sigma_w^2 = 1.3$. This means that the largest share of variability is traceable to the physical, topographical and land cover differences between the plots. An additional evidence resides in the fact that the value of $\tilde{F}$, equal to 3.1, is greater than the critical value of 1.9, and therefore the null hypothesis of absence of treatment effect, i.e. the effect of plot location in the present case,

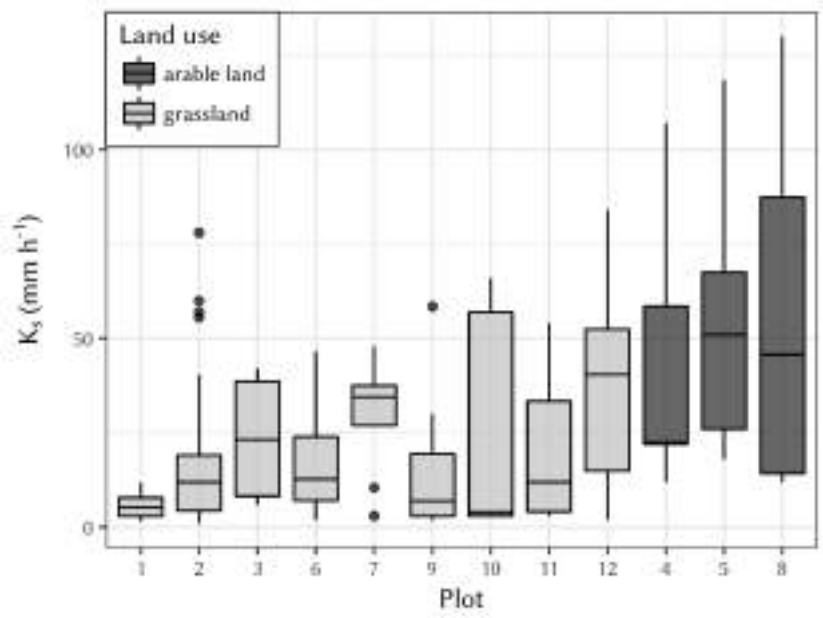

Figure 6.4 - Boxplots of saturated hydraulic conductivity, K_s, for the different measurement plots. Dark-grey boxplots represent plots located in arable areas, light-grey boxplots represent plots located in grassland areas. The box represents the interquartile range, i.e. difference between the third and the first quartiles. The horizontal black line represents the median of each plot. The dark-grey dots, usually representing possible outliers, were nevertheless considered as acceptable occurrences of K_s as they lie in the typical K_s domain.

must be rejected.

In the interest of further analyzing the origin of the treatment effect, the main variability source represented by the land use was considered. The whole set of K_s observations was divided into arable and grassland areas ($J = 2$), regardless of the specific type of crop cultivated in the field and the type of natural vegetation (e.g. forest, meadow, orchard). Table 6.3b shows the ANOVA result when land use is considered as source of variability. The variance associated with the measurement error and the random nature of K_s, i.e. σ_w^2, is 1.4, and is thus almost negligible compared to $\sigma_b^2 = 23.7$ indicating that land use is most likely the main driver for the observed K_s variations across the catchment. The value of the F-ratio of 17.2 is much larger than the critical $\tilde{F}$ of 3.9 associated with a significance level of 5 %, indicating that the group effect is not negligible and the means of the two groups are significantly different from each other.

Table 6.3 - Results of ANOVA analyses. df = degree of freedom (df_b;df_w;df_t); SS = sums of squares (SS_b;SS_w;SS_t); σ^2 = variance (σ_b^2;σ_w^2); $\tilde{F}$ = variance ratio; $\tilde{F}_{crit}$ = critical value of the F-ratio. All variances (SS, σ^2) relate to the logarithms of K_s.

(a) All measurements grouped by plot

Source of variation	df	SS	σ^2	$\tilde{F}$	$\tilde{F}_{crit}$
Plot (between)	11	44.7	4.1	3.1	1.9
Error (within)	119	156.9	1.3		
Total	130	201.5			

(b) All measurements grouped by land use

Source of variation	df	SS	σ^2	$\tilde{F}$	$\tilde{F}_{crit}$
Land use (between)	1	23.7	23.7	17.2	3.9
Error (within)	129	177.8	1.4		
Total	130	201.5			

(c) Grassland measurements grouped by plot

Source of variation	df	SS	σ^2	$\tilde{F}$	$\tilde{F}_{crit}$
Plot (between)	8	19.1	2.4	1.7	2.0
Error (within)	98	137.0	1.4		
Total	106	156.2			

(d) Arable land measurements grouped by plot

Source of variation	df	SS	σ^2	$\tilde{F}$	$\tilde{F}_{crit}$
Plot (between)	2	1.8	0.9	1.0	3.5
Error (within)	21	19.9	0.9		
Total	23	21.7			

Finally, since both land use and measurement plot location are responsible for a non-negligible treatment or group effect, it is interesting to understand if both factors cause saturated hydraulic conductivity to vary in space, or rather if the two are related with each other and K_s spatial variability is actually due to only one of them. In other words, we want to understand if K_s varies with plot location because of different physical and topographical soil characteristics specific of each plot or only because every plot exhibits a different land use. To this end, the whole sample of K_s observations was split into two sub-samples – the first one consisted of measurements performed in grassland areas and the second of measurements performed in arable areas – and within each sub-sample an analysis of variance was carried out considering as source of variation the plot location. Results of the analyses are shown in Table 6.3c-d. In both cases, variances associated with treatment (between) and error (within) have approximately the same values, and the F-ratio is always lower than the critical value, indicating that plot location does not explain the spatial variability, and that measurements on different plots with the same land use can be considered as sampled from the same population because the null hypothesis of equality of each group mean to the grand mean cannot be rejected.

The great influence of land use on the observed K_s variability is evident when the Probability Density Functions (PDFs) of K_s observations are divided into the two sub-samples previously defined (Figure 6.5). Saturated hydraulic conductivity is usually assumed as log-normally distributed (Nielsen et al., 1973; Warrick et al., 1977; Dagan and Bresler, 1983; M. L. Sharma et al., 1987) and, although the PDFs of both grassy and arable fields follow a log-normal distribution as tested with the Shapiro-Wilk test (Shapiro and Wilk, 1965) on the log-transformed data, they exhibit different shapes. In arable fields, the PDF is flatter, the peak is lower and less pronounced, the variation range is larger and the median is 34.5 mm h^{-1} as compared to 12 mm h^{-1} in grassy fields (Table 6.1). This means that agricultural practices and a homogeneous land cover influence the random nature of saturated hydraulic conductivity, which still varies randomly inside each group. Clearly, land use strongly influences K_s in agricultural settings and data collected in arable and grassland areas should not be considered as stemming from the same population.

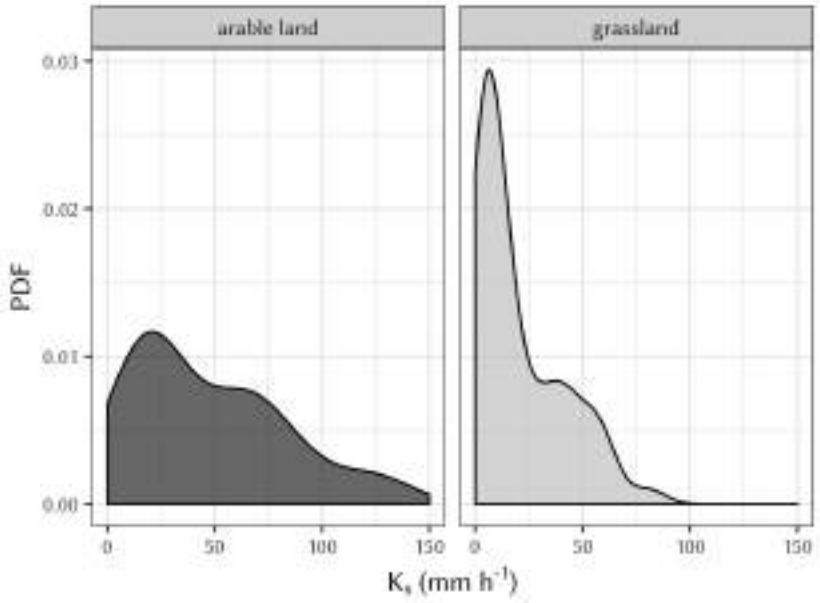

Figure 6.5 - Probability Density Functions (PDFs) of observed saturated hydraulic conductivity, K_s, values on both arable (dark-grey) and grassy (light-grey) fields.

6.3.2 Minimum number of samples for estimating areal average saturated hydraulic conductivity

The uncertainty analysis aimed at determining the minimum number of samples required for estimating a reliable K_s geometric mean, $\bar{K}_s$, for a specific area was carried out using the data from plots 2, 11-12 and 7. These plots had the same land use, different areas (about 500 m^2, 200 m^2 and 80 m^2, respectively) and different number of total observations. However, considering that the measurements were performed with the same spatial resolution, the plots approximately had the same measurement density (about 1 observation per 10 m^2). Figure 6.6 shows the 95 % confidence intervals of $\bar{K}_s$ normalized by the geometric mean of the specific plots. For a specific number of measurements, n, the plot with smaller area results in a narrower normalized confidence interval. For example, for $n = 6$, the width of plot 7 normalized confidence interval of 1.2 is much narrower than those of plots 2 and 11-12 (2.2 and 2.0, respectively).

Although the normalization influences the width of the confidence interval

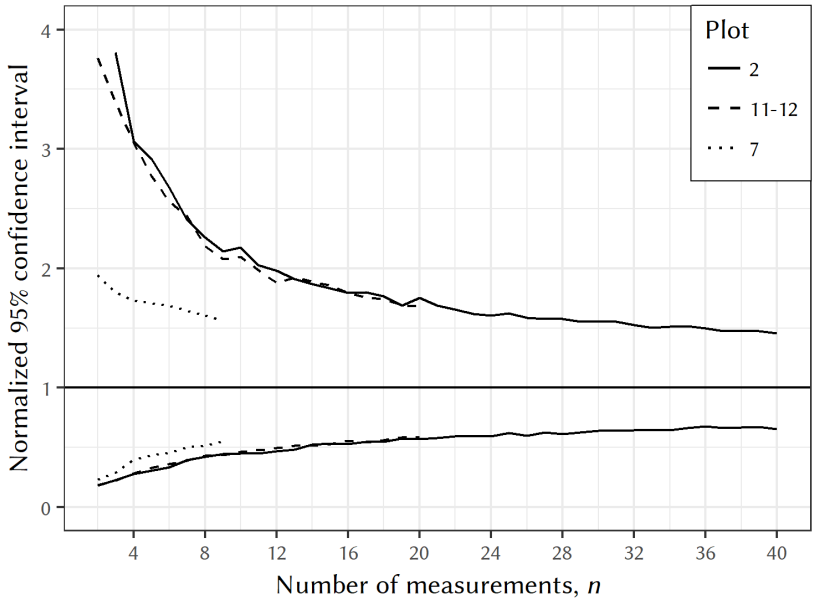

Figure 6.6 - Normalized 95 % confidence intervals of the saturated hydraulic conductivity geometric mean K_s obtained via non-parametric bootstrap method for 3 grassy plots.

because of the different values of the geometric mean of the three plots (Table 6.2), it does not affect the results in terms of the reliability exhibited by the same value of n with changing areas. Specifically, for $n = 6$ the widths of the confidence intervals without normalization by the geometric mean have different trends (29.7, 34.8 and 21.3 $\mathrm{mm\,h^{-1}}$ for plots 7, 11-12 and 2, respectively), but the corresponding average relative errors of the geometric means of the three plots (62, 107 and 117 %, respectively), confirm a higher reliability of the geometric mean estimates for smaller areas. These findings are likely related to the lower variability captured in grassy fields when a smaller area is sampled while, in larger areas, local soil heterogeneities (e.g. macropores, wormholes, cracks, local slope) have a higher chance to be encountered. Furthermore, the differences appear to be fairly limited if plots 11-12 and 2 are compared in terms of both the width of the normalized 95 % confidence interval (Figure 6.6) and the average relative errors. This suggests that, beyond a certain extent, all the local soil heterogeneities characterizing the plot are captured.

Our study does not involve a specific analysis of spatial correlations be-

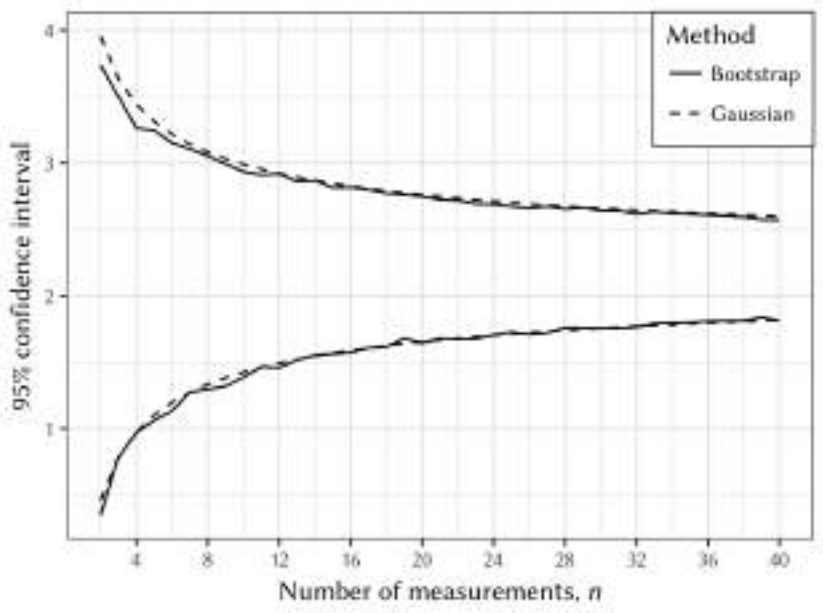

Figure 6.7 - 95 % confidence interval of the saturated hydraulic conductivity geometric mean obtained applying the non-parametric bootstrap method (solid curve) and for a Gaussian variable (dashed curve). Plot 2, log-transformed data.

cause of the relatively small number of samples on the smaller plots. The hypothesis of independent observations, upon which the bootstrap method is based, was adopted following Ahmed et al. (2015).

Based on the hypothesis of independent data, the confidence interval of plot 2, characterized by a statistically significant sample, was also computed adopting a Gaussian distribution for the log-transformed K_s data. Its trend is shown in Figure 6.7 together with that provided by the non-parametric bootstrap method applied to log-transformed K_s data. As expected, no significant differences can be observed.

Figure 6.8 shows the reduction of the confidence interval with increasing number of measurements for the three plots. The reduction was obtained as the difference between the width of the non-normalized confidence interval associated with n measurements and the width associated with $n - 1$ measurements. On every plot, the reduction is large for small n. For example, if 4 measurements are used to calculate the confidence interval instead of 3, the width of the confidence interval decreases by 5, 7 and 4.3 $\mathrm{mm\,h^{-1}}$ for

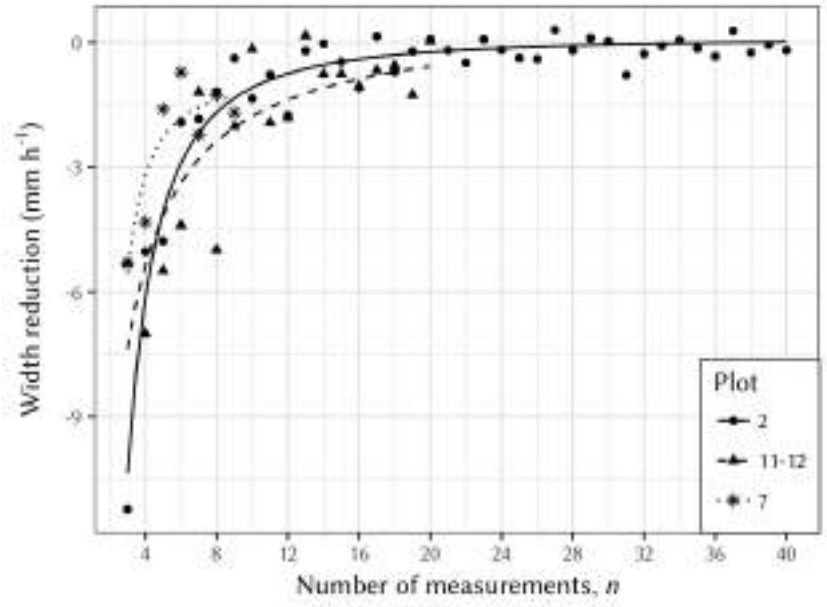

Figure 6.8 - Reduction of the width of the non-normalized confidence interval of the saturated hydraulic conductivity geometric mean obtained using one extra measurement in the bootstrap method. For a specific n the corresponding point represents the difference between the width associated with n measurements and with $n-1$ measurements.

plots 2, 11-12 and 7, respectively. On the other hand, as n increases, the reduction decreases and tends asymptotically towards zero. This is particularly evident from the interpolated curve of plot 2, even though the same behavior is detected for plots 11-12 and 7. From this it can be deduced that the benefit – in terms of width reduction – gained by performing one extra measurement on each plot is high for small n and decreases with plot extent up to a point, specific to each plot, where the average reduction rate becomes almost constant, i.e. the interpolated curve becomes horizontal. Therefore, the n associated with this point can be considered as the minimum number of measurements necessary to enter the "zone" where the confidence interval is stable. For example, the interpolated curve of plot 2 is almost constant for n greater than 12, suggesting that the reduction of the confidence interval width for more than 12 measurements is negligible.

A further remark concerns the possible influence of spatial correlations on the analysis. The presence of spatial correlations would have the effect of

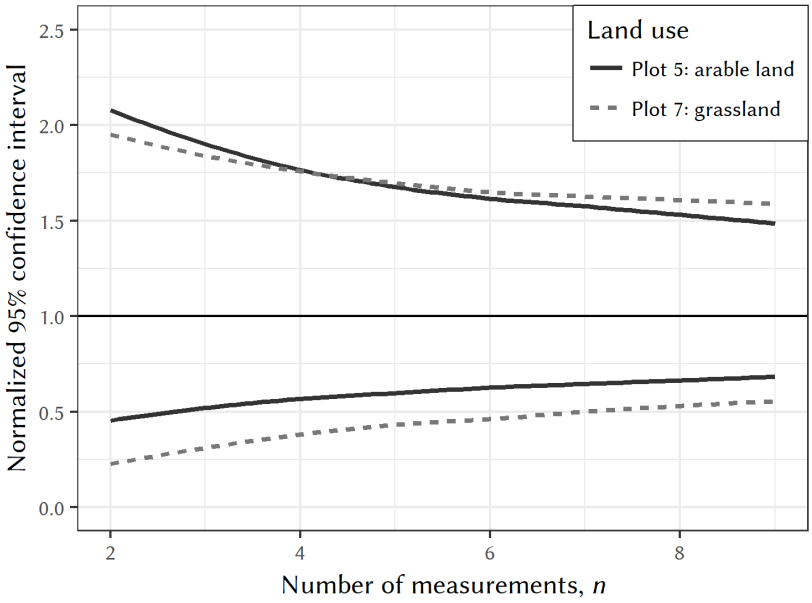

Figure 6.9 - Normalized 95 % confidence intervals by the K_s geometric mean, obtained via the non-parametric bootstrap method for a grassy and an arable plot. The x-axis represents the number of measurements used for each plot.

reducing the width of the confidence interval for a specific n as compared to uncorrelated data ("single realization case" of Skøien and Blöschl, 2006). The same confidence in the estimates of the geometric mean would be therefore achieved with a smaller number of observations. Consequently, the minimum number of measurements would depend on the spatial correlation structure of the plot investigated which would make the application of our results to other areas difficult. On the other hand, the assumption of independent data allows to transfer the results regardless of the plot correlation structure, even though they may represent an upper limit of the density of the required measurements if correlations are present.

In order to gain insight into the relationship between grassy and arable fields in terms of accuracy in the $\bar{K}_s$ estimation, the same uncertainty analysis was carried out on plots 5 and 7, which possess the same number of observations, the same area, but different land use. Figure 6.9 shows that the confidence intervals for the grassland areas are wider than for the arable areas, independently of the number of measurements n used for the derivation,

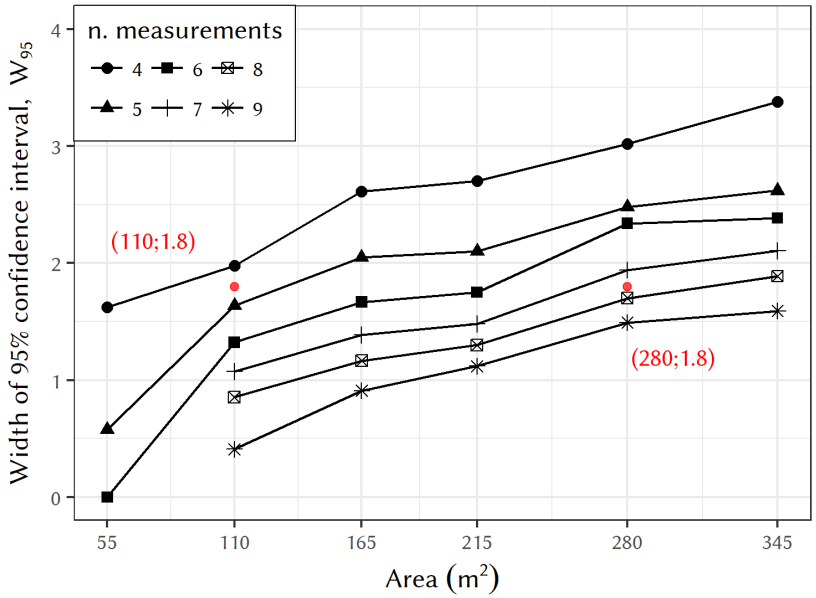

Figure 6.10 - Width of the 95 % confidence intervals normalized by the saturated hydraulic conductivity, K_s, geometric mean plotted against plot size. Lines represent the number of measurements used for the evaluation of the confidence interval and the geometric mean.

which is due to the larger variability of K_s in the grassland areas highlighted in the spatial analysis (§ 6.3.1). This result justifies the choice of focusing the consecutive analysis only on grassy fields, because, for the same plot size, the minimum number of measurements derived for natural conditions always ensures a greater accuracy in arable environments.

In planning a field campaign one must decide the number and the location of the measurements in relation to the time required to collect a single observation and the time available. The second step of the uncertainty analysis is aimed at assisting in that choice. In order to be able to compare the combined effect of plot size and number of measurements on the accuracy of the final areal estimation of $\bar{K}_s$, six sub-plots were derived from plot 2 in an attempt to minimize the differences between the analyzed areas. Ideally, the only distinguishing aspects of the sub-plots are size and total number of measurements available. For each sub-plot the 95 % confidence intervals of $\bar{K}_s$ normalized by the geometric mean of the specific sub-plot was generated through the non-parametric bootstrap method. The width of the normalized 95 % con-

fidence interval, W_{95}, obtained with a specific number of measurements n as a function of the plot size is shown in Figure 6.10. On a plot of specific dimensions, a better estimate of the average saturated hydraulic conductivity can be achieved by increasing the number of measurements in the area, in accordance with the findings of Skøien and Blöschl (2006). For example, if a plot of 165 m^2 is sampled at 5 locations, the width of the confidence interval is about twice the average K_s, but if 8 measurements are made on the same plot the width is halved (slightly less than $1 \cdot \bar{K}_s$), i.e. the reliability associated with the $\bar{K}_s$ estimation is almost doubled. On the other hand, when the same number of samples is taken in increasing areas, the width of the confidence interval increases as well, indicating how the samples progressively lose the ability of representing the true value of $\bar{K}_s$. If 7 measurements are performed over an area of 110 m^2, the width of the confidence interval is $1.1 \cdot \bar{K}_s$, but the uncertainty almost doubles whenever the same number of samples is taken on a plot of 345 m^2 ($W_{95} = 2.1 \cdot \bar{K}_s$).

As mentioned before, the confidence intervals are obtained with the non-parametric bootstrap method which is based on the hypothesis of independent data. Although the increase in uncertainty with increasing areas could be partially due to a progressive decorrelation, this is not the case because in the derivation of the confidence intervals spatial correlations are not considered. One possible explanation may be the increased likelihood of encountering soil local heterogeneities in larger areas. Additionally, if one considers a sub-area of plot 2 of 120 m^2 the contained measured K_s are characterized by a variance of about 170 $mm^2\,h^{-2}$. When the sub-area is extended up to 300 m^2 the variance increases as well and it is equal to 350 $mm^2\,h^{-2}$. Finally, if the sub-area is further extended up to 450 m^2 the variance reaches the value of 410 $mm^2\,h^{-2}$, and for greater areas the variance value fluctuates in the range 350-400 $mm^2\,h^{-2}$. This trend confirms that when the sampled area increases more variability is encountered and therefore the uncertainty on the estimation of the K_s geometric mean value increases as well.

Figure 6.10 is also useful to derive a minimum number of samples that have to be taken in an area of specific dimensions for a tradeoff between accuracy (or uncertainty) and time required for the measurements. Selection of the accuracy level should consider the expected $\bar{K}_s$ value of the study since

the average error is relative to it. For example, if a width of 1.5 is selected for a silty loam soil, for which a K_s of about $1.6\,\mathrm{mm\,h^{-1}}$ is expected (Corradini et al., 1997), the estimated value of $\bar{K}_s$ can vary on average between 0.4 and $2.8\,\mathrm{mm\,h^{-1}}$. However, if the same width is chosen for a sandy loam soil, for which a K_s of about $25\,\mathrm{mm\,h^{-1}}$ is expected (Corradini et al., 1997), the estimated value of $\bar{K}_s$ will vary on average between 6.25 and $43.75\,\mathrm{mm\,h^{-1}}$. Furthermore, the level of accuracy should be selected in relation to the final purpose of the measurement campaign. For instance, if the peak discharge of a stream is to be estimated by a rainfall-runoff model with the intention of designing a weir system along the stream, required accuracy of $\bar{K}_s$ could be inferred from the required accuracy of the flood estimate by error propagation.

The accuracy level suggested by (Ahmed et al., 2015) varies in the range of 1.8-2.2. When the reference value is taken as 1.8, Figure 6.10 suggests that for a plot of $110\,\mathrm{m^2}$ at least 5 measurements are needed to obtain a width of the normalized 95 % confidence interval equal to or smaller than the reference value. Similarly, on a plot of $280\,\mathrm{m^2}$ at least 8 samples should be taken in order to estimate average saturated hydraulic conductivity.

Chapter 7

Determination of a pedotransfer function for field-scale saturated hydraulic conductivity

The assessment of K_s is essential at the field scale to properly represent the effect of soil heterogeneity on the infiltration process in distributed rainfall-runoff models. Area infiltration models, such as those of Smith and Goodrich (2000) (§ 2.4.1) or Govindaraju et al. (2001) (§ 2.4.2), have in common the essential requirement of a spatial characterization of K_s, which in the absence of sampled data can be synthetically approximated by a log-normal random field with values of $\bar{K}_s$ and $CV(K_s)$ fixed in advance.

Measurements of K_s observed in-situ through classical devices are always influenced by local discontinuities in soil matrix, such as cracks, worm holes or roots which often determine preferential flow paths for infiltration (Picciafuoco et al., 2018b). Only recently a global database of infiltration measurements useful to investigate the problems linked with the determination of K_s has been assembled (Rahmati et al., 2018).

An alternative approach to estimate K_s at the point scale relies upon the use of pedotransfer functions (§ 3.2.1). The complexity of existing PTFs varies from simple tables that provide hydraulic parameters for particular textural classes (Wösten et al., 1995; Tietje and Hennings, 1996), i.e. class pedotransfer functions, to linear regression-based approaches (Minasny et al., 1999;

Pachepsky et al., 2001), and artificial neural networks (ANN) models (Schaap et al., 2001; Parasuraman et al., 2006; Sedaghat et al., 2016), i.e. continuous pedotransfer functions.

As above-mentioned, in order to apply models for estimating field-scale infiltration, K_s as a random variable can be represented through $\bar{K}_s$ and $CV(K_s)$ of each catchment region. In principle, the last two quantities could be estimated using pedotransfer functions. However, PTFs already developed allow to derive K_s only at the point scale and therefore (i) a procedure of upscaling, linked with the spatial resolution of the available soil properties, or alternatively (ii) a formulation of PTFs able to provide directly $\bar{K}_s$ should be set out. In addition, criteria useful to predict $CV(K_s)$ at the field scale by PTFs should be defined. The objectives 3 and 4 (§ 1) of this investigation have been addressed by approach (ii) set up by the following methodology.

7.1 Training and testing data-sets

The K_s observations collected at the HOAL catchment (Tables 4.4 and 6.1) were used to derive a new data-set used for calibrating and validating two PTFs. The results obtained in § 6.3.2 suggest that the minimum number of measurements necessary for estimating a representative geometric mean value of saturated hydraulic conductivity, $\bar{K}_s$, in a plot of 80 m^2 is six. Such a number of samples corresponds to a width of the normalized 95 % confidence interval of $\bar{K}_s$ of about 1, meaning that the uncertainty associated to the non-normalized $\bar{K}_s$ estimate is equal to $1 \cdot \bar{K}_s$. Following these results, in each of the 12 measurement plots (Figure 4.8), sub-areas of approximately 80 m^2 were considered and the contained K_s observations were averaged six at a time. Henceforth, the geometric mean calculated from six K_s values averaged over 80 m^2 is termed field-scale saturated hydraulic conductivity, $\bar{K}_s^f$. In addition, values of *om*, *cl*, *si*, *sa*, *s* and *el* derived from the sampled nodes (Figure 4.8) included in the sub-areas were averaged and together with the $\bar{K}_s^f$ data constituted the database used for calibrating and validating the pedotransfer function. Table 7.1 summarizes the basic statistics of the aforementioned database. The average error on the mean of the $\bar{K}_s^f$ values (equal to 13.2 mm h^{-1}) obtained with six measurements is equal to 6.6 mm h^{-1},

Table 7.1 - Basic statistics of the complete database. Min = minimum value; Max = maximum value; Mean = arithmetic mean; St.dev = standard deviation; *CV* = coefficient of variation; *om* = organic matter content; *cl* = clay content; *si* = silt content; *sa* = sand content; *s* = slope angle; *el* = elevation; $\bar{K}_s^f$ = field-scale saturated hydraulic conductivity.

Statistics	*om* (%)	*cl* (%)	*si* (%)	*sa* (%)	(°)	*el* (m a.s.l.)	$\bar{K}_s^f$ (mm h^{-1})
Min	1.9	18.2	69.3	6.3	3.5	263.6	2.7
Max	3.2	22.8	73.7	10.2	8.9	314.7	48.6
Mean	2.6	20.3	70.8	8.9	6.1	272.7	13.2
St.dev.	0.3	0.9	1.2	1.0	0.8	14.2	9.5
CV (%)	9.6	4.2	1.6	10.9	13.3	5.2	71.8

therefore it is considered acceptable for this investigation because it produces deviations of the geometric mean within the observed $\bar{K}_s^f$ domain.

Bearing in mind that averaged values are being considered, it is possible to note the little variation of soil textural properties: *om* and *sa* coefficients of variation stand at about 10 % indicating limited spatial variability of the two parameters across the measurement plots, not to mention *cl* and *si* percentages which are characterized by even smaller *CV*s, equal to 4.2 % and 1.7 %, respectively. Furthermore, slope angles and elevation vary little across the measurement plots as well. Notwithstanding small changes in soil characteristics, $\bar{K}_s^f$ ranges over two orders of magnitude with a minimum of 2.7 mm h^{-1}, a maximum of 48.6 mm h^{-1} and a *CV* of 71.8 %.

Nevertheless, possible relationships between $\bar{K}_s^f$ and the other examined soil properties can be traced in Figure 7.1. The field-scale saturated hydraulic conductivity has a positive trend in relation to *si* and *el*, whereas it exhibits a negative relationship with *om*, *sa* and *s*. Almost no connection can be observed between $\bar{K}_s^f$ and *cl*. The presence of a significant relationship between the field-scale saturated hydraulic conductivity values and the respective soil attributes justifies the choice of further analyzing this bond through the development of a pedotransfer function.

In order to calibrate and validate a PTF the complete database was split in two parts: approximately 2/3 of the data constituted the training data-set used to calibrate the coefficients of the pedotransfer function, while the remaining

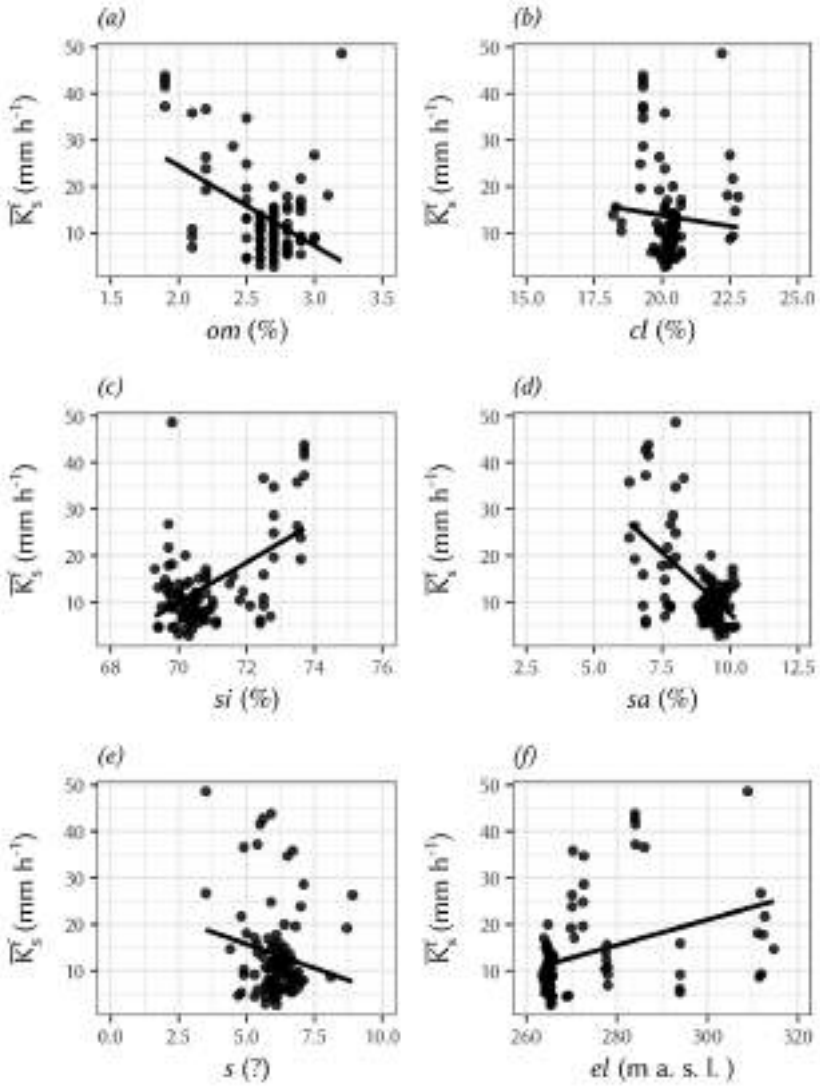

Figure 7.1 - Field-scale saturated hydraulic conductivity, $\bar{K}_s^f$, plotted against (a) organic matter content, *om*; (b) clay content, *cl*; (c) silt content, *si*; (d) sand content, *sa*; (e) slope angle, *s*; (f) elevation, *el*.

1/3 of the data constituted the testing data-set used for validating the derived PTF. The testing data-set was generated from the complete database by carefully selecting the observations in order to meet the following requirements: (a) at least one observation from each measurement plot must be present in the training data-set and (b) the selection must be performed according to the probability distribution of the data.

Finally, the definition of the coefficients of the PTF was carried out with a regression technique over the training data-set. Due to the absence of information on parameters frequently used in the definition of a pedotransfer function for saturated hydraulic conductivity such as bulk density, soil water content, and total or effective porosity (Ahuja et al., 1984; Jabro, 1992; Spychalski et al., 2007), in order to improve the prediction capabilities, the parameters *om*, *cl*, *si*, *sa* were also considered raised to the power of two as can be found in many published PTFs (Brakensiek et al., 1984; Saxton et al., 1986; Wösten et al., 1999). This choice could have the consequence of introducing a certain degree of collinearity among the independent variables, condition that was checked as described in the following section.

7.2 Development of the pedotransfer function for $\bar{K}_s$

In order to calibrate a PTF to estimate an unknown parameter (dependent variable) on a training data-set composed of both the dependent variable and the independent ones, regression techniques are often employed.

Consider the standard model for multiple linear regression,

$$\boldsymbol{y} = \boldsymbol{X}\boldsymbol{\beta} + \boldsymbol{\varepsilon} \tag{7.1}$$

where the matrix of regressors $\boldsymbol{X}$ is $(n \times p)$ and rank p, the unknown parameter vector $\boldsymbol{\beta}$ is $(p \times 1)$, the vector of dependent variables $\boldsymbol{y}$ is $(n \times 1)$, and the error vector $\boldsymbol{\varepsilon}$ is $(n \times 1)$.

The objective is finding the $\boldsymbol{\beta}$ that minimizes the sum of squared errors:

$$\min_{\boldsymbol{\beta}} ||\boldsymbol{y} - \boldsymbol{X}\boldsymbol{\beta}||_2^2 \tag{7.2}$$

where the subscript 2 indicates the L2-norm of the vector. Assuming that $\boldsymbol{\varepsilon}$ is normally distributed, with $\mathrm{E}(\boldsymbol{\varepsilon}) = 0$ and $\mathrm{Var}(\boldsymbol{\varepsilon}) = \sigma^2$, and that the errors are uncorrelated the ordinary least squares (OLS) estimator $\hat{\boldsymbol{\beta}}$ of $\boldsymbol{\beta}$ is:

$$\hat{\boldsymbol{\beta}} = \left(\boldsymbol{X}'\boldsymbol{X}\right)^{-1}\boldsymbol{X}'\boldsymbol{y} \tag{7.3}$$

The $\left(\boldsymbol{X}'\boldsymbol{X}\right)^{-1}$ matrix always exists if the regressors are linearly independent, that is, if no column of the $\boldsymbol{X}$ matrix is a linear combination of the other columns. It can also be demonstrated that the variance-covariance matrix of the regression coefficients is:

$$\text{Var}(\hat{\boldsymbol{\beta}}) = \sigma^2 \left(\boldsymbol{X}'\boldsymbol{X}\right)^{-1} \tag{7.4}$$

If we let $\boldsymbol{C} = \left(\boldsymbol{X}'\boldsymbol{X}\right)^{-1}$, the variance of the $\hat{\beta}_j$ coefficient is $\sigma^2 C_{j,j}$ and the covariance between $\hat{\beta}_i$ and $\hat{\beta}_j$ is $\sigma^2 C_{i,j}$. Finally, the vector of fitted values $\hat{\boldsymbol{y}}$ corresponding to the observed values $\boldsymbol{y}$ is:

$$\hat{\boldsymbol{y}} = \boldsymbol{X}\hat{\boldsymbol{\beta}} \tag{7.5}$$

Inferences such as those illustrated can be easily performed when the regressors are orthogonal, i.e. there is no linear relationship among them. However, when there are near-linear dependencies among the regressors the inferences can be misleading or erroneous and the model is said to be affected by multicollinearity. In such circumstances, the $\boldsymbol{C}$ matrix tends to infinity and the regression coefficients (7.3) and their variance-covariance matrix (7.4) become very large and may change erratically in response to small changes in the model or the data. According to Wold et al. (1984) ridge regression is one of the methods that can be used to accomplish a stabilization of the regression estimates. In order to stabilize the parameter and to control the general instability associated with the least squares estimates, one can use:

$$\hat{\boldsymbol{\beta}}^* = \left[\boldsymbol{X}'\boldsymbol{X} + k\boldsymbol{I}\right]^{-1} \boldsymbol{X}'\boldsymbol{y} \tag{7.6}$$

where $\boldsymbol{I}$ is the identity matrix ($p \times p$), $\hat{\boldsymbol{\beta}}^*$ is the ridge regression estimator of $\boldsymbol{\beta}$, and $k > 0$ is a positive quantity added to the diagonal of $\boldsymbol{X}'\boldsymbol{X}$. The ridge estimator can also be considered as the solution of the least squares problem with penalty $k||\boldsymbol{\beta}||_2^2$

$$\min_{\boldsymbol{\beta}} = ||\boldsymbol{y} - \boldsymbol{X}\boldsymbol{\beta}||_2^2 + k||\boldsymbol{\beta}||_2^2 \tag{7.7}$$

The parameter k is the Lagrange multiplier used to resolve the minimization problem, and represents the bias introduced in order to reduce both the

variance associated to the regression coefficients and the magnitude of the coefficients themselves, as such it is named shrinkage parameter. In order to account for possible different units among the regressors, the components of the $\boldsymbol{X}$ matrix are often standardized by subtracting from each $x_{i,j}$ the corresponding column means (m_j) and dividing the results by the column standard deviations (sd_j). This is particularly helpful when the selection of k is performed observing the ridge trace plot because all the coefficients assume the same magnitude, as explained later.

According to Hoerl and Kennard (1970a,b), the best method for achieving a better estimate of $\hat{\boldsymbol{\beta}}^*$ is using the ridge trace plot to select a single value of k and a unique $\hat{\boldsymbol{\beta}}^*$. The ridge trace is the plot of $\hat{\beta}_j^*$ for increasing k and the selection criterion should consider that (a) coefficients will not have unreasonable absolute values (this is why standardizing $\boldsymbol{X}$ is important), (b) coefficients with apparently incorrect signs at $k = 0$ will have changed to have the proper sign, and (c) coefficients will not significantly change their values beyond the selected k. Furthermore, Golub et al. (1979) suggest the generalized cross-validation (GCV) method as an alternative approach to estimate k. In particular, the optimal k value is the one that minimizes the GCV statistic which can be calculated as (Liu and Jiang, 2012):

$$\mathrm{GCV}(\hat{\boldsymbol{\beta}}^*) = \frac{\left(\boldsymbol{y} - \boldsymbol{X}\hat{\boldsymbol{\beta}}^*\right)' \left(\boldsymbol{y} - \boldsymbol{X}\hat{\boldsymbol{\beta}}^*\right)}{\left(n - \mathrm{tr}(\boldsymbol{H})\right)^2} \tag{7.8}$$

where $\boldsymbol{H} = \boldsymbol{X}\left(\boldsymbol{X}'\boldsymbol{X}\right)^{-1}\boldsymbol{X}'$.

In order to establish if the problem of multicollinearity exists, it is possible to derive the Variance Inflation Factors (VIFs, Marquardt, 1970) defined for the j-th regressor as:

$$\mathrm{VIF}_j = C_{j,j} = \left(1 - R_j^2\right)^{-1} \tag{7.9}$$

where R_j^2 is the coefficient of determination obtained when x_j is regressed on the remaining $p - 1$ regressors; when x_j is nearly linearly dependent on some subset of the remaining regressors, R_j^2 is near unity and $C_{j,j}$ is large. Since the variance of the j-th regression coefficient is $\sigma^2 C_{j,j}$ (7.4), we can view VIF_j as the factor by which the variance of $\hat{\beta}_j$ is increased due to near-linear

dependences among the regressors. According to Montgomery et al. (2012) one or more large VIFs indicate multicollinearity and practical experience indicates that values exceeding 10 are an indication that the associated regression coefficients are poorly estimated.

In this investigation two PTFs were developed. The first PTF, PTF_{MLR}, was derived performing a multiple linear regression (MLR) analysis on a sub-set of independent variables, whose selection is a step of fundamental importance in the regression procedure. In this context, for example Puckett et al. (1985) performed a correlation analysis and computed correlation coefficients between pairs of variables; those properties with correlation coefficients, ρ, greater than 0.7 were selected for the regression. Ferrer Julià et al. (2004) performed a correlation analysis and chose as independent variables those which presented the best correlation values with the dependent variable. In this work the independent variables used to derive the PTF_{MLR} were those presenting at least a "moderate" (Evans, 1996) correlation with the dependent variable $\bar{K}_s^f$. Once the regressors were selected, MLR was performed after having tested the assumptions of normal distribution of the errors and absence of multicollinearity with the Shapiro-Wilk test (Shapiro and Wilk, 1965) and VIFs inspection, respectively. The second PTF, PTF_R, was derived considering as regressors all the independent variables available. As a consequence, multicollinearity in the matrix of regressors was detected by VIFs inspection. Multiple linear regression could not be applied and therefore the ridge regression technique was chosen to calibrate the pedotransfer function.

7.2.1 Evaluation criteria

In order to compare the results of the developed PTFs during the calibration and validation phases their accuracy and reliability were analyzed. Following Pachepsky et al. (1998), accuracy is considered as the correspondence between measured and estimated data for the data-set from which a PTF has been developed, and reliability as the correspondence between measured and estimated data for data-sets other than the one used to develop a PTF. In this study, the accuracy of the PTFs was evaluated in the calibration phase, while the reliability was evaluated in the validation step, through the

Root Mean Square Error (RMSE):

$$\text{RMSE} = \sqrt{\frac{1}{N}\sum_{i=1}^{N}\left(\log_{10}\left(\bar{K}^{f}_{s_{m,i}}\right) - \log_{10}\left(\bar{K}^{f}_{s_{e,i}}\right)\right)^{2}} \tag{7.10}$$

and the Geometric Mean Error Ratio (GMER):

$$\text{GMER} = \exp\left(\frac{1}{N}\sum_{i=1}^{N}\ln(\epsilon_i)\right) \tag{7.11}$$

where subscript m stands for "measured data" and subscript e for "estimated data", N is the number of data points, and ϵ is the error ratio calculated as:

$$\epsilon_i = \frac{\bar{K}^{f}_{s_{e,i}}}{\bar{K}^{f}_{s_{m,i}}} \tag{7.12}$$

A RMSE of 0 corresponds to a perfect match between observed and estimated values while the optimal value of GMER is 1. A less than 1 GMER indicates underestimation of the predictive model.

7.3 Generation of a continuous map

Using the pedotransfer functions, $\bar{K}_s$ maps were estimated at a resolution of 25×25 m to minimize the effect of the interpolation step – whose influence in the prediction increases as the map resolution gets finer – and to highlight the performance of PTFs considered. Two alternative approaches were adopted (Figure 7.2). The first option, method A, consisted of first spatially interpolating the independent variables available on the 50×50 m grid onto the 25×25 m grid and then applying a PTF at the 25×25 m grid. The second option, method B, consisted of first applying the PTF to estimate $\bar{K}_s$ on the locations where the independent variables are known (i.e., the 50×50 m grid), and then spatially interpolating those values to obtain the 25×25 m $\bar{K}_s$ grid. The spatial interpolation technique used in both methods was the ordinary kriging (Matheron, 1963).

Finally, a visual comparison of the $\bar{K}_s$ maps of the catchment obtained was carried out, along with a quantitative comparison with the measured $\bar{K}_s$. The

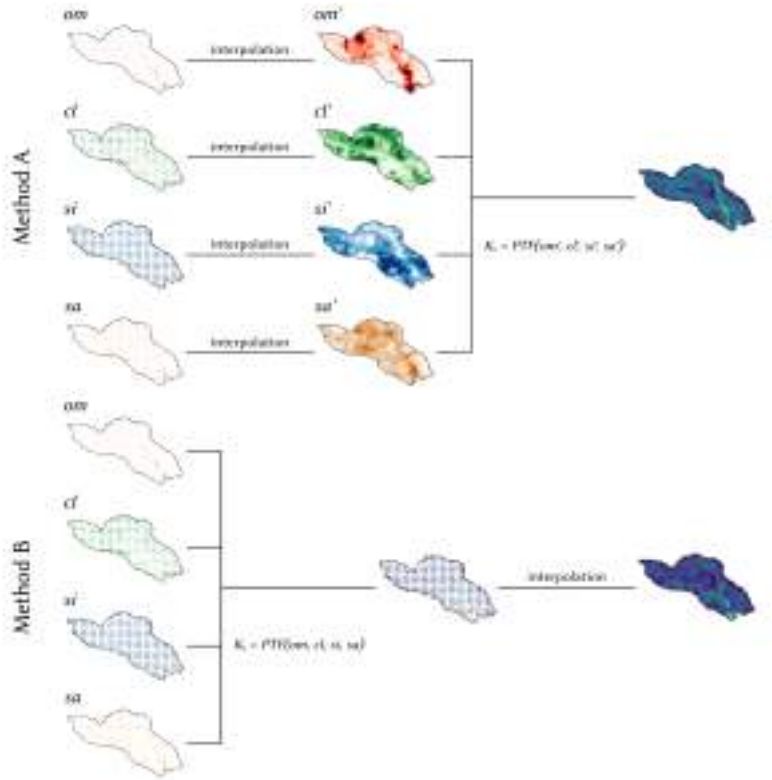

Figure 7.2 - Qualitative illustration of the steps followed by the two methods: A, the PTF is applied to the interpolated independent variables and B, the PTF is applied to punctual data and then interpolation is performed.

latter was performed with the purpose of having a criterion to establish which combination of PTF and methodology (A or B) performed better in terms of reproducing $\bar{K}_s$ spatial variability. However, it was not used for quantitatively evaluating the correspondence between measured and predicted values as the measured $\bar{K}_s$ are associated with a support area of 80 m^2, while the $\bar{K}_s$ of each pixel of the maps are associated with a support area of 625 m^2.

7.4 Results

7.4.1 PTF calibration and validation

The first pedotransfer function, PTF_{MLR}, has been calibrated through multiple linear regression technique. A correlation analysis has been performed

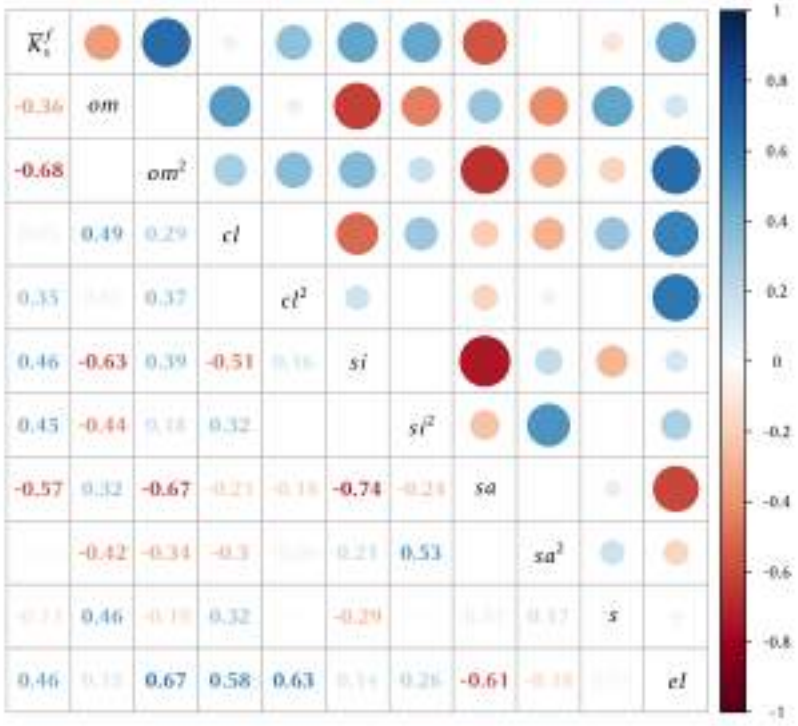

Figure 7.3 - Correlation matrix among the different parameters available: field-scale saturated hydraulic conductivity, $\bar{K}_s^f$, organic matter content, om, the square of the organic matter content, om^2, clay content, cl, the square of the clay content, cl^2, silt content, si, the square of the sil content, si^2, sand content, sa, the square of the sand content, sa^2, slope angle, s, and elevation, el. The size of the circles is proportional to the correlation coefficient ρ, while the color scale goes from very strong positive correlation (blue) towards zero correlation (white) down to very strong negative correlation (red).

in order to establish the existing level of correlation between the dependent variable, $\bar{K}_s^f$, and the other independent variables available. Figure 7.3 shows the correlation among the different possible regressors: the color scale goes from very strong positive correlation (blue) towards zero correlation (white) down to very strong negative correlation (red). According to Evans (1996) only om^2 presents a strong correlation with $\bar{K}_s^f$, while moderate correlation can be detected in relation to si, si^2, sa and el and weak or very weak correlation exists between $\bar{K}_s^f$ and om, cl, cl^2, sa^2 and s. For such reason in the development of the PTF_{MLR} only those parameters at least moderately correlated (i.e., ρ greater than 0.4) to the dependent variable were chosen as regressors.

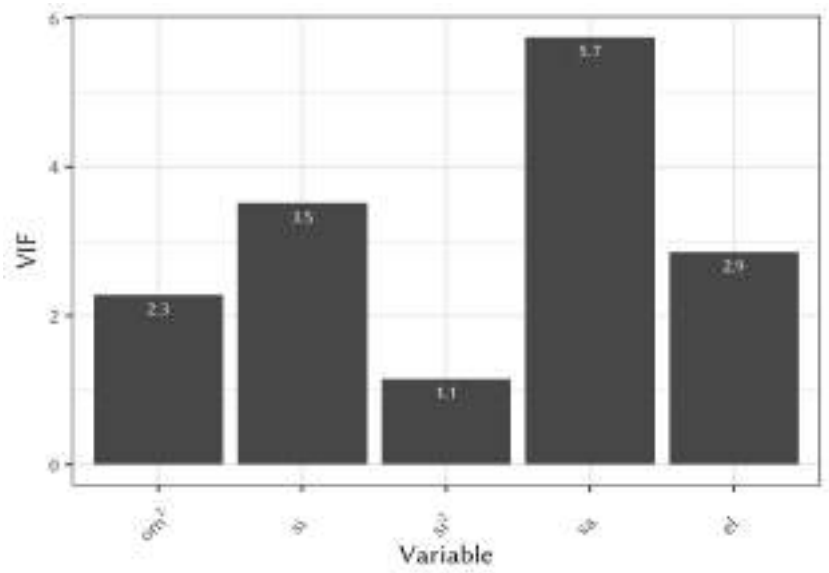

Figure 7.4 - Variance inflation factors (VIF) associated to the regressors chosen to develop the pedotransfer function via multiple linear regression (PTF_{MLR}). The independent variables are the square of the organic matter content, om^2, the silt content, si, the square of the silt content, si^2, the sand content, sa, and the elevation, el.

Estimates of the $\hat{\beta}_j$ regression coefficients have been carried out applying equation (7.3) on the training data-set (results can be found in appendix A) and successively verifying the assumptions of normally-distributed errors by means of the Shapiro-Wilk test (Shapiro and Wilk, 1965), and of absence of multicollinearity in the matrix $\boldsymbol{X}$ by analyzing the variance inflation factors associated to the different regressors. Figure 7.4 shows the magnitude of the VIF_j factors, i.e. the indices that quantify how much the variances associated to the $\hat{\beta}_j$ estimated regression coefficients are affected by near-linear dependencies among the regressors. Since all the VIFs assumed values of the same order of magnitude and equal to or lower than the empirical limit of 10 (Montgomery et al., 2012), it could be concluded that multicollinearity was not affecting the problem.

The final step concerned the application of the newly-developed PTF_{MLR} to both the training and the testing data-sets and the determination of the evaluation criteria in order to assess the pedotransfer function accuracy and reliability. At first, equation (A.1) has been applied to the training data-set to

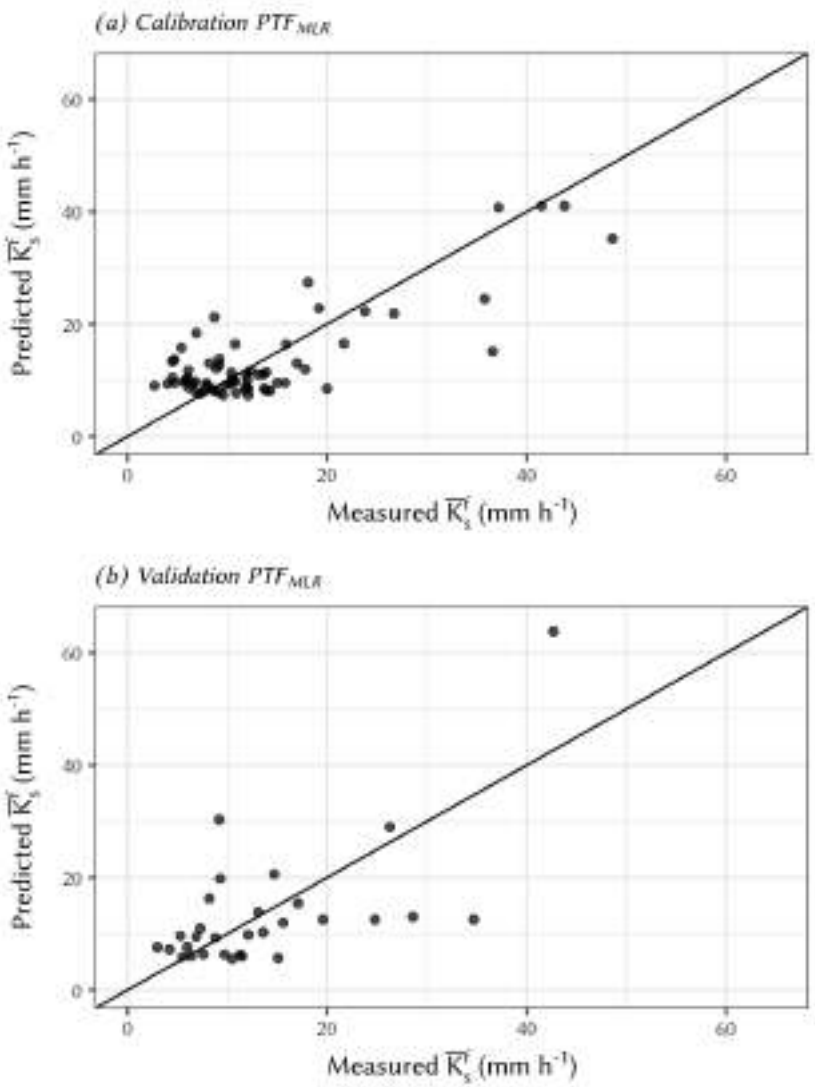

Figure 7.5 - Measured versus predicted field-scale saturated hydraulic conductivity, $\bar{K}_s^f$, values obtained applying the pedotransfer function derived with multiple linear regression (PTF_{MLR}) to the training (a) and testing (b) data-sets. The black line is the 1:1 line.

estimate the very same observations the pedotransfer function was developed with. Figure 7.5a shows the results of the calibration procedure, the closer the points are to the black line the higher is the accuracy of the PTF_{MLR}. The accuracy of the PTF_{MLR} is remarkable for $\bar{K}_s^f$ lower than approximately 20 mm h^{-1} while a tendency to underestimate the measured values can be observed for $\bar{K}_s^f$ ranging between 20 mm h^{-1} and 40 mm h^{-1}. The overall

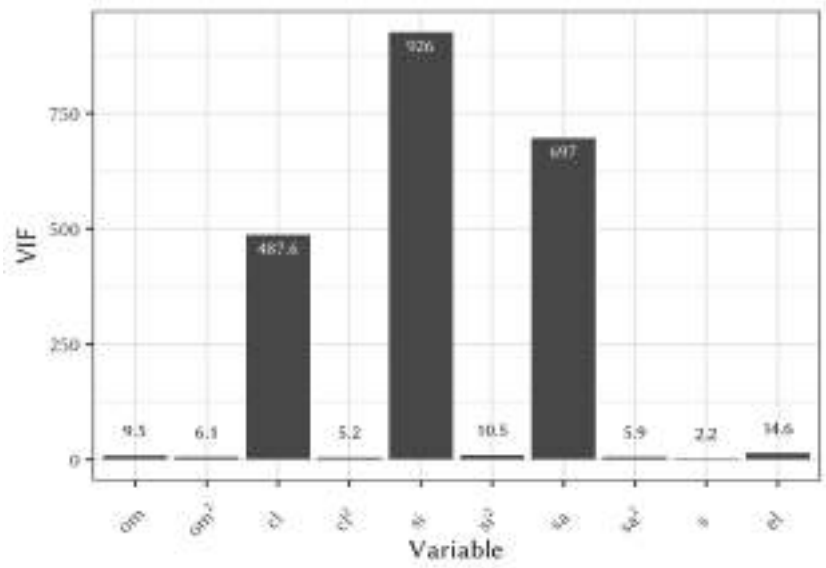

Figure 7.6 - Variance inflation factors (VIFs) associated to the regressors chosen to develop the pedotransfer function via ridge regression (PTF_R). The independent variables are the organic matter content, *om*, the square of the organic matter content, om^2, the clay content, *cl*, the square of the clay content, cl^2, the silt content, *si*, the square of the silt content, si^2, the sand content, *sa*, the square of the sand content, sa^2, the slope angle, *s*, and the elevation, *el*.

performance is quantified by a RMSE equal to 0.21 and a GMER of 1.09, both values supporting the suitability of the multiple linear regression as they are close to the optimum figures (0 and 1, respectively). Successively, equation (A.1) has been applied to the testing data-set in order to validate the PTF_{MLR} and to evaluate its reliability in predicting $\bar{K}_s^f$ values other than those used in the calibration (Figure 7.5b). Similarly to the calibration data-set, the measured $\bar{K}_s^f$ are adequately predicted up to approximately $20\,\mathrm{mm\,h^{-1}}$ whereas a clear propensity to underestimate the observed values is traceable for $\bar{K}_s^f$ between $20\,\mathrm{mm\,h^{-1}}$ and $40\,\mathrm{mm\,h^{-1}}$. The indices RMSE and GMER for the validation data-set assume the values of 0.24 and 0.98, respectively, resulting comparable with those obtained during the calibration stage.

The second pedotransfer function, PTF_R, has been calibrated considering all the available independent variables. In this case MLR technique could not be applied. In fact, the assumptions of normal distribution of the errors and absence of multicollinearity should be met, however from the inspection of the VIFs associated to the matrix $\boldsymbol{X}$ (Figure 7.6) it becomes obvious that

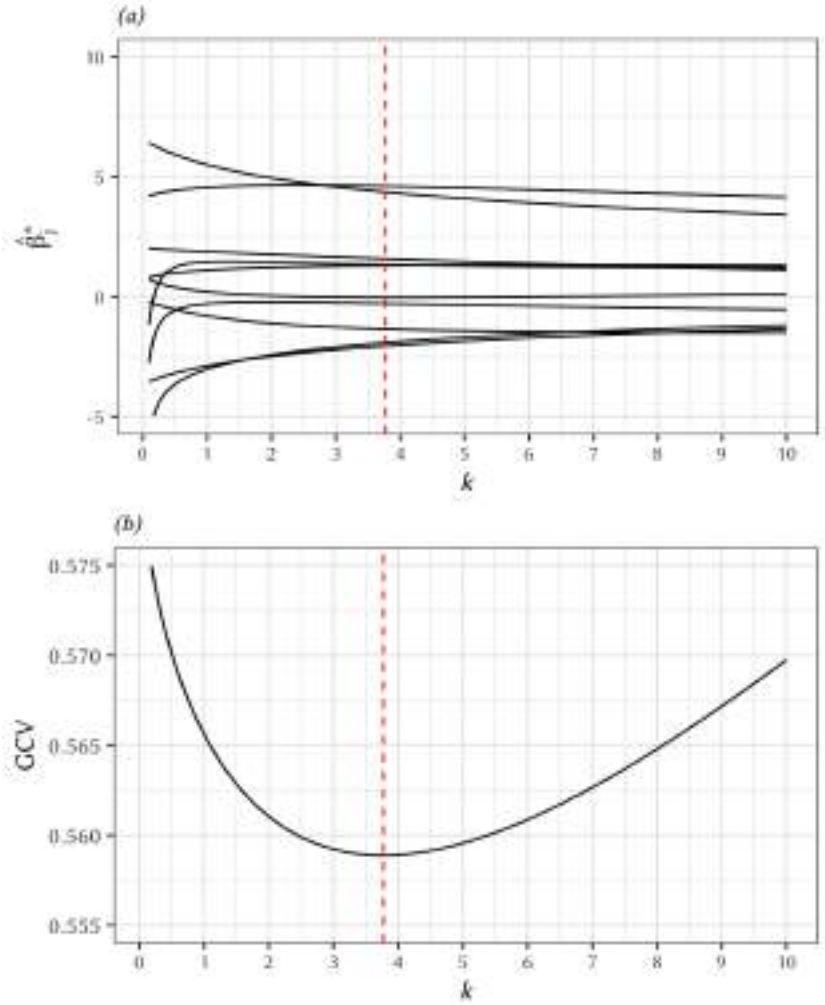

Figure 7.7 - Shrinkage parameter k selection: (a) the ridge trace plot represents how a single regression coefficient $\hat{\beta}_j^*$ changes for different possible shrinkage parameters; (b) the minimum GCV statistic is associated to the best shrinkage parameter.

multicollinearity is affecting the system because five out of ten VIFs have a value greater than the empirical limit of 10. Moreover, the factors associated to *cl*, *si* and *sa* are two orders of magnitude larger than the others, indicating that if a multiple linear regression was applied the corresponding resulting coefficients would have large variances and thus poor prediction capability.

Therefore, ridge regression has been employed and both the methods suggested by Hoerl and Kennard (1970a,b) and Golub et al. (1979) have been applied to select the shrinkage parameter k. The ridge trace plot (Figure 7.7a)

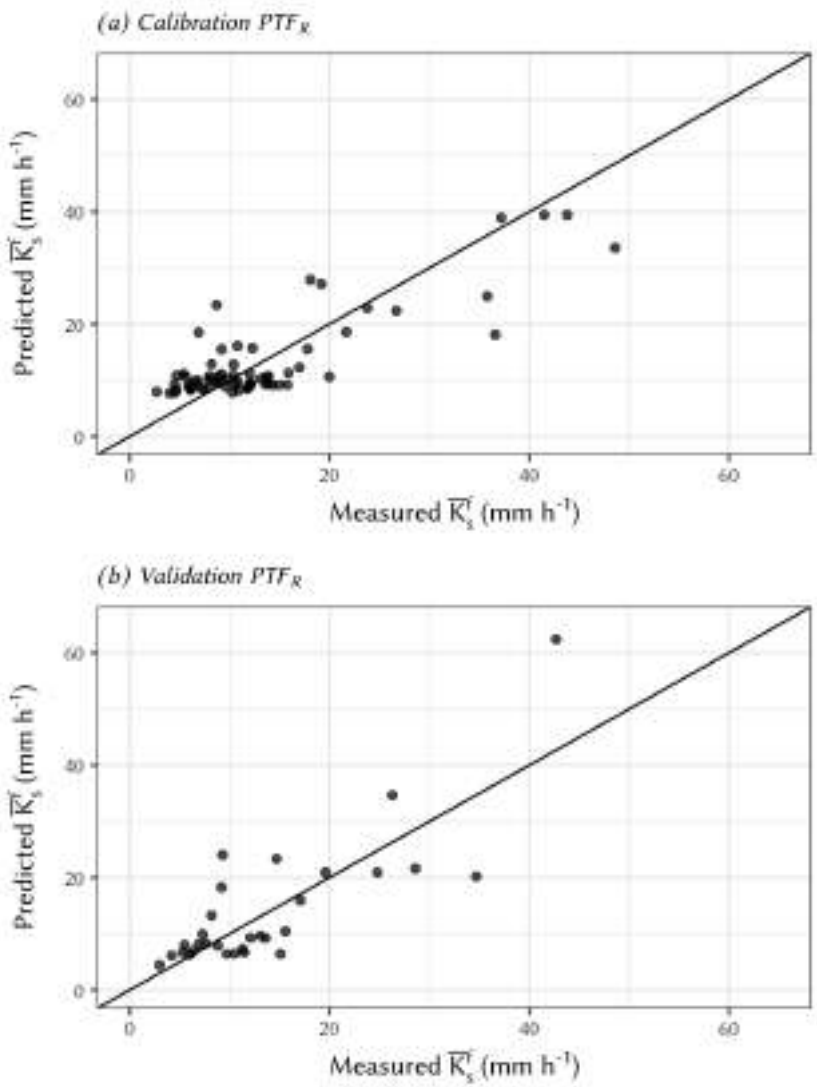

Figure 7.8 - Measured versus predicted field-scale saturated hydraulic conductivity, $\bar{K}_s^f$, values obtained applying the pedotransfer function derived with ridge regression (PTF_R) to the training (a) and testing (b) data-sets. The black line is the 1:1 line.

has been obtained calculating through equation (7.6) several $\hat{\boldsymbol{\beta}}^*$ for multiple trial values of k ranging from 0 to 10 and each line of the plot represents how a single coefficient $\hat{\beta}_j^*$ changes for different possible shrinkage parameters. Similarly, the GCV-k plot (Figure 7.7b) was generated with equation (7.8) using the same trial shrinkage parameters and thus the same $\hat{\boldsymbol{\beta}}^*$. Finally, the selected k has been the one that provided the smallest GCV which, at the

same time, also satisfied the conditions for the k selection by using the ridge trace plot set out in Hoerl and Kennard (1970a,b).

Successively, the developed PTF_R (A.2) has been applied to the training data-set in order to evaluate the calibration phase performance. Figure 7.8a shows a remarkable accuracy for$\bar{K}_s^f$ lower than approximately 30 mm h^{-1} and a slight tendency to underestimate the measured values greater than 30 mm h^{-1}. The calibration RMSE and GMER are equal to 0.18 and 1.09, respectively. Similarly, equation (A.2) has been applied to the testing data-set in order to validate the PTF_R and to evaluate its reliability in predicting $\bar{K}_s^f$ values other than those used in the calibration (Figure 7.8b). In most cases the points lie close to the black line, indicating a very close relationship between measured and predicted values. The indices RMSE and GMER of the validation phase assume the values of 0.18 and 1.01, respectively, hence comparable with those obtained during the calibration stage.

7.4.2 Maps generation

The two pedotransfer functions developed present similar performance in terms of RMSE and GMER in both the calibration and the validation stages, although the PTF_R produces errors which on average are smaller than those obtained with the PTF_{MLR}. In order to be able to provide a complete characterization of the differences of the two regression methodologies applied, a comparison of the maps generated for the whole catchment has been also carried out.

Method A provides for the application of the PTF to the spatially interpolated independent variables which were obtained by applying the ordinary kriging technique to the values of *om*, *cl*, *si* and *sa* available on the nodes of the 50×50 m grid. The experimental variograms were fitted with an exponential model because it provided the smallest residual sum of squares, as suggested in Oliver and Webster (2014). Figure 7.9 shows the catchment $\bar{K}_s$ map obtained by applying PTF_{MLR} to the interpolated independent variables with a spatial resolution of 25×25 m. The majority of the predicted values lie on the blue portion of the color scale, i.e. around 20 mm h^{-1}, while a few appear to be greater than 40 mm h^{-1} or smaller than 20 mm h^{-1}. Table 7.2

Table 7.2 - Basic statistics of the $\bar{K}_s$ values of the maps obtained applying the PTFs derived with both the multiple linear regression technique (PTF_{MLR}) and the ridge regression technique (PTF_R). Min = minimum value; Max = maximum value; Mean = arithmetic mean; St.dev = standard deviation; *CV* = coefficient of variation.

	Method A		Method B	
Statistics	PTF_{MLR}	PTF_R	PTF_{MLR}	PTF_R
Min ($mm\,h^{-1}$)	10.7	2.7	7.4	1.0
Max ($mm\,h^{-1}$)	45.6	43.9	43.8	56.7
Mean ($mm\,h^{-1}$)	15.0	14.5	14.6	13.9
St.dev. ($mm\,h^{-1}$)	1.9	5.7	3.0	5.9
CV (%)	12.7	36.8	20.5	42.4

summarizes the basic statistics evaluated on the $\bar{K}_s$ predicted values, the minimum is 10.7 $mm\,h^{-1}$ while the maximum is 45.6 $mm\,h^{-1}$, and the coefficient of variation is equal to 12.7 % which is rather unusual for saturated hydraulic conductivity, even considering averaged values. Figure 7.10 is the result of the application of PTF_R to the spatially interpolated independent variables. Although the majority of the predicted $\bar{K}_s$ values lie in the central portion of the color scale, the map is characterized by a higher spatial variability compared to Figure 7.9. The higher spatial variability is also reflected by a *CV* of 36.8 % (Table 7.2) and a wider variation range characterized by a minimum of 2.7 $mm\,h^{-1}$ and a maximum of 43.9 $mm\,h^{-1}$.

Successively, method B was adopted for generating a continuous $\bar{K}_s$ map of the study area. The first step was the application of the two PTFs to the independent variables measured on the nodes of the 50×50 m grid, while the second step was the application of the ordinary kriging spatial interpolation technique to derive a $\bar{K}_s$ continuous map with a spatial resolution of 25×25 m. The exponential model was used to fit the empirical variograms obtained with both PTF_{MLR} and PTF_R because in either case it provided the smallest residual sum of squares. Figure 7.11 is the map generated from the spatial interpolation of the $\bar{K}_s$ values when PTF_{MLR} was applied. The minimum value of the $\bar{K}_s$ predicted (Table 7.2) is 7.4 $mm\,h^{-1}$, which is smaller compared to the minimum obtained with the same PTF but method A. Similar observations can

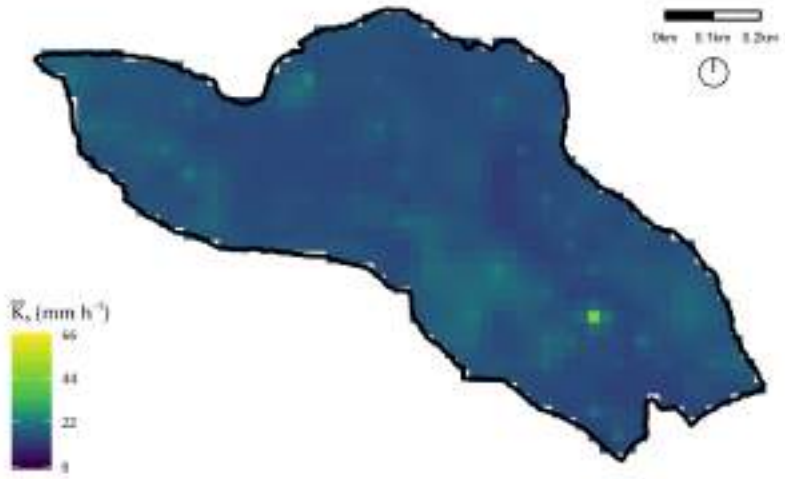

Figure 7.9 - Map of the study area obtained using the pedotransfer function obtained with multiple linear regression (PTF_{MLR}) and method A (first spatial interpolation of the independent variables and then application of the PTF).

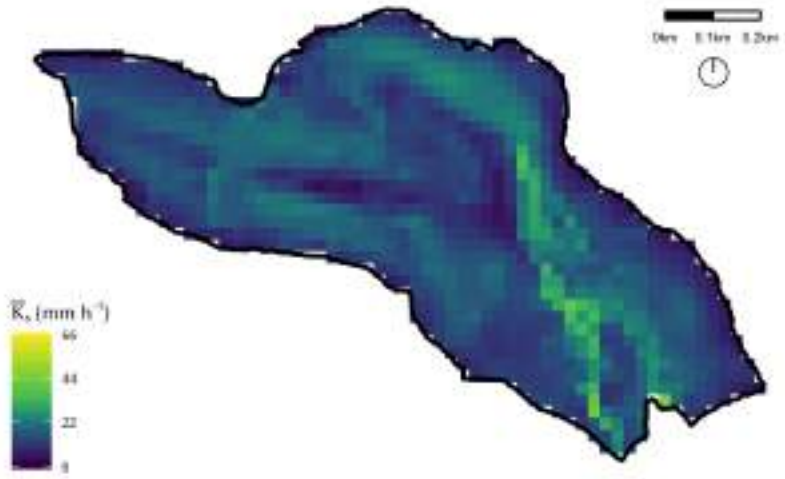

Figure 7.10 - Map of the study area obtained using the pedotransfer function obtained with ridge regression (PTF_R) and method A (first spatial interpolation of the independent variables and then application of the PTF).

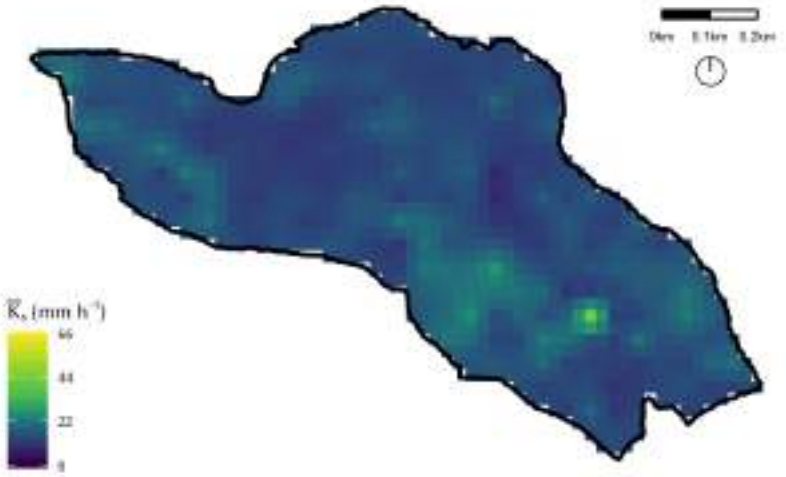

Figure 7.11 - Map of the study area obtained using the pedotransfer function obtained with multiple linear regression (PTF_{MLR}) and method B (first application of the PTF to the independent variables and then spatial interpolation).

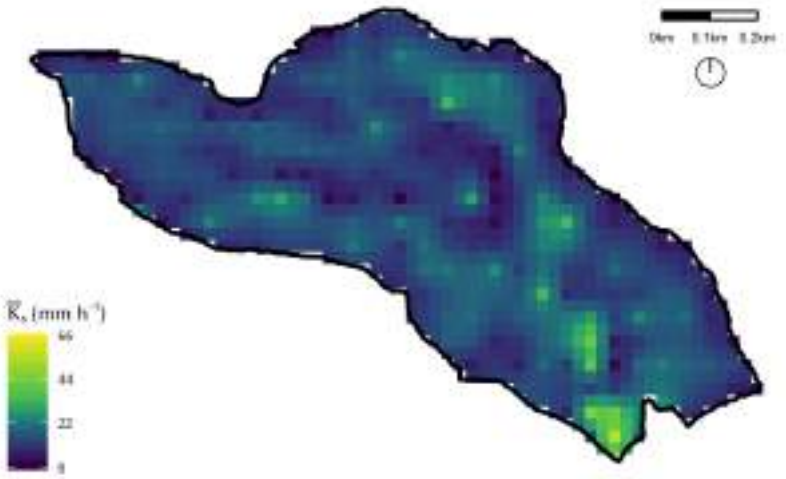

Figure 7.12 - Map of the study area obtained using the pedotransfer function obtained with ridge regression (PTF_R) and method B (first application of the PTF to the independent variables and then spatial interpolation).

be made about the maximum value which is equal to 43.8 mm h^{-1} and smaller than the one obtained with method A. The map is also characterized by a higher spatial variability compared to the one in Figure 7.9, traceable in a less uniform color distribution and in a greater CV of 20.5 %. Finally, Figure 7.12 is the resulting map achieved with method B and PTF_R. The spatial distribution of the $\bar{K}_s$ predicted values appears more random and thus less influenced by the catchment morphology compared to the map obtained with the same PTF but method A (Figure 7.10). The variation range is the widest among all the maps generated ought to a minimum value of 1 mm h^{-1} and a maximum of 56.7 mm h^{-1} (Table 7.2), as well as the CV, equal to 42.4 %.

7.5 Discussion

A moderate correlation is detected among $\bar{K}_s^f$ and soil characteristics which is fairly anticipated due to the close relationship between infiltration and soil composition. Texture alone was reported to be a good predictor of saturated hydraulic conductivity in sandy soils (Jaynes and Tyler, 1984; El-Kadi, 1985) and clay content was the principal parameter to be correlated with K_s in Puckett et al. (1985). In the present case however, clay content exhibits scarce correlation to $\bar{K}_s^f$ which makes it unsuitable for the regression analysis. On the other hand, organic matter content is found to be a good predictor of field-scale saturated hydraulic conductivity, as it was for Rawls et al. (1982, 1983) and Wösten et al. (1999) who successfully used it as PTF input. A strong relationship between *om* and K_s is not always observed, in fact Ferrer Julià et al. (2004) detected almost no correlation between them in their study to construct a saturated hydraulic conductivity map of Spain. Nevertheless, they decided to use *om* as input in the developed PTF due to the well-known influence of this soil characteristic on water behavior. The negative correlation with *sa* is unusual, however it can be explained by the fact that the locations of the measurements presenting low values of sand percentage also coincide with those areas of the catchment where agricultural practices take place. In the study area, land management operations have the effect of increasing the maximum values observed Picciafuoco et al. (2018b) and this is the reason why higher $\bar{K}_s^f$ values correspond to low percentages

of sand and not the opposite as one would expect.

7.5.1 PTF calibration and validation

The soil textural and topographical characteristics are used for calibrating and validating two pedotransfer functions for estimating the geometric mean saturated hydraulic conductivity using two different regression techniques. Textural composition is often used as predictor for saturated hydraulic conductivity as well as other soil parameters such as effective porosity, bulk density or saturated soil moisture (Saxton et al., 1986; Wösten, 1997; Suleiman and Ritchie, 2001; Spychalski et al., 2007), but unfortunately this extra information was not available in this study. On the other hand, slope was hardly ever used as predictor despite its well-known influence on infiltration (Morbidelli et al., 2018).

In both cases, $\mathrm{PTF_{MLR}}$ and $\mathrm{PTF_R}$, the calibration procedure (Figure 7.5a and Figure 7.8a) is successful for $\bar{K}_s^f$ values lower than approximately 30 mm h^{-1}. Due to the characteristic log-normal shape of the $\bar{K}_s^f$ probability density function the majority of the observations assume values lower than 30 mm h^{-1} making the regression more accurate in this area of the measured-predicted plane. On the contrary, regression for $\bar{K}_s^f$ greater than 30 mm h^{-1} appears to be less accurate, with measured values always underestimated with $\mathrm{PTF_R}$; the performance is slightly better if $\mathrm{PTF_{MLR}}$ is applied. Overall, the average errors committed in the calibration stage by the two PTFs are comparable, being the RMSE equal to 0.21 and 0.18 for $\mathrm{PTF_{MLR}}$ and $\mathrm{PTF_R}$, respectively, and they are in accordance with those that can be found in literature. For example, Schaap and Leij (1998) used neural network-based PTFs to predict saturated hydraulic conductivity from different sets of soil properties including texture, bulk density, and retention points at 10 and 33 kPa. They obtained RMSE indices in the calibration stage ranging from 0.83, if only texture was used, to 0.66 if all the variables were utilized in the prediction. Parasuraman et al. (2006) employed artificial neural networks to model K_s at the field scale of two distinct sites using bulk density and sand, silt and clay contents. The RMSEs obtained in the calibration stage ranged from 0.21 to 0.23 for the first site and from 0.36 to 0.38 for the second site, depending on the input variables

utilized and the ensemble algorithm. Twarakavi et al. (2009) derived a set of four PTFs using the same database utilized to develop the software ROSETTA (Schaap et al., 2001) but applying a new methodology called support vector machines (SVM). They were able to obtain saturated hydraulic conductivity estimates of the training data-set with RMSEs between 0.71 and 0.55 for the four SVM-based PTFs developed.

In the validation stage PTF_R provides better results compared to PTF_{MLR} for $\bar{K}_s^f$ values lower than approximately $10\,mm\,h^{-1}$ (Figure 7.5b and Figure 7.8b), with the points aligned to and closely located to the 1:1 line. The measured values are better predicted by PTF_R also for $\bar{K}_s^f$ between $20\,mm\,h^{-1}$ and $40\,mm\,h^{-1}$, being the points in this interval closer to the bisector, however both PTFs poorly reproduce measured $\bar{K}_s^f$ greater than $40\,mm\,h^{-1}$ likely due to insufficient information in the calibration stage. On average PTF_R provides better predictions compared to PTF_{MLR} that can be quantified by an RMSE equal to 0.18 for the former and equal to 0.24 for the latter, nonetheless the errors committed are comparable with those that can be found in literature. Schaap and Leij (1998) obtained RMSEs relative to the validation stage ranging from 0.84 to 0.71 for the different PTFs developed. Parasuraman et al. (2006) attained RMSEs that varied from 0.20 to 0.23 for the first site and from 0.48 to 0.50 for the second site when the ANN-based PTF was used with the testing data-set. Twarakavi et al. (2009) achieved RMSEs values related to the validation data-set between 0.72 and 0.56 for the four SVM-based PTFs developed.

7.5.2 Maps generation

In terms of map generation capability, the two PTFs developed in this study present substantial differences independently of the method (A or B) chosen. From a merely qualitative analysis, the maps obtained with PTF_{MLR} (Figure 7.9 and Figure 7.11) highlight the scarce aptitude of the function to reproduce the high spatial variability that usually characterizes saturated hydraulic conductivity. At a glance the two charts appear flat in the color pattern as if the catchment were characterized by an almost homogeneous $\bar{K}_s$ distribution. On the other hand, the maps obtained applying PTF_R (Fig-

ure 7.10 and Figure 7.12) appear more varied and definitely more inclined to spatially describe a parameter such K_s which changes erratically within a few meters. In addition, the two maps allow a discussion on the influence of the method (A or B) applied on the final result. It appears that method A is affected by the morphology of the site, in fact the landscape can be easily deduced by Figure 7.10 where the stream and forested areas are characterized by a higher variability while the cultivated areas show more uniform values. This variability pattern is supported by the previous findings of Picciafuoco et al. (2018b) who highlighted how in the study area saturated hydraulic conductivity variability, in terms of CV, reduces of about 25 % in the agricultural areas compared to the forested land. On the other hand, method B seems to be significantly influenced by the location of the soil survey sites (light-grey squares in Figure 4.8) where the independent variables have been measured. In Figure 7.12 many pixels stand out because their value is significantly different from those of the surrounding tiles. Furthermore, those pixels appear to be located on a grid and their locations coincide with the locations where the soil surface has been sampled to measure *om*, *cl*, *si* and *sa*. These results are probably related to the smoothing effect that often affects ordinary kriging estimates (Isaaks and Srivastava, 1989). As a consequence of the smoothing effect, small values are usually overestimated while large values are underestimated. Furthermore, this effect is uneven in space, being zero at the data locations and increases as the location of the estimated point gets further away from the data locations (Journel et al., 2000). The smoothing is less discernible if method A is applied most likely because it affects the estimates of the textural components, which are characterized by a small variability across the catchment $\bar{K}_s$. The application of the pedotransfer function counterbalances the smoothing effect and, as a result, the generated spatial variability of the map presents a less even distribution of the estimates. On the contrary, in method B the spatial interpolation step represents the last phase of the map generation process, therefore the smoothing effect is more apparent because it influences directly the $\bar{K}_s$ estimates.

The qualitative analysis of the maps highlights the inability of $\mathrm{PTF_{MLR}}$ to represent $\bar{K}_s$ spatial variability. However, to fully comprehend which of the two methodologies examined deliver the best result a more quantitative anal-

ysis based on real observations should be carried out. For example, more $\bar{K}$ samples could be taken in areas of the catchment different from those already measured and used for the PTF calibration. These extra samples could be then compared with the maps obtained with methods A and B and evaluation criteria could be calculated to deliver a quantitative comparison. Failing to provide such information at present, the predicted values of average saturated hydraulic conductivity (Table 7.2) can be compared with those obtained averaging the in-situ observations (Table 7.1). Nevertheless, a preliminary remark is necessary: the sampled K_s were averaged on areas of about 80 m^2 while the $\bar{K}_s$ obtained from the application of the two above-mentioned methods are representative of much larger areas (about 625 m^2). For such reason, the following comparison must be handled with care considering it as a discussion aimed at understanding the positive aspects of one methodology applied over the other. In terms of minimum values predicted PTF_R does a better job resulting in $\bar{K}_s$ equal to 2.7 $mm\,h^{-1}$ (A) and 1 $mm\,h^{-1}$ (B) in comparison to 10.7 $mm\,h^{-1}$ (A) and 7.4 $mm\,h^{-1}$ (B) obtained with PTF_{MLR}. In both cases the minima are closer to the one obtained averaging the in-situ observations, equal to 2.7 $mm\,h^{-1}$. However, the maximum $\bar{K}_s$ predicted with PTF_{MLR}, equal to 45.6 $mm\,h^{-1}$ (A) and 43.8 $mm\,h^{-1}$ (B), is more similar to the one actually observed in the field of 48.6 $mm\,h^{-1}$ compared to the maxima obtained with PTF_R, especially when method B is applied. As far as the mean value is concerned, both PTFs provide good estimates regardless of the method applied. The greatest differences though can be observed if CVs are analyzed. A reduction of the coefficient of variation associated to the PTF-derived values compared to the one observed averaging the in-situ measurements is expected because of the different scales that characterize the two quantities compared. Nonetheless, the CVs achieved utilizing PTF_{MLR}, equal to 12.7 % (A) and 20.5 % (B), are much lower compared to those obtained with PTF_R, equal to 36.8 % (A) and 42.4 % (B). Neither of the PTFs developed is capable of reproducing the variability of the original sample, characterized by a CV of 71.8 %, but PTF_R is definitely the one providing the best results. Despite the higher CVs observed when method B is applied, method A provides better results because the derived map is influenced by the catchment morphology, which is what one would expect for a map representing the pattern of a soil parameter.

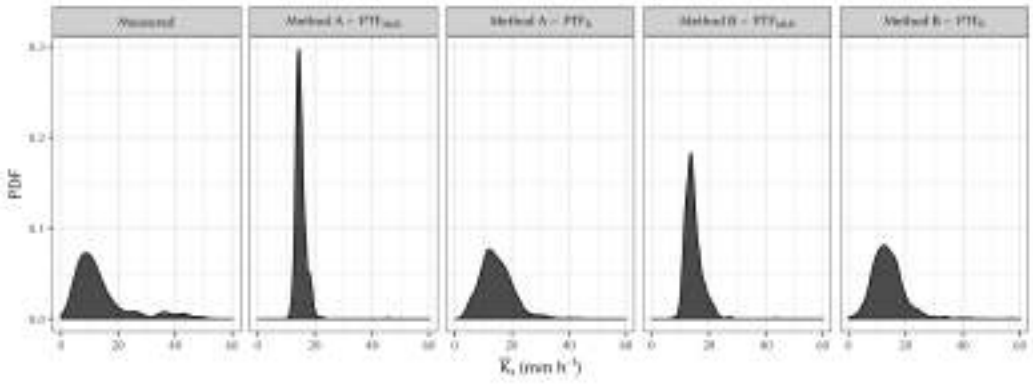

Figure 7.13 - Probability density functions characterizing the set of measured field-scale saturated hydraulic conductivity, $\bar{K}_s^f$, values, and the sets derived from the maps. The maps have been obtained using the pedotransfer functions derived with multiple linear regression (PTF_{MLR}) and ridge regression (PTF_R) and applying methods A (first spatial interpolation of the independent variables and then application of the PTF) and B (first application of the PTF to the independent variables and then spatial interpolation).

The striking argument which delineates PTF_R as the best option is the observations of the different probability density functions (PDFs) associated to the set of $\bar{K}_s$ measured in-situ, $\bar{K}_s^f$, and the sets derived from the maps. Once again, differences in sample size and representative scale between measured and PTF-derived probability density functions should be taken into account and therefore a quantitative analysis is not completely appropriate. However, Figure 7.13 clearly shows, even if in a qualitative manner, that PTF_{MLR} provides PDFs with both methods that dramatically change from the reference one, i.e. the PDF describing the sampled $\bar{K}_s^f$ frequency.

It was demonstrated how the PTF_R developed for the study area allows to derive satisfactory estimates of average saturated hydraulic conductivity, not only in terms of mean but also in terms of variability. The particular soil characteristics of the catchment analyzed offer the opportunity to underline how oftentimes using basic PTFs can lead to profoundly incorrect results. In this particular case, the use of a class pedotransfer function (§ 3.2.1), i.e. PTFs that estimate K_s only from the textural classes as for example the one implemented in the first hierarchical level of the ROSETTA software, would result in a catchment characterized only by three values of $\bar{K}_s^f$ being the 75 % of topsoil classified as silty loam, the 20 % as silty clay loam and 5 % as silt.

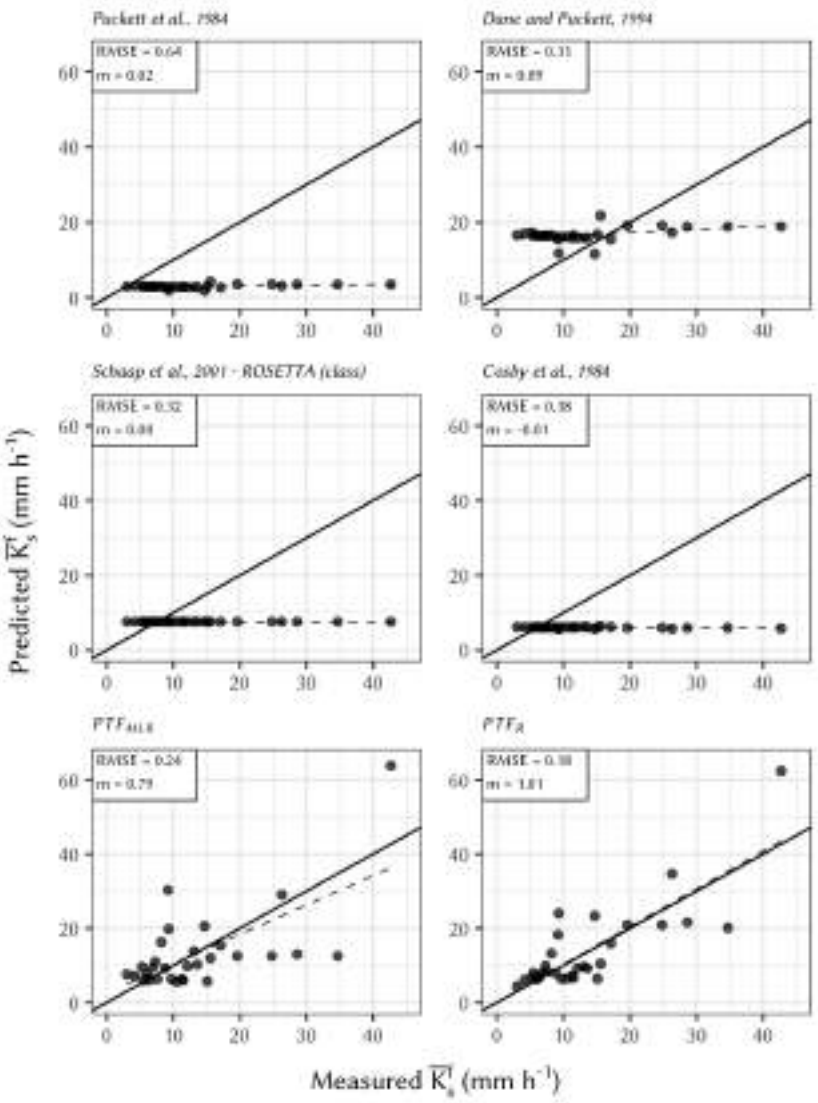

Figure 7.14 - Measured versus predicted field-scale saturated hydraulic conductivity, $\bar{K}_s^f$, values obtained applying literature PTFs (first and second row) and the PTFs developed in this study (third row) to the testing data-set. RMSE is the root mean square error and m is the slope of the fitting line (dashed line). The black line is the 1:1 line.

Even if the RMSE that one would obtain applying the class PTF present in ROSETTA to the testing data-set of this study still assumed an acceptable magnitude, the spatial variability structure of $\bar{K}_s^f$ would be completely lost (Figure 7.14). To strongly remark the necessity of deriving a specific PTF for the interested area instead of using one of those available in literature,

five pedotransfer functions developed for other studies were applied to the testing data-set and their ability in terms of RMSE were compared to those characterizing the PTFs generated in this study (Figure 7.14). As expected all the PTFs developed for different catchments and different scales produce RMSEs higher than those associated to PTF_{MLR} and PTF_{R}, even if the average errors provided for example by the PTFs of Dane and Puckett (1994) and ROSETTA (Schaap et al., 2001) equal to 0.31 and 0.32, respectively, do not significantly deviate from those relative to PTF_{MLR} and PTF_{R}. If only RMSE were considered, one would conclude that the application in the case study of the abovementioned PTFs is feasible, however when the predicted values are analyzed the conclusion would be quite the opposite. If one draws the best fitting line of the points on the measured-predicted plane (dashed line in Figure 7.14) the slope, m, can be used as indicator of the goodness of prediction, the closer m is to 1, the closer the best fitting line is to the bisector, the more accurate are the predictions. It is possible to note that all the PTFs selected from literature generate RMSEs comparable with those that can be found in other studies (Schaap and Leij, 1998; Twarakavi et al., 2009), but the predicted values are extremely inaccurate and vary on a range of few mm h^{-1}, the $\bar{K}_s^f$ variability is not reproduced and the best fitting line is basically horizontal.

Chapter 8

Conclusions

1. The experimental rainfall-runoff approach, with measurements of deep flow obtained in controlled experiments performed at the laboratory and plot scale, has been found to provide a reliable estimate of the areal-average value of K_s. It can be therefore used as a benchmark to compare areal-average estimates obtained through point measurements of K_s carried out at a discrete number of locations with classical devices. The accuracy in the estimate of the areal-average K_s values by each of the three selected devices is not appropriate. The GP leads in any case to large errors, and the CTP gives more limited overestimates but provides an unexpectedly large spatial heterogeneity of K_s in the laboratory soil. It is possible to note that, on the basis of a three-dimensional analysis of infiltration from the disc tension infiltrometer developed by Haverkamp et al. (1994) and Smettem et al. (1994), the equations used in the CTP to estimate K_s from point measurements of cumulative infiltration are not rigorous. However, the estimate of K_s can be only partly affected from the use of inappropriate equations because these cannot justify the unexpected large variability of K_s in the laboratory soil. The DRI provides estimates in the laboratory and at the plot scale but the variability of point measurements at the laboratory scale appears to be more reliable. The K_s spatial variability obtained by point measurements in the plot is linked with the soil heterogeneity even though large differences due to the sensitivity of measurements to small variations

in the standard procedures cannot be excluded. The last conclusion is supported by the results obtained in the laboratory experiments. Thus, although the DRI may be a good tool to capture the nature of the K_s spatial variability, it is required a different calibration to convert individual measurements to realistic values. Since actual values are not always known, this poses a serious challenge. It is important to remark that some factors, indicated as responsible for the conflicting results obtained in previous comparative investigations carried out in natural soils, should not have significantly affected the results of the experiments carried out in this investigation. The processes of sealing and erosion as well as the presence of entrapped air and preferential-flow zones cannot account for the low accuracy of the selected point measurement devices. The causes of the observed discrepancies still remain an open issue that deserves to be addressed before we are able to definitely use these instruments to assess both local measurements and field variability.

2. In order to understand the controls on K_s horizontal variability in agricultural environments the DRI was used considering that this device remains a valid tool to highlight K_s spatial variation because of its low sensitivity to small variations in the standard measurement procedure, which quite often influence measurements in natural environments. Furthermore, the low cost of the instrument, as well as the ease of installation and operation, allowed parallel measurements. While soil texture varies little in the small Austrian catchment, K_s varies by two orders of magnitude, with a minimum of 1 mm h^{-1} and a maximum of 130 mm h^{-1}. The variation range in arable areas is wider than in grassland (pasture, forest) areas. The minima are similar, but the maximum value of K_s on cultivated plots is 50 % greater than those on the grassy plots. Soil management practices and uniform land cover in the cultivated areas are considered the main causes of the lower spatial variability of K_s, with a CV 25 % smaller than in the areas with natural vegetation. An analysis of variance indicates that the main control on the K_s spatial variability has to be ascribed to the land cover. Its influence is also reflected by the fact that two separate PDFs should be considered for

the K_s spatial variability in natural or agricultural settings.
An uncertainty analysis has been also performed to determine the minimum number of measurements necessary for estimating the geometric mean of K_s for a specific area. From the analysis of three grassy plots with the same measurement density, it is clear that the uncertainty, expressed in terms of width reduction of the 95 % confidence interval, decreases rapidly as the number of measurements increases up to a certain value. Here the reduction stabilizes and, after this point, the increase of the number of observations provides little benefit in accuracy. The width of the confidence interval obtained with a specific number of measurements increases with plot size most likely because of the higher chance to encounter soil local heterogeneities such as macropores, wormholes, different root systems or preferential flow paths. However, the increase appears to be limited beyond a certain extent, suggesting that all the local soil heterogeneities characterizing the plot are captured, but further analyses on this should be performed. The chart of the confidence interval width as a function of number of measurements and plot size can be used to assist in sampling design. The chart could be used for estimating the minimum number of DRI measurements in other catchments that exhibit similar geo-morphological characteristics, i.e. an agricultural setting, slope angles less than 10° and silty soils. If spatial correlations of K_s are present, the proposed procedure represents an upper limit of the uncertainty to be expected.

3. The same data-set has been used to develop two pedotransfer functions by the techniques of multiple linear regression and ridge regression. The two predictive functions PTF_{MLR} and PTF_R, respectively, have been compared in terms of accuracy, reliability and capability of reproducing $\bar{K}_s$ variability for map generation. The PTF_R with better estimates and smaller average errors can be considered a valid alternative to the classical multiple linear regression technique. This conclusion is also supported by a comparison of the maps generated for the whole area of interest by applying the two predictive functions together with a spatial interpolation technique required to obtain an appropriate spatial resolution.

4. The maps obtained with two different procedures by the PTF_{MLR} result in an almost uniform distribution of hydraulic conductivity which is not realistic in the study catchment. On the other hand, the corresponding maps generated with the PTF_R have a much more variable spatial pattern and a more reliable coefficient of variation. Furthermore, the statistical characteristics of the PTF_R-related maps are similar to those associated with the original $\bar{K}_s$ measurements. Finally, the procedure with interpolation of the input soil parameters and successive application of the PTF_R provides a $\bar{K}_s$ map influenced by the catchment morphology, which is what one would expect for a map representing the pattern of a soil parameter.

Acknowledgements

The author would like to acknowledge financial support provided by the Austrian Science Funds (FWF) as part of the Vienna Doctoral Programme on Water Resource Systems (DK W1219-N22) and the Italian Ministry of Education, University and Research (PRIN 2015).

Bibliography

Abdelbaki, A. M. (2016), "Using automatic calibration method for optimizing the performance of Pedotransfer functions of saturated hydraulic conductivity", *Ain Shams Engineering Journal*, 7, (2), 653-662, DOI: 10.1016/j.asej.2015.05.012.

Ahmed, F., J. S. Gulliver, and J. Nieber (2015), "Field infiltration measurements in grassed roadside drainage ditches: Spatial and temporal variability", *Journal of Hydrology*, 530, 604-611, DOI: 10.1016/j.jhydrol.2015.10.012.

Ahuja, L. R., S. A. El-Swaify, and A. Rahman (1976), "Measuring Hydrologic Properties of Soil With a Double-ring Infiltrometer and Multiple-depth Tensiometers." *Soil Science Society of America Journal*, 40, (4), 494-499, DOI: 10.2136/sssaj1976.03615995004000040016x.

Ahuja, L. R. (1983), "Modeling Infiltration into Crusted Soils by the Green—Ampt Approach", *Soil Science Society of America Journal*, 47, (3), 412-418, DOI: 10.2136/sssaj1983.03615995004700030004x.

Ahuja, L. R., J. W. Naney, and D. R. Nielsen (1984), "Scaling Soil Water Properties and Infiltration Modeling", *Soil Science Society America Journal*, 48, (5), 970-973, DOI: 10.2136/sssaj1984.03615995004800050003x.

Ahuja, L. R., F. Fiedler, G. H. Dunn, J. G. Benjamin, and A. Garrison (1998), "Changes in Soil Water Retention Curves Due to Tillage and Natural Reconsolidation", *Soil Science Society of America Journal*, 62, (5), 1228-1233, DOI: 10.2136/sssaj1998.03615995006200050011x.

Alletto, L. and Y. Coquet (2009), "Temporal and spatial variability of soil bulk density and near-saturated hydraulic conductivity under two contrasted tillage management systems", *Geoderma*, 152, (1-2), 85-94, DOI: 10.1016/j.geoderma.2009.05.023.

Angulo-Jaramillo, R., J.-P. Vandervaere, S. Roulier, J.-L. Thony, J.-P. Gaudet, and M. Vauclin (2000), "Field measurement of soil surface hydraulic properties by

disc and ring infiltrometers: A review and recent developments", *Soil and Tillage Research*, 55, (1-2), 1-29, DOI: 10.1016/S0167-1987(00)00098-2.

Armstrong, R. A., S. V. Slade, and F. Eperjesi (2000), "An introduction to analysis of variance (ANOVA) with special reference to data from clinical experiments in optometry", *Ophthalmic and Physiological Optics*, 20, (3), 235-241, DOI: 10.1046/j.1475-1313.2000.00502.x.

Arya, L. M., D. A. Farrell, and G. R. Blake (1975), "A Field Study of Soil Water Depletion Patterns in Presence of Growing Soybean Roots : I . Determination of Hydraulic Properties of the Soil", *Soil Science Society of America Journal*, 39, 424-430, DOI: 10.2136/sssaj1975.03615995003900030021x.

Arya, L. M. and J. F. Paris (1981), "A Physicoempirical Model to Predict the Soil Moisture Characteristic from Particle-Size Distribution and Bulk Density Data1", *Soil Science Society of America Journal*, 45, (6), 1023-1030, DOI: 10.2136/sssaj1981.03615995004500060004x.

Assouline, S. and Y. Mualem (1997), "Modeling the dynamics of seal formation and its effect on infiltration as related to soil and rainfall characteristics", *Water Resources Research*, 33, (7), 1527-1536, DOI: 10.1029/96WR02674.

Assouline, S. and Y. Mualem (2002), "Infiltration during soil sealing: The effect of areal heterogeneity of soil hydraulic properties", *Water Resources Research*, 38, (12), 22–1–22-9, DOI: 10.1029/2001WR001168.

Assouline, S. and Y. Mualem (2006), "Runoff from heterogeneous small bare catchments during soil surface sealing", *Water Resources Research*, 42, (12), DOI: 10.1029/2005WR004592.

Bagarello, V., M. Iovino, and D. Elrick (2004), "A Simplified Falling-Head Technique for Rapid Determination of Field-Saturated Hydraulic Conductivity", *Soil Science Society of America Journal*, 68, (1), 66-73, DOI: 10.2136/sssaj2004.0066.

Bagarello, V., G. Baiamonte, M. Castellini, S. Di Prima, and M. Iovino (2014), "A comparison between the single ring pressure infiltrometer and simplified falling head techniques", *Hydrological Processes*, 28, (18), 4843-4853, DOI: 10.1002/hyp.9980.

Baiamonte, G., V. Bagarello, F. D'Asaro, and V. Palmeri (2017), "Factors Influencing Point Measurement of Near-surface Saturated Soil Hydraulic Conductivity in a Small Sicilian Basin", *Land Degradation & Development*, 28, (3), 970-982, DOI: 10.1002/ldr.2674.

Basha, H. A. (2011a), "Infiltration models for semi-infinite soil profiles", *Water Resources Research*, 47, (8), DOI: 10.1029/2010WR010253.

Basha, H. A. (2011b), "Infiltration models for soil profiles bounded by a water table", *Water Resources Research*, 47, (10), DOI: 10.1029/2011WR010872.

Bear, J. (1972), *Dynamics of Fluids in Porous Media*, New York.

Blöschl, G., A. P. Blaschke, M. Broer, C. Bucher, G. Carr, X. Chen, A. Eder, M. Exner-Kittridge, A. Farnleitner, A. Flores-Orozco, P. Haas, P. Hogan, A. Kazemi Amiri, M. Oismüller, J. Parajka, R. Silasari, P. Stadler, P. Strauss, M. Vreugdenhil, W. Wagner, and M. Zessner (2016), "The Hydrological Open Air Laboratory (HOAL) in Petzenkirchen: a hypothesis-driven observatory", *Hydrology and Earth System Sciences*, 20, (1), 227-255, DOI: 10.5194/hess-20-227-2016.

Blöschl, G. and M. Sivapalan (1995), "Scale issues in hydrological modelling: A review", *Hydrological Processes*, 9, (3-4), 251-290, DOI: 10.1002/hyp.3360090305.

Boers, T. M., F. J. M. P. van Deurzen, L. A. A. J. Eppink, and R. E. Ruytenberg (1992), "Comparison of infiltration rates measured with an infiltrometer, a rainulator and a permeameter for erosion research in SE Nigeria", *Soil Technology*, 5, (1), 13-26, DOI: 10.1016/0933-3630(92)90003-J.

Boisvert, J., T. Pultz, R. Brown, and B. Brisco (1996), "Potential of Synthetic Aperture Radar for Large-Scale Soil Moisture Monitoring: A Review", *Canadian Journal of Remote Sensing*, 22, (1), 2-13, DOI: 10.1080/07038992.1996.10874632.

Bonell, M., B. K. Purandara, B. Venkatesh, J. Krishnaswamy, H. A. K. Acharya, U. V. Singh, R. Jayakumar, and N. Chappell (2010), "The impact of forest use and reforestation on soil hydraulic conductivity in the Western Ghats of India: Implications for surface and sub-surface hydrology", *Journal of Hydrology*, 391, (1-2), 47-62, DOI: 10.1016/j.jhydrol.2010.07.004.

Bouma, J. (1987), "Transfer functions and threshold values: from soil characteristics to land qualities. Workshop on Quantified Land Evaluation Process", *International Institute for Aerosphere Survey and Earth Science*, 6, 106-110.

Bouma, J., P. Droogers, M. P. W. Sonneveld, C. J. Ritsema, J. E. Hunink, W. W. Immerzeel, and S. Kauffman (2011), "Hydropedological insights when considering catchment classification", *Hydrology and Earth System Sciences*, 15, (6), 1909-1919, DOI: 10.5194/hess-15-1909-2011.

Brakensiek, D. L., W. J. Rawls, and G. R. Stephenson (1984), "Modifying SCS hydrologic soil groups and curve numbers for rangeland soils", *ASAE paper no. PNR-84203*.

Breusch, T. S. and A. R. Pagan (1979), "A Simple Test for Heteroscedasticity and Random Coefficient Variation", *Econometrica*, 47, (5), 1287-1294, DOI: 10.2307/1911963.

Brooks, R. H. and A. T. Corey (1964), "Hydraulic Properties of Porous Media", *Hydrologic Paper No. 3*, 27.

Brown, R. N., C. Percivalle, S. Narkiewicz, and S. DeCuollo (2010), "Relative rooting depths of native grasses and amenity grasses with potential for use on roadsides in New England", *HortScience*, 45, (3), 393-400.

Brutsaert, W. (1967), "Some methods of calculating unsaturated permeability", *Transactions of the ASAE*, 10, (3), 400-404.

Bullock, M. S., S. D. Nelson, and W. D. Kemper (1988), "Soil Cohesion as Affected by Freezing, Water Content, Time and Tillage", *Soil Science Society of America Journal*, 52, (3), 770-776, DOI: 10.2136/sssaj1988.03615995005200030031x.

Burgy, R. H. and J. N. Luthin (1956), "A Test of the single- and double-ring types of infiltrometers", *Transactions American Geophysical Union*, 37, (2), 189-192.

Campbell, G. S. (1974), "A simple method for determining unsaturated conductivity from moisture retention data", *Soil Science*, 117, (6), 311-314, DOI: 10.1097/00010694-197406000-00001.

Carpenter, J. and J. Bithell (2000), "Bootstrap confidence intervals: when, which, what? A practical guide for medical statisticians", *Statistics in Medicine*, 19, (9), 1141-1164, DOI: 10.1002/(SICI)1097-0258(20000515)19:9<1141::AID-SIM479>3.0.CO;2-F.

Chen, L., S. Sela, T. Svoray, and S. Assouline (2013), "The role of soil-surface sealing, microtopography, and vegetation patches in rainfall-runoff processes in semiarid areas", *Water Resources Research*, 49, (9), 5585-5599, DOI: 10.1002/wrcr.20360.

Chen, Z. Q., R. S. Govindaraju, and M. L. Kavvas (1994), "Spatial averaging of unsaturated flow equations under infiltration conditions over areally heterogeneous fields: 1. Development of models", *Water Resources Research*, 30, (2), 523-533, DOI: 10.1029/93WR02885.

Chow, V. T., D. R. Maidment, and L. W. Mays (1988), *Applied Hydrology*, Editions McGraw-Hill, New York, p. 572.

Clothier, B. E. and I. White (1981), "Measurement of Sorptivity and Soil Water Diffusivity in the Field", *Soil Science Society of America Journal*, 45, (2), 241, DOI: 10.2136/sssaj1981.03615995004500020003x.

Coquet, Y., P. Vachier, and C. Labat (2005), "Vertical variation of near-saturated hydraulic conductivity in three soil profiles", *Geoderma*, 126, (3-4), 181-191, DOI: 10.1016/j.geoderma.2004.09.014.

Cornelis, W. M., J. Ronsyn, M. Van Meirvenne, and R. Hartmann (2001), "Evaluation of Pedotransfer Functions for Predicting the Soil Moisture Retention Curve", *Soil*

Science Society of America Journal, 65, (3), 638-648, DOI: 10.2136/sssaj2001.653638x.

Corradini, C., F. Melone, and R. E. Smith (1994), "Modeling infiltration during complex rainfall sequences", *Water Resources Research*, 30, (10), 2777-2784, DOI: 10.1029/94WR00951.

Corradini, C., F. Melone, and R. E. Smith (1997), "A unified model for infiltration and redistribution during complex rainfall patterns", *Journal of Hydrology*, 192, (1-4), 104-124, DOI: 10.1016/S0022-1694(96)03110-1.

Corradini, C., F. Melone, and R. E. Smith (2000), "Modeling local infiltration for a two-layered soil under complex rainfall patterns", *Journal of Hydrology*, 237, (1-2), 58-73, DOI: 10.1016/S0022-1694(00)00298-5.

Corradini, C., R. S. Govindaraju, and R. Morbidelli (2002), "Simplified modelling of areal average infiltration at the hillslope scale", *Hydrological Processes*, 16, (9), 1757-1770, DOI: 10.1002/hyp.394.

Corradini, C., A. Flammini, R. Morbidelli, and R. S. Govindaraju (2011), "A conceptual model for infiltration in two-layered soils with a more permeable upper layer: From local to field scale", *Journal of Hydrology*, 410, (1-2), 62-72, DOI: 10.1016/j.jhydrol.2011.09.005.

Dagan, G. and E. Bresler (1983), "Unsaturated flow in spatially variable fields: 1. Derivation of model of infiltration and redistribution", *Wat. Resour. Res.* 19, (2), 413-420, DOI: 10.1029/WR019i002p00413.

Dane, J. H. and W. E. Puckett (1994), "Field soil hydraulic properties based on physical and mineralogical information", in *Proceedings of the international workshop on indirect methods for estimating the hydraulic properties of unsaturated soils*, University of California, Riverside, 389-403.

Darcy, H. (1856), *Détermination des lois d'écoulement de l'eau à travers le sable*, Victor Dalmont, Paris, pp. 590-594.

Dexter, A. R., E. A. Czyż, and O. P. Gaţe (2004), "Soil structure and the saturated hydraulic conductivity of subsoils", *Soil and Tillage Research*, 79, (2), 185-189, DOI: 10.1016/j.still.2004.07.007.

Dirksen, C. (1991), "Unsaturated hydraulic conductivity", in *Soil Analysis Physical Methods*, ed. by K. A. Smith and C. Mullins, Marcel Dekker, New York, 209-270.

Dirksen, C. and S. Matula (1994), "Automatic Atomized Water Spray System for Soil Hydraulic Conductivity Measurements", *Soil Science Society of America Journal*, 58, (2), 319-325, DOI: 10.2136/sssaj1994.03615995005800020009x.

Dixon, R. M. and D. R. Linden (1972), "Soil Air Pressure and Water Infiltration Under Border Irrigation", *Soil Science Society of America Journal*, 36, (6), 948-953, DOI: 10.2136/sssaj1972.03615995003600060032x.

Durner, W. and K. Lipsius (2005), "Determining Soil Hydraulic Properties", in *Encyclopedia of Hydrological Sciences*, John Wiley & Sons, chap. 75, 1121-1143.

Durner, W. and H. Flühler (2005), "Soil Hydraulic Properties", in *Encyclopedia of Hydrological Sciences*, John Wiley & Sons, chap. 74, 1103-1119.

Durner, W. and D. Or (2005), "Soil Water Potential Measurement", in *Encyclopedia of Hydrological Sciences*, John Wiley & Sons, chap. 73, 1089-1102.

Emmerich, W. E. (2003), "Season and erosion pavement influence on saturated soil hydraulic conductivity", *Soil Science*, 168, (9), 637-645, DOI: 10.1097/01.ss.0000090804.06903.3b.

Essig, E. T., C. Corradini, R. Morbidelli, and R. S. Govindaraju (2009), "Infiltration and deep flow over sloping surfaces: Comparison of numerical and experimental results", *Journal of Hydrology*, 374, (1-2), 30-42, DOI: 10.1016/j.jhydrol.2009.05.017.

Evans, J. D. (1996), *Straightforward Statistics for the Behavioral Sciences*, p. 624.

Ferrer Julià, M., T. Estrela Monreal, A. Sánchez del Corral Jiménez, and E. García Meléndez (2004), "Constructing a saturated hydraulic conductivity map of Spain using pedotransfer functions and spatial prediction", *Geoderma*, 123, (3-4), 257-277, DOI: 10.1016/j.geoderma.2004.02.011.

Gardner, C. M. K., T. J. Dean, and J. D. Cooper (1998), "Soil Water Content Measurement with a High-Frequency Capacitance Sensor", *Journal of Agricultural Engineering Research*, 71, (4), 395-403, DOI: 10.1006/jaer.1998.0338.

Gardner, W. R. (1958), "Some steady-state solutions of the unsaturated moisture flow equation with application to evaporation from a water table", *Soil Science*, 85, (4), 228-232, DOI: 10.1097/00010694-195804000-00006.

Ghezzehei, T. A. and D. Or (2003), "Stress-induced volume reduction of isolated pores in wet soil", *Water Resources Research*, 39, (3), DOI: 10.1029/2001WR001137.

Golub, G. H., M. Heath, and G. Wahba (1979), "Generalized Cross-Validation as a Method for Choosing a Good Ridge Parameter", *Technometrics*, 21, (2), 215-223, DOI: 10.1080/00401706.1979.10489751.

Goodrich, D. C., J.-M. Faurès, D. A. Woolhiser, L. J. Lane, and S. Sorooshian (1995), "Measurement and analysis of small-scale convective storm rainfall variability", *Journal of Hydrology*, 173, (1-4), 283-308, DOI: 10.1016/0022-1694(95)02703-R.

Govindaraju, R. S., R. Morbidelli, and C. Corradini (2001), "Areal Infiltration Modeling over Soils with Spatially Correlated Hydraulic Conductivities", *Journal of Hydrologic Engineering*, 6, (2), 150-158, DOI: 10.1061/(ASCE)1084-0699(2001)6:2(150).

Govindaraju, R. S., C. Corradini, and R. Morbidelli (2006), "A semi-analytical model of expected areal-average infiltration under spatial heterogeneity of rainfall and soil saturated hydraulic conductivity", *Journal of Hydrology*, 316, (1-4), 184-194, DOI: 10.1016/j.jhydrol.2005.04.019.

Govindaraju, R. S., C. Corradini, and R. Morbidelli (2012), "Local- and field-scale infiltration into vertically non-uniform soils with spatially-variable surface hydraulic conductivities", *Hydrological Processes*, 26, (21), 3293-3301, DOI: 10.1002/hyp.8454.

Green, W. and G. Ampt (1911), "Studies on soil physics: 1. The flow of air and water through soils", *Journal of Agricultural Science*, 4, (1), 1-24.

Gupta, R. K., R. P. Rudra, W. T. Dickinson, N. K. Patni, and G. J. Wall (1993), "Comparison of Saturated Hydraulic Conductivity measured by Various Field Methods", *Transactions of the ASAE*, 36, (1), 51-55, DOI: 10.13031/2013.28313.

Gupta, R. K., R. P. Rudra, W. T. Dickinson, and G. J. Wall (1994), "Spatial and seasonal variations in hydraulic conductivity in relation to four determination techniques", *Canadian Water Resources Journal*, 19, (2), 103-113, DOI: 10.4296/cwrj1902103.

Haverkamp, R. and J.-Y. Parlange (1986), "Predicting the water-retention curve from particle-size distribution: 1. Sandy soils without organic matter", *Soil Science*, 142, (6), 325-339, DOI: 10.1097/00010694-198612000-00001.

Haverkamp, R., P. J. Ross, K. R. J. Smettem, and J.-Y. Parlange (1994), "Three-dimensional analysis of infiltration from the disc infiltrometer: 2. Physically based infiltration equation", *Water Resources Research*, 30, (11), 2931-2935, DOI: 10.1029/94WR01788.

Hillel, D. and W. R. Gardner (1970), "Transient infiltration into crust-topped profiles", *Soil Science*, 109, (2), 69-76.

Hillel, D., V. D. Krentos, and Y. Stylianou (1972), "Procedure and test of an internal drainage method for measuring soil hydraulic characteristics in situ", *Soil Science*, 114, (5), 395-400, DOI: 10.1097/00010694-197211000-00011.

Hoerl, A. E. and R. W. Kennard (1970a), "Ridge Regression: Applications to Nonorthogonal Problems", *Technometrics*, 12, (1), 69-82, DOI: 10.1080/00401706.1970.10488635.

Hoerl, A. E. and R. W. Kennard (1970b), "Ridge Regression: Biased Estimation for Nonorthogonal Problems", *Technometrics*, 12, (1), 55-67, DOI: 10.1080/00401706.1970.10488634, arXiv: 9809069v1 [arXiv:gr-qc].

Hu, W., D. She, M. Shao, K. P. Chun, and B. Si (2015), "Effects of initial soil water content and saturated hydraulic conductivity variability on small watershed runoff simulation using LISEM", *Hydrological Sciences Journal*, 60, (6), 1137-1154, DOI: 10.1080/02626667.2014.903332.

Hubbert, M. K. (1956), "Darcy's law and the field equations of the flow of underground fluids", *AIME Petroleum Transaction*, 207, 222-239.

Huisman, J. A., S. S. Hubbard, J. D. Redman, and A. P. Annan (2003), "Measuring Soil Water Content with Ground Penetrating Radar", *Vadose Zone Journal*, 2, (4), 476-491.

Isaaks, E. H. and R. M. Srivastava (1989), "An Introduction to Applied Geostatistics", *Oxford University Press, New York*, 561.

Jabro, J. D. (1992), "Estimation of Saturated Hydraulic Conductivity of Soils From Particle Size Distribution and Bulk Density Data", *Transactions of the ASAE*, 35, (2), 557-560, DOI: 10.13031/2013.28633.

Jackson, T. J. (1993), "III. Measuring surface soil moisture using passive microwave remote sensing", *Hydrological Processes*, 7, (2), 139-152, DOI: 10.1002/hyp.3360070205.

Jaynes, D. B. and E. J. Tyler (1984), "Using soil physical properties to estimate hydraulic conductivity", *Soil Science*, 138, (4), 298-305, DOI: 10.1097/00010694-198410000-00007.

Journel, A. G., P. C. Kyriakidis, and S. Mao (2000), "Correcting the Smoothing Effect of Estimators: A Spectral Postprocessor", *Mathematical Geology*, 32, (7), 787-812, DOI: 10.1023/A:1007544406740.

El-Kadi, A. I. (1985), "On estimating the hydraulic properties of soil, Part 2. A new empirical equation for estimating hydraulic conductivity for sands", *Advances in Water Resources*, 8, (3), 148-153, DOI: 10.1016/0309-1708(85)90055-7.

Kern, J. S. (1995), "Evaluation of Soil Water Retention Models Based on Basic Soil Physical Properties", *Soil Science Society of America Journal*, 59, (4), 1134, DOI: 10.2136/sssaj1995.03615995005900040027x.

Krajewski, W. F., G. J. Ciach, and E. Habib (2003), "An analysis of small-scale rainfall variability in different climatic regimes", *Hydrological Sciences Journal*, 48, (2), 151-162, DOI: 10.1623/hysj.48.2.151.44694.

Lai, J. and L. Ren (2007), "Assessing the Size Dependency of Measured Hydraulic Conductivity Using Double-Ring Infiltrometers and Numerical Simulation", *Soil Science Society of America Journal*, 71, (6), 1667-1675, DOI: 10.2136/sssaj2006.0227.

Lai, J., Y. Luo, and L. Ren (2010), "Buffer Index Effects on Hydraulic Conductivity Measurements Using Numerical Simulations of Double-Ring Infiltration", *Soil Science Society of America Journal*, 74, (5), 1526-1536, DOI: 10.2136/sssaj2009.0450.

Lassabatère, L., R. Angulo-Jaramillo, J. M. Soria Ugalde, R. Cuenca, I. Braud, and R. Haverkamp (2006), "Beerkan Estimation of Soil Transfer Parameters through Infiltration Experiments—BEST", *Soil Science Society of America Journal*, 70, (2), 521-532, DOI: 10.2136/sssaj2005.0026.

Leij, F. J., T. A. Ghezzehei, and D. Or (2002), "Analytical Models for Soil Pore-Size Distribution After Tillage", *Soil Science Society of America Journal*, 66, (4), 1104-1114, DOI: 10.2136/sssaj2002.1104.

Linsley, R. K., J. B. Franzini, D. L. Freyberg, and G. Tchobanoglous (1992), *Water Resources Engineering*, McGraw-Hill.

Liu, X.-Q. and H.-Y. Jiang (2012), "Optimal generalized ridge estimator under the generalized cross-validation criterion in linear regression", *Linear Algebra and its Applications*, 436, (5), 1238-1245, DOI: 10.1016/j.laa.2011.08.032.

Loague, K. and G. A. Gander (1990), "Spatial variability of infiltration on a small rangeland catchment", *Soil Science Society of America Journal*, 26, (5), 957-971.

Maller, R. A. and M. L. Sharma (1981), "An analysis of areal infiltration considering spatial variability", *Journal of Hydrology*, 52, (1-2), 25-37, DOI: 10.1016/0022-1694(81)90093-7.

Mapa, R. B., R. E. Green, and L. Santo (1986), "Temporal Variability of Soil Hydraulic Properties with Wetting and Drying Subsequent to Tillage1", *Soil Science Society of America Journal*, 50, (5), 1133-1138, DOI: 10.2136/sssaj1986.03615995005000050008x.

Marquardt, D. W. (1970), "Generalized Inverses, Ridge Regression, Biased Linear Estimation, and Nonlinear Estimation", *Technometrics*, 12, (3), 591-612, DOI: 10.2307/1267205.

Marshall, T. J. and G. B. Stirk (1950), "The effect of lateral movement of water in soil on infiltration measurements", *Australian Journal of Agricultural Research*, 1, (3), 253-265, DOI: 10.1071/AR9500253.

Matheron, G. (1963), "Principles of Geostastistics", *Economic Geology*, 58, 1246-1266.

McKay, M. D., R. J. Beckman, and W. J. Connover (1979), "A Comparison of three methods for selecting values of input vairables in the analysis of output from a computer code", *Tecnometrics*, 21, (2), 239-245.

McKenzie, N., K. Coughlan, and H. Cresswell (2002), *Soil physical measurement and interpretation for land evaluation*, Csiro Publishing, vol. 5.

McWhorter, D. B. (1971), *Infiltration Affected by Flow of Air*, 49, Colo. State Univ., Fort Collins, p. 53.

Minasny, B., A. B. McBratney, and K. L. Bristow (1999), "Comparison of different approaches to the development of pedotransfer functions for water-retention curves", *Geoderma*, 93, (3-4), 225-253, DOI: 10.1016/S0016-7061(99)00061-0.

Mohanty, B. P., M. D. Ankeny, R. Horton, and R. S. Kanwar (1994), "Spatial analysis of hydraulic conductivity measured using disc infiltrometer", *Water Resources Research*, 30(9), (9), 2489-2498.

Montgomery, D. C., E. A. Peck, and G. G. Vining (2012), *Introduction to Linear Regression Analysis*.

Morbidelli, R., C. Corradini, and R. S. Govindaraju (2006), "A field-scale infiltration model accounting for spatial heterogeneity of rainfall and soil saturated hydraulic conductivity", *Hydrological Processes*, 20, (7), 1465-1481, DOI: 10.1002/hyp.5943.

Morbidelli, R., C. Corradini, C. Saltalippi, A. Flammini, and E. Rossi (2011), "Infiltration-soil moisture redistribution under natural conditions: experimental evidence as a guideline for realizing simulation models", *Hydrology and Earth System Sciences*, 15, (9), 2937-2945, DOI: 10.5194/hess-15-2937-2011.

Morbidelli, R., C. Saltalippi, A. Flammini, E. Rossi, and C. Corradini (2014), "Soil water content vertical profiles under natural conditions: matching of experiments and simulations by a conceptual model", *Hydrological Processes*, 28, (17), 4732-4742, DOI: 10.1002/hyp.9973.

Morbidelli, R., C. Saltalippi, A. Flammini, M. Cifrodelli, C. Corradini, and R. S. Govindaraju (2015), "Infiltration on sloping surfaces: Laboratory experimental evidence and implications for infiltration modeling", *Journal of Hydrology*, 523, 79-85, DOI: 10.1016/j.jhydrol.2015.01.041.

Morbidelli, R., C. Saltalippi, A. Flammini, M. Cifrodelli, T. Picciafuoco, C. Corradini, and R. S. Govindaraju (2016), "Laboratory investigation on the role of slope on infiltration over grassy soils", *Journal of Hydrology*, 543, 542-547, DOI: 10.1016/j.jhydrol.2016.10.024.

Morbidelli, R., C. Saltalippi, A. Flammini, M. Cifrodelli, and C. Corradini (2017), "A laboratory experimental system for infiltration studies", *Hydrology Research*, 48, (3), 741-748, DOI: 10.2166/nh.2016.066.

Morbidelli, R., C. Saltalippi, A. Flammini, and R. S. Govindaraju (2018), "Role of slope on infiltration: A review", *Journal of Hydrology*, 557, 878-886, DOI: 10.1016/j.jhydrol.2018.01.019.

Morel-Seytoux, H. J. (1973), "Two-phase flows in porous media", *Advances in Hydroscience*, 9, 119-202.

Moret-Fernández, D., C. González-Cebollada, B. Latorre, and V. Pérez (2015), "A modified hood infiltrometer to estimate the soil hydraulic properties from the transient water flow measurements", *Journal of Hydrology*, 530, 554-560, DOI: 10.1016/j.jhydrol.2015.10.014.

Mualem, Y. (1976), "A new model for predicting the hydraulic conductivity of unsaturated porous media", *Water Resources Research*, 12, (3), 513-522, DOI: 10.1029/WR012i003p00513.

Mualem, Y. and S. Assouline (1989), "Modeling soil seal as a nonuniform layer", *Water Resources Research*, 25, (10), 2101-2108, DOI: 10.1029/WR025i010p02101.

Mualem, Y., S. Assouline, and D. Eltahan (1993), "Effect of rainfall-induced soil seals on soil water regime: Wetting processes", *Water Resources Research*, 29, (6), 1651-1659, DOI: 10.1029/93WR00096.

Muñoz-Carpena, R., C. M. Regalado, J. Álvarez-Benedi, and F. Bartoli (2002), "Field evaluation of the new Philip-Dunne permeameter for measuring saturated hydraulic conductivity", *Soil Science*, 167, (1), 9-24, DOI: 10.1097/00010694-200201000-00002.

Nemes, A., M. G. Schaap, and J. H. M. Wösten (2003), "Functional Evaluation of Pedotransfer Functions Derived from Different Scales of Data Collection", *Soil Science Society of America Journal*, 67, (4), 1093-1102, DOI: 10.2136/sssaj2003.1093.

Nielsen, D. R., J. W. Biggar, and K. T. Erh (1973), "Spatial variability of field-measured soil-water properties", *Hilgardia*, 42, (7), 215-259, DOI: 10.3733/hilg.v42n07p215.

Nielsen, D. R., M. T. van Genuchten, and J. W. Biggar (1986), "Water flow and solute transport processes in the unsaturated zone", *Water Resources Research*, 22, (9S), 89S-108S, DOI: 10.1029/WR022i09Sp0089S.

Nimmo, J. R. (2002), "Guidelines for method selection [water retention and storage]", in *Methods of Soil Analysis: Part 4 - Physical Methods, Soil Science Society of America Book Series No. 5*, ed. by J. H. Dane and G. C. Topp, Madison, 717-720.

Oliver, M. and R. Webster (2014), "A tutorial guide to geostatistics: Computing and modelling variograms and kriging", *CATENA*, 113, 56-69, DOI: 10.1016/j.catena.2013.09.006.

Pachepsky, Y. A., W. J. Rawls, and D. J. Timlin (1998), "The Current Status of Pedotransfer Functions: Their Accuracy, Reliability, and Utility in Field- and Regional-Scale Modeling", in *Assessment of Non-Point Source Pollution in the Vadose Zone*, ed. by D. L. Corwin, K. Loague, and T. R. Ellsworth, American Geophysical Union, vol. 108, 223-234, DOI: 10.1029/GM108p0223.

Pachepsky, Y. A., D. J. Timlin, and W. J. Rawls (2001), "Soil Water Retention as Related to Topographic Variables", *Soil Science Society of America Journal*, 65, (6), 1787-1795, DOI: 10.2136/sssaj2001.1787.

Paltineanu, I. C. and J. L. Starr (1997), "Real-time Soil Water Dynamics Using Multisensor Capacitance Probes: Laboratory Calibration", *Soil Science Society of America Journal*, 61, (6), 1576, DOI: 10.2136/sssaj1997.03615995006100060006x.

Papanicolaou, A. T. N., M. Elhakeem, C. G. Wilson, C. L. Burras, L. T. West, H. H. Lin, B. Clark, and B. E. Oneal (2015), "Spatial variability of saturated hydraulic conductivity at the hillslope scale: Understanding the role of land management and erosional effect", *Geoderma*, 243-244, 58-68, DOI: 10.1016/j.geoderma.2014.12.010.

Parasuraman, K., A. Elshorbagy, and B. C. Si (2006), "Estimating Saturated Hydraulic Conductivity In Spatially Variable Fields Using Neural Network Ensembles", *Soil Science Society of America Journal*, 70, (6), 1851-1859, DOI: 10.2136/sssaj2006.0045.

Parlange, J.-Y. and D. E. Hill (1979), "Air and water movement in porous media: compressibility effects", *Soil Science*, 127, 257-263.

Parlange, J.-Y., I. Lisle, R. D. Braddock, and R. E. Smith (1982), "The three-parameter infiltration equation", *Soil Science*, 133, (6), 337-341, DOI: 10.1097/00010694-198206000-00001.

Perroux, K. M. and I. White (1988), "Designs for Disc Permeameters", *Soil Science Society of America Journal*, 52, (5), 1205-1215, DOI: 10.2136/sssaj1988.03615995005200050001x.

Philip, J. R. (1957a), "The theory of infiltration: 1. The infiltration equation and its solution", *Soil Science*, 83, (5), 345-358.

Philip, J. R. (1957b), "The theory of infiltration: 2. The profile of infinity", *Soil Science*.

Philip, J. R. (1957c), "The theory of infiltration: 4. Sorptivity and algebraic infiltration equations", *Soil Science*, 84, (3), 257-264.

Philip, J. R. (1969), "Theory of Infiltration", *Advances in Hydroscience*, 5, 215-296, DOI: 10.1016/B978-1-4831-9936-8.50010-6.

Philip, J. R. (1991), "Hillslope infiltration: Planar slopes", *Water Resources Research*, 27, (1), 109-117, DOI: 10.1029/90WR01704.

Philip, J. R. (1998), "Infiltration into crusted soils", *Water Resources Research*, 34, (8), 1919-1927, DOI: 10.1029/98WR01207.

Picciafuoco, T., R. Morbidelli, A. Flammini, C. Saltalippi, C. Corradini, P. Strauss, and G. Blöschl (2018a), "A pedotransfer function for field-scale saturated hydraulic conductivity of a small watershed", *Hydrological Processes*, Submitted.

Picciafuoco, T., R. Morbidelli, A. Flammini, C. Saltalippi, C. Corradini, P. Strauss, and G. Blöschl (2018b), "On the estimation of spatially representative plot scale saturated hydraulic conductivity", *Journal of Hydrology*, Submitted.

Poesen, J. (1984), "The influence of slope angle on infiltration rate and Hortonian overland flow", *Zeitschrift für Geomorpholgie, Supplement Band*, 49, 116-131.

Puckett, W. E., J. H. Dane, and B. F. Hajek (1985), "Physical and Mineralogical Data to Determine Soil Hydraulic Properties", *Soil Science Society of America Journal*, 49, (4), 831-836, DOI: 10.2136/sssaj1985.03615995004900040008x.

Ragab, R. and J. D. Cooper (1993), "Variability of unsaturated zone water transport parameters: implications for hydrological modelling. 1. In situ measurements", *Journal of Hydrology*, 148, (1-4), 109-131, DOI: 10.1016/0022-1694(93)90255-8.

Rahmati, M., L. Weihermüller, J. Vanderborght, Y. A. Pachepsky, L. Mao, S. H. Sadeghi, N. Moosavi, H. Kheirfam, C. Montzka, K. Van Looy, B. Toth, Z. Hazbavi, W. Al Yamani, A. A. Albalasmeh, M. Z. Alghzawi, R. Angulo-Jaramillo, A. C. D. Antonino, G. Arampatzis, R. A. Armindo, H. Asadi, Y. Bamutaze, J. Batlle-Aguilar, B. Béchet, F. Becker, G. Blöschl, K. Bohne, I. Braud, C. Castellano, A. Cerdà, M. Chalhoub, R. Cichota, M. Císlerová, B. Clothier, Y. Coquet, W. Cornelis, C. Corradini, A. P. Coutinho, M. B. de Oliveira, J. R. de Macedo, M. F. Durães, H. Emami, I. Eskandari, A. Farajnia, A. Flammini, N. Fodor, M. Gharaibeh, M. H. Ghavimipanah, T. A. Ghezzehei, S. Giertz, E. G. Hatzigiannakis, R. Horn, J. J. Jiménez, D. Jacques, S. D. Keesstra, H. Kelishadi, M. Kiani-Harchegani, M. Kouselou, M. Kumar Jha, L. Lassabatere, X. Li, M. A. Liebig, L. Lichner, M. V. López, D. Machiwal, D. Mallants, M. S. Mallmann, J. D. de Oliveira Marques, M. R. Marshall, J. Mertens, F.

Meunier, M. H. Mohammadi, B. P. Mohanty, M. Pulido-Moncada, S. Montenegro, R. Morbidelli, D. Moret-Fernández, A. A. Moosavi, M. R. Mosaddeghi, S. B. Mousavi, H. Mozaffari, K. Nabiollahi, M. R. Neyshabouri, M. V. Ottoni, T. B. Ottoni Filho, M. R. Pahlavan-Rad, A. Panagopoulos, S. Peth, P.-E. Peyneau, T. Picciafuoco, J. Poesen, M. Pulido, D. J. Reinert, S. Reinsch, M. Rezaei, F. P. Roberts, D. Robinson, J. Rodrigo-Comino, O. C. Rotunno Filho, T. Saito, H. Suganuma, C. Saltalippi, R. Sándor, B. Schütt, M. Seeger, N. Sepehrnia, E. Sharifi Moghaddam, M. Shukla, S. Shutaro, R. Sorando, A. A. Stanley, P. Strauss, Z. Su, R. Taghizadeh-Mehrjardi, E. Taguas, W. G. Teixeira, A. R. Vaezi, M. Vafakhah, T. Vogel, I. Vogeler, J. Votrubova, S. Werner, T. Winarski, D. Yilmaz, M. H. Young, S. Zacharias, Y. Zeng, Y. Zhao, H. Zhao, and H. Vereecken (2018), "Development and analysis of the Soil Water Infiltration Global database", *Earth System Science Data*, 10, (3), 1237-1263, DOI: 10.5194/essd-10-1237-2018.

Rawls, W. J., D. L. Brakensiek, and K. E. Saxton (1982), "Estimation of Soil Water Properties", *Transactions of the ASAE*, 25, (5), 1316-1320, DOI: 10.13031/2013.33720.

Rawls, W. J., D. L. Brakensiek, and B. Soni (1983), "Agricultural Management Effects on Soil Water Processes Part I: Soil Water Retention and Green and Ampt Infiltration Parameters", *Transactions of the ASAE*, 26, (6), 1747-1752, DOI: 10.13031/2013.33837.

Rawls, W. J. and D. L. Brakensiek (1985), "Prediction of Soil Water Properties for Hydrologic Modelling", in *Proceedings of a Symposium Watershed Management in the Eighties,* ed. by E. B. Jones and T. J. Ward, New York, 293-299.

Rawls, W. J., T. J. Gish, and D. L. Brakensiek (1991), "Estimating Soil Water Retention from Soil Physical Properties and Characteristics", in *Advances in Soil Science*, vol. 16, 213-234, DOI: 10.1007/978-1-4612-3144-8_5.

Reynolds, W. D. and D. E. Erlick (1985), "In Situ Measurement of Field-Saturated Hydraulic Conductivity, Sorptivity, and the α-Parameter Using the Guelph Permeameter", *Soil Science*, 140, (4), 292-302, DOI: 10.1097/00010694-198510000-00008.

Reynolds, W. D., B. T. Bowman, R. R. Brunke, C. F. Drury, and C. S. Tan (2000), "Comparison of Tension Infiltrometer, Pressure Infiltrometer, and Soil Core Estimates of Saturated Hydraulic Conductivity", *Soil Science Society of America Journal*, 64, (2), 478-484, DOI: 10.2136/sssaj2000.642478x.

Robinson, D. A., S. B. Jones, J. M. Wraith, D. Or, and S. P. Friedman (2003), "A Review of Advances in Dielectric and Electrical Conductivity Measurement in Soils

Using Time Domain Reflectometry", *Vadose Zone Journal*, 2, (4), 444-475, DOI: 10.2136/vzj2003.4440.

Römkens, M. J. M., R. L. Baumhardt, J.-Y. Parlange, F. D. Whisler, M. B. Parlange, and S. N. Prasad (1986a), "Effect of rainfall characteristics on seal hydraulic conductance", *Assessment of Soil Surface Sealing and Crusting*, ed. by F. Callebaut, D. Gabriels, and M. De Boodt, 228-235.

Römkens, M. J. M., R. L. Baumhardt, M. B. Parlange, F. D. Whisler, J.-Y. Parlange, and S. N. Prasad (1986b), "Rain-induced surface seals: their effect on ponding and infiltration", *Annales Geophysicae*, 4, 417-424.

Ronayne, M. J., T. B. Houghton, and J. D. Stednick (2012), "Field characterization of hydraulic conductivity in a heterogeneous alpine glacial till", *Journal of Hydrology*, 458-459, 103-109, DOI: 10.1016/j.jhydrol.2012.06.036.

Russo, D. and E. Bresler (1981), "Soil Hydraulic Properties as Stochastic Processes: I. An Analysis of Field Spatial Variability", *Soil Science Society of America Journal*, 45, (4), 682-687, DOI: 10.2136/sssaj1981.03615995004500040002x.

Russo, D. and E. Bresler (1982), "A univariate versus a multivariate parameter distribution in a stochastic-conceptual analysis of unsaturated flow", *Water Resources Research*, 18, (3), 483-488, DOI: 10.1029/WR018i003p00483.

Saghafian, B., P. Y. Julien, and F. L. Ogden (1995), "Similarity in Catchment Response: 1. Stationary Rainstorms", *Water Resources Research*, 31, (6), 1533-1541, DOI: 10.1029/95WR00518.

Sander, G. C., J.-Y. Parlange, and W. L. Hogarth (1988), "Air and water flow, II. Gravitational flow with an arbitrary flux boundary condition", *Journal of Hydrology*, 99, (3-4), 225-234, DOI: 10.1016/0022-1694(88)90050-9.

Sander, G. C., J. Norbury, and S. W. Weeks (1993), "An exact solution to the nonlinear diffusion-convection equation for two-phase flow", *The Quarterly Journal of Mechanics and Applied Mathematics*, 46, (4), 709-727, DOI: 10.1093/qjmam/46.4.709.

Santos, M. J., M. C. Goncalves, and L. S. Pereira (1999), "Determinig the unsaturated soil hydraulic conductivity in the entire suction range using a two-step method", in *Proceeding of the International Workshop on Characterization and Measurement of the Hydraulic Properties of Unsaturated Porous Media*, ed. by M. T. van Genuchten, F. J. Leij, and L. Wu, University of California, Riverside, 303-312.

Saxton, K. E., W. J. Rawls, J. S. Romberger, and R. I. Papendick (1986), "Estimating Generalized Soil-water Characteristics from Texture", *Soil Science Society of Amer-*

ica Journal, 50, (4), 1031-1036, DOI: 10.2136/sssaj1986.03615995005000040039x.

Scanlon, B. R., B. J. Andraski, and J. Bilskie (2002), "Miscellaneous methods for measuring matric or water potential", in *Methods of Soil Analysis: Part 4 - Physical Methods, Soil Science Society of America Book Series No. 5*, ed. by J. H. Dane and G. C. Topp, Soil Science Society of America, Madison, 643-670.

Schaap, M. G. and F. J. Leij (1998), "Database-related accuracy and uncertainty of pedotransfer functions", *Soil Science*, 163, (10), 765-779, DOI: 10.1097/00010694-199810000-00001.

Schaap, M. G., F. J. Leij, and M. T. van Genuchten (2001), "ROSETTA: a computer program for estimating soil hydraulic parameters with hierarchical pedotransfer functions", *Journal of Hydrology*, 251, (3-4), 163-176, DOI: 10.1016/S0022-1694(01)00466-8.

Schaap, M. G. (2005), "Models for Indirect Estimation of Soil Hydraulic Properties", in *Encyclopedia of Hydrological Sciences*, John Wiley & Sons, chap. 76, 1145-1150.

Schulze-Makuch, D., D. A. Carlson, D. S. Cherkauer, and P. Malik (1999), "Scale dependency of hydraulic conductivity in heterogeneous media", *Groundwater*, 37, (6), 904-919, DOI: 10.1111/j.1745-6584.1999.tb01190.x.

Schwärzel, K. and J. Punzel (2007), "Hood Infiltrometer—A New Type of Tension Infiltrometer", *Soil Science Society of America Journal*, 71, (5), 1438-1447, DOI: 10.2136/sssaj2006.0104.

Sedaghat, A., H. Bayat, and A. A. Safari Sinegani (2016), "Estimation of soil saturated hydraulic conductivity by artificial neural networks ensemble in smectitic soils", *Eurasian Soil Science*, 49, (3), 347-357, DOI: 10.1134/S106422931603008X.

Shapiro, S. S. and M. B. Wilk (1965), "An Analysis of Variance Test for Normality (Complete Samples)", *Biometrika*, 52, (3/4), 591-611, DOI: 10.2307/2333709.

Sharma, K. D., H. P. Singh, and O. P. Pareek (1983), "Rainwater infiltration into a bare loamy sand", *Hydrological Sciences Journal*, 28, (3), 417-424, DOI: 10.1080/02626668309491980.

Sharma, M. L. (1979), "Spatial variability and its effect on infiltration", in *Proceeding of the Hydrology Water Resources Symposium*, Perth, Australia, 69-73.

Sharma, M. L., R. J. W. Barron, and M. S. Fernie (1987), "Areal distribution of infiltration parameters and some soil physical properties in lateritic catchments", *Journal of Hydrology*, 94, (1-2), 109-127, DOI: 10.1016/0022-1694(87)90035-7.

Sidiras, N. and C. H. Roth (1987), "Infiltration measurements with double-ring infiltrometers and a rainfall simulator under different surface conditions on an Oxisol",

Soil and Tillage Research, 9, (2), 161-168, DOI: 10.1016/0167-1987(87)90082-1.

Šimůnek, J., O. Wendroth, and M. T. van Genuchten (1999), "Estimating unsaturated soil hydraulic properties from laboratory tension disc infiltrometer experiments", *Water Resources Research*, 35, (10), 2965-2979, DOI: 10.1029/1999WR900179.

Singh, V. P. (2017), *Handbook of applied hydrology*, Vol. 2, McGraw-Hill Education.

Sivapalan, M. and E. F. Wood (1986), "Spatial Heterogeneity and Scale in the Infiltration Response of Catchments", in *Scale Problems in Hydrology*, 81-106, DOI: 10.1007/978-94-009-4678-1_5.

Skøien, J. O. and G. Blöschl (2006), "Sampling Scale Effects in Random Fields and Implications for Environmental Monitoring", *Environmental Monitoring and Assessment*, 114, (1-3), 521-552, DOI: 10.1007/s10661-006-4939-z.

Smettem, K. R. J., J.-Y. Parlange, P. J. Ross, and R. Haverkamp (1994), "Three-dimensional analysis of infiltration from the disc infiltrometer: 1. A capillary-based theory", *Water Resources Research*, 30, (11), 2925-2929, DOI: 10.1029/94WR01787.

Smith, R. E. and J.-Y. Parlange (1978), "A parameter-efficient hydrologic infiltration model", *Water Resources Research*, 14, (3), 533-538, DOI: 10.1029/WR014i003p00533.

Smith, R. E. and D. C. Goodrich (2000), "Model For Rainfall Excess Patterns on Randomly Heterogeneous Areas", *Journal of Hydrologic Engineering*, 5, (4), 355-362, DOI: 10.1061/(ASCE)1084-0699(2000)5:4(355).

Smith, R. E. (1990), "Analysis of Infiltration through a Two-Layer Soil Profile", *Soil Science Society of America Journal*, 54, (5), 1219-1227, DOI: 10.2136/sssaj1990.03615995005400050004x.

Smith, R. E. (2002), *Infiltration Theory for Hydrologic Applications*, American Geophysical Union.

Snedecor, G. W. and W. G. Cochran (1980), *Statistical Methods*, 7th, Iowa State University Press, p. 507.

Sobieraj, J. A., H. Elsenbeer, and G. Cameron (2004), "Scale dependency in spatial patterns of saturated hydraulic conductivity", *Catena*, 55, (1), 49-77, DOI: 10.1016/S0341-8162(03)00090-0.

Spychalski, M., C. Kaźmierowski, and Z. Kaczmarek (2007), "Estimation of saturated hydraulic conductivity on the basis of drainage porosity", *Electronic Journal of Polish Agricultural Universities*, 10, (1).

Stephens, D. B., K. Lambert, and D. Watson (1983), "Influence of entrapped air on field determinations of hydraulic properties in the vadose zone", in *Proc. Conf. on Vadose Zone Characterization and Monitoring*, National Water Well Association, Columbus, Ohio, Las Vegas, Nevada.

Suleiman, A. A. and J. T. Ritchie (2001), "Estimating Saturated Hydraulic Conductivity from Soil Porosity", *Transactions of the ASAE*, 44, (2), 235-339, DOI: 10.13031/2013.4683.

Swartzendruber, D. and T. C. Olson (1961a), "Model study of the double-ring infiltrometer as affected by depth of wetting and particle size", *Soil Science*, 92, (4), 219-225, DOI: 10.1097/00010694-196110000-00001.

Swartzendruber, D. and T. C. Olson (1961b), "Sand-model study of buffer effects in the double-ring infiltrometer", *Soil Science Society of America Journal*, 25, (1), 5-8.

Taha, A., J. M. Gresillon, and B. E. Clothier (1997), "Modelling the link between hillslope water movement and stream flow: application to a small Mediterranean forest watershed", *Journal of Hydrology*, 203, (1-4), 11-20, DOI: 10.1016/S0022-1694(97)00081-4.

Taskinen, A., H. Sirviö, and M. Bruen (2008), "Statistical analysis of the effects on overland flow of spatial variability in soil hydraulic conductivity", *Hydrological Sciences Journal*, 53, (2), 387-400, DOI: 10.1623/hysj.53.2.387.

Thorup-Kristensen, K., M. S. Cortasa, and R. Loges (2009), "Winter wheat roots grow twice as deep as spring wheat roots, is this important for N uptake and N leaching losses?", *Plant and Soil*, 322, (1), 101-114, DOI: 10.1007/s11104-009-9898-z.

Tietje, O. and M. Tapkenhinrichs (1993), "Evaluation of Pedo-Transfer Functions", *Soil Science Society of America Journal*, 57, (4), 1088-1095, DOI: 10.2136/sssaj1993.03615995005700040035x.

Tietje, O. and V. Hennings (1996), "Accuracy of the saturated hydraulic conductivity prediction by pedo-transfer functions compared to the variability within FAO textural classes", *Geoderma*, 69, (1-2), 71-84, DOI: 10.1016/0016-7061(95)00050-X.

Topp, G. C., J. L. Davis, and A. P. Annan (1980), "Electromagnetic determination of soil water content: Measurements in coaxial transmission lines", *Water Resources Research*, 16, (3), 574-582, DOI: 10.1029/WR016i003p00574.

Topp, G. C. and W. D. Reynolds (1998), "Time domain reflectometry: a seminal technique for measuring mass and energy in soil", *Soil and Tillage Research*, 47, (1-2), 125-132, DOI: 10.1016/S0167-1987(98)00083-X.

Topp, G. C. and T. P. Ferré (2005), "Measuring Soil Water Content", in *Encyclopedia of Hydrological Sciences*, John Wiley & Sons, chap. 72, 1077-1088.

Tossell, R. W., W. T. Dickinson, R. P. Rudra, and G. J. Wall (1987), "A portable rainfall simulator", *Canadian Agricultural Engineering*, 29, (2), 155-162.

Touma, J., G. Vachaud, and J.-Y. Parlange (1984), "Air and water flow in a sealed, ponded vertical soil column: Experiment and model", *Soil Science*, 137, (3), 181-187, DOI: 10.1097/00010694-198403000-00008.

Tseng, P.-H. and W. A. Jury (1993), "Simulation of field measurement of hydraulic conductivity in unsaturated heterogeneous soil", *Water Resources Research*, 29, (7), 2087-2099, DOI: 10.1029/93WR00578.

Twarakavi, N. K. C., J. Šimůnek, and M. G. Schaap (2009), "Development of Pedotransfer Functions for Estimation of Soil Hydraulic Parameters using Support Vector Machines", *Soil Science Society of America Journal*, 73, (5), 1443-1452, DOI: 10.2136/sssaj2008.0021.

Van Es, H. M., C. B. Ogden, R. L. Hill, R. R. Schindelbeck, and T. Tsegaye (1999), "Integrated Assessment of Space, Time, and Management-Related Variability of Soil Hydraulic Properties", *Soil Science Society of America Journal*, 63, (6), 1599-1608, DOI: 10.2136/sssaj1999.6361599x.

Van Genuchten, M. T. (1980), "A closed form equation for predicting the hydraulic conductivity of unsaturated soils", *Soil Science Society of America Journal*, 44, (5), 892-898.

Van Genuchten, M. T. and D. R. Nielsen (1985), "On describing and predicting the hydraulic properties of unsaturated soils", *Annales De Geophysique*, 3, 615-628.

Vanderlinden, K., D. Gabriels, and J. V. Giráldez (1998), "Evaluation of infiltration measurements under olive trees in Córdoba", *Soil and Tillage Research*, 48, (4), 303-315, DOI: 10.1016/S0167-1987(98)00137-8.

Vandervaere, J.-P., M. Vauclin, R. Haverkamp, C. Peugeot, J.-L. Thony, and M. Gilfedder (1998), "A simple model of infiltration into crusted soils", *Soil Science*, 163, 9-21.

Verbist, K. M. J., W. M. Cornelis, S. Torfs, and D. Gabriels (2013), "Comparing Methods to Determine Hydraulic Conductivities on Stony Soils", *Soil Science Society of America Journal*, 77, (1), 25-42, DOI: 10.2136/sssaj2012.0025.

Vieira, S. R., D. R. Nielsen, and J. W. Biggar (1981), "Spatial Variability of Field-Measured Infiltration Rate", *Soil Science Society of America Journal*, 45, (6), 1040-1048, DOI: 10.2136/sssaj1981.03615995004500060007x.

Von Hippel, A. R. (1954), "Theory", in *Dielectric Materials and Applications*, ed. by A. R. Von Hippel, M.I.T. Technology Press and John Wiley & Sons, New York, 3-46.

Wagger, M. G. and H. P. Denton (1989), "Influence of Cover Crop and Wheel Traffic on Soil Physical Properties in Continuous No-Till Corn1", *Soil Science Society of America Journal*, 53, (4), 1206-1210, DOI: 10.2136/sssaj1989.03615995005300040036x.

Wagner, B., V. R. Tarnawski, V. Hennings, U. Müller, G. Wessolek, and R. Plagge (2001), "Evaluation of pedo-transfer functions for unsaturated soil hydraulic conductivity using an independent data set", *Geoderma*, 102, (3-4), 275-297, DOI: 10.1016/S0016-7061(01)00037-4.

Wang, Z., J. Feyen, D. R. Nielsen, and M. T. van Genuchten (1997), "Two-phase flow infiltration equations accounting for air entrapment effects", *Water Resources Research*, 33, (12), 2759-2767, DOI: 10.1029/97WR01708.

Warrick, A. W., G. J. Mullen, and D. R. Nielsen (1977), "Scaling field-measured soil hydraulic properties using a similar media concept", *Water Resources Research*, 13, (2), 355-362, DOI: 10.1029/WR013i002p00355.

Weeks, S. W., G. C. Sander, and J.-Y. Parlange (2003), "n-Dimensional first integral and similarity solutions for two-phase flow", *The ANZIAM Journal*, 44, (3), 365-380, DOI: 10.1017/S1446181100008087.

Weir, G. J. and W. M. Kissling (1992), "The influence of airflow on the vertical infiltration of water into soil", *Water Resources Research*, 28, (10), 2765-2772, DOI: 10.1029/92WR00803.

White, I. and M. J. Sully (1987), "Macroscopic and microscopic capillary length and time scales from field infiltration", *Water Resources Research*, 23, (8), 1514-1522, DOI: 10.1029/WR023i008p01514.

Wind, G. P. (1968), "Capillary conductivity data estimated by a simple method", in *Water in the Unsaturated Zone, Proceedings of the Wageningen Symposium*, ed. by P. E. Rijtema and H. Wassink, International Association of Scientific Hydrology, Gent/Brugge/Paris, 181-191.

Wold, S., A. Ruhe, H. Wold, and W. J. Dunn III (1984), "The Collinearity Problem in Linear Regression. The Partial Least Squares (PLS) Approach to Generalized Inverses", *SIAM Journal on Scientific and Statistical Computing*, 5, (3), 735-743, DOI: 10.1137/0905052.

Wooding, R. A. and H. J. Morel-Seytoux (1976), "Multiphase Fluid Flow Through Porous Media", *Annual Review of Fluid Mechanics*, 8, (1), 233-274, DOI: 10.1146/annurev.fl.08.010176.001313.

Wooding, R. A. (1968), "Steady Infiltration from a Shallow Circular Pond", *Water Resources Research*, 4, (6), 1259-1273, DOI: 10.1029/WR004i006p01259.

Woolhiser, D. A., R. E. Smith, and J. V. Giráldez (1996), "Effects of Spatial Variability of Saturated Hydraulic Conductivity on Hortonian Overland Flow", *Water Resources Research*, 32, (3), 671-678, DOI: 10.1029/95WR03108.

Wösten, J. H. M., P. A. Finke, and M. J. W. Jansen (1995), "Comparison of class and continuous pedotransfer functions to generate soil hydraulic characteristics", *Geoderma*, 66, (3-4), 227-237, DOI: 10.1016/0016-7061(94)00079-P.

Wösten, J. H. M. (1997), "Chapter 10 Pedotransfer functions to evaluate soil quality", *Developments in Soil Science*, 25, 221-245, DOI: 10.1016/S0166-2481(97)80037-2.

Wösten, J. H. M., A. Lilly, A. Nemes, and C. Le Bas (1999), "Development and use of a database of hydraulic properties of European soils", *Geoderma*, 90, (3-4), 169-185, DOI: 10.1016/S0016-7061(98)00132-3.

Wösten, J. H. M., Y. A. Pachepsky, and W. J. Rawls (2001), "Pedotransfer functions: bridging the gap between available basic soil data and missing soil hydraulic characteristics", *Journal of Hydrology*, 251, (3-4), 123-150, DOI: 10.1016/S0022-1694(01)00464-4.

Wu, L., L. Pan, M. J. Roberson, and P. J. Shouse (1997), "Numerical evaluation of ring-infiltrometers under various soil conditions", *Soil Science*, 162, (11), 771-777, DOI: 10.1097/00010694-199711000-00001.

Zegelin, S. J., I. White, and D. R. Jenkins (1989), "Improved field probes for soil water content and electrical conductivity measurement using time domain reflectometry", *Water Resources Research*, 25, (11), 2367-2376, DOI: 10.1029/WR025i011p02367.

Ziegler, A. D., J. N. Negishi, R. C. Sidle, S. Noguchi, and A. R. Nik (2006), "Impacts of logging disturbance on hillslope saturated hydraulic conductivity in a tropical forest in Peninsular Malaysia", *CATENA*, 67, (2), 89-104, DOI: 10.1016/j.catena.2006.02.008.

Zimmermann, B. and H. Elsenbeer (2008), "Spatial and temporal variability of soil saturated hydraulic conductivity in gradients of disturbance", *Journal of Hydrology*, 361, (1-2), 78-95, DOI: 10.1016/j.jhydrol.2008.07.027.

Appendix A

Pedotransfer functions

The equation of the PTF obtained using the multiple linear regression technique (PTF_{MLR}) is:

$$\bar{K}_s^f = -2.24 + 46.2\, om^2 + 36.0\, si + 32.0\, si^2 + 23.7\, sa + 0.1\, el \tag{A.1}$$

The equation of the PTF obtained using the ridge regression technique (PTF_R) is:

$$\bar{\boldsymbol{K}}_s^f = 13.5 + \tilde{\boldsymbol{X}}\hat{\boldsymbol{\beta}}^* \tag{A.2}$$

where $\tilde{\boldsymbol{X}}$ is the standardized matrix of regressors, $\bar{\boldsymbol{K}}_s^f$ is the vector of the derived field-scale saturated hydraulic conductivity values, $\hat{\boldsymbol{\beta}}^*$ is the vector of the ridge coefficients equal to:

$$\hat{\boldsymbol{\beta}}^{*T} = \begin{bmatrix} -1.35 & 4.62 & -1.91 & 1.30 & 1.34 & 4.36 & -0.28 & -2.05 & 1.52 & -0.03 \end{bmatrix}$$

In order to estimate the $\bar{\boldsymbol{K}}_s^f$ vector with regressors other than those used in the calibration, the standardized matrix $\tilde{\boldsymbol{X}}$ has to be generated according to the following transformation:

$$\tilde{x}_{i,j} = \frac{x_{i,j} - m_j}{sd_j} \tag{A.3}$$

where m_j and sd_j are the j-th elements of the vectors $\boldsymbol{m}$ and $\boldsymbol{sd}$, respectively in $\mathrm{mm\,h^{-1}}$:

$$\boldsymbol{m} = \begin{bmatrix} 0 & 0 & 0 & 0 & 0 & 0 & 0 & 0 & 5.89 & 273 \end{bmatrix}$$

$$\boldsymbol{sd} = \begin{bmatrix} 0.12 & 0.12 & 0.12 & 0.12 & 0.12 & 0.12 & 0.12 & 0.12 & 0.78 & 14.32 \end{bmatrix}$$

It is absolutely fundamental to remark that the matrix $\tilde{\boldsymbol{X}}$ needs to be generated considering the exact following order of the columns: om, om^2, cl, cl^2, si, si^2, sa, sa^2, s, el with the units previously described.